NMR Study of Magnetism and Superconductivity in Heavy-Fermion Systems under Pressure

Yu Kawasaki

OSAKA UNIVERSITY

GRADUATE SCHOOL OF ENGINEERING SCIENCE
DEPARTMENT OF PHYSICAL SCIENCE
DIVISION OF MATERIAL PHYSICS

2000

Abstract

We have performed NMR and NQR studies on several types of heavy-fermion (HF) compounds with different ground states in a series of CeT_2Si_2, where T stands for transition metals; superconductor $CeCu_2Si_2$, antiferromagnets $CePd_2Si_2$ and $CeRh_2Si_2$, and paramagnet $CeRu_2Si_2$ showing a pseudo-metamagnetic transition. A common feature in these compounds is that they are located close to a quantum critical region, where a magnetic order occurs at nearly zero temperature ($T \rightarrow 0$), and their magnetic properties are largely affected by a magnetic instability.

One of the most attracting feature in the HF system is the unconventional superconductivity (SC) characterized by the proximity to magnetic instability. It is necessary to investigate magnetic properties in the vicinity of magnetic to SC phase boundary for a full understanding of possible mechanism of the SC. Therefore, Cu-NQR studies on two near stoichiometric $Ce_{1+x}Cu_{2+y}Si_2$, close to magnetic criticality, were performed under hydrostatic pressures, and the results are presented in Chapter 3.

In $Ce_{0.99}Cu_{2.02}Si_2$, an anomalous ground state so-called A-phase sets in, dominated by critical magnetic fluctuations. By applying a small pressure which enhances the Kondo temperature, the magnetic A-phase with low frequency fluctuations changes into the SC phase without passing through a quantum critical point, while $T_c \sim 0.65$ K stays nearly constant up to 15 kbar. The transition from A- to SC phase is of a first-order type, and occurs close to the antiferromagnetic (AF) instability. However, it is suggested that the energy difference between these states may be very small and/or degenerate, since any hysteresis behavior in the A-phase development can not be seen at all by the cooling process. We propose that low-energy spin-fluctuations observed in the magnetic A-phase may be regarded as an intermediate state between the static magnetic order and SC.

In $Ce_{0.975}Cu_2Si_2$ which undergoes a static magnetic order at ambient pressure below $T_N \sim 0.6$ K, no SC has been induced up to 19.4 kbar. It is considered that the pressure-induced SC is sensitive to the sample quality.

In Chapter 4, we present Si-NMR studies of the HF antiferromagnets $CePd_2Si_2$ (T_N = 10 K) and $CeRh_2Si_2$ (T_N = 36 K) at ambient pressure, which undergo the pressure-induced superconducting transition. The NMR results in $CePd_2Si_2$ are consistent with those obtained from previous neutron-diffraction (ND) experiments.

In contrast, the NMR results in $CeRh_2Si_2$ are unconventional. Further splitting in the

NMR spectrum at $T_{N2} = 25$ K was found, indicating that two AF domains coexist with different wave vectors and saturation moments, M_{AF}. A remarkable finding is that the size in M_{AF}(NMR) obtained from NMR, 0.36 μ_B and 0.22 μ_B, are significantly smaller than M_{AF}(ND) from ND, 1.86 μ_B and 1.69 μ_B. This suggests that a correlation time in fluctuations of f-electron moments is longer than the characteristic time of observation for thermal neutrons but shorter than that for NMR. $CeRh_2Si_2$ is the first cerium-based HF compound exhibiting the probe dependent M_{AF} which was observed in uranium-based HF superconductors UPt_3 and URu_2Si_2 in the ordered state.

Chapter 5 describes Ru-NMR and NQR studies of $CeRu_2Si_2$ up to a magnetic field $H \sim 15.5$ T, which has revealed that the dramatic evolution in the HF state takes place through the pseudo-metamagnetic transition at $H_M \sim 7.7$ T. The HF state in $H < 3$ T is characterized by the $1/T_1T$ = constant relation below 8 K, whereas the $1/T_1T$ at H_M continues to increase upon cooling down to 1.4 K, suggesting a very low characteristic energy. As H increases above H_M, the value of $1/T_1T$ = constant being valid far below 8 K is successively reduced with much smaller values than that for $H < 3$ T. Appearance of the peak in $1/T_1T$ at higher T points to an unusual renormalization process for $4f$ electrons, in which a spin-polarized Fermi liquid state is formed. The novel crossover in the HF state takes place not only in the H variation but also in the T variation across the metamagnetic transition in $CeRu_2Si_2$. The H-T pseudo phase diagram was developed from the $1/T_1$ and other experimental results.

Table of Contents

Chapter 1

Introduction

1.1 General introduction and survey

It has been twenty years since a discovery of a class of intermetallic compounds, so-called heavy-fermion (HF) system [1]. These materials have represented one of the most intriguing type of ground states in condensed matter physics, and extensive studies have been carried out with special interests in order to elucidate underlying physical mechanisms.

1.1.1 Heavy-fermion system

These compounds, in general, contain cerium, ytterbium, or uranium, characterized by their unfilled f-shell. Their remarkable features appear in the low-temperature region. Common properties are enhanced electronic specific-heat coefficients, e.g., γ up to 1000 mJ/mol·K^2, and equally enhanced Pauli susceptibilities along with huge quadratic resistivity coefficients. It is basically accepted that these properties are understood in the framework of the Fermi liquid theory with strongly renormalized quasi-particles of large effective mass. In the high-temperature region, a conventional paramagnetic local-moment regime is valid.

These phenomena are discussed in connection with the Kondo effect, a compensation of local f moments below the Kondo temperature ($T_{\rm K}$) by an antiferromagnetic exchange interaction with conduction electrons, although the theory of the Kondo effect treats a single magnetic impurity in a non-magnetic metal. Obviously such a situation of a singular magnetic property is not realized in the HF systems, in which magnetic atoms are regularly situated on the crystal lattice. Disparities between the single Kondo impurity model and the real HF system appear below $T_{\rm K}$. In the HF system, localized f-electrons at high temperatures are delocalized via a hybridization with conduction electrons, forming a HF band of strongly correlated quasi-particles with a largely enhanced density of states at the Fermi energy.

In addition, the Rudermann-Kittel-Kasuya-Yosida (RKKY) interactions among local moments, which is mediated by conduction electrons, also develops with decreasing tem-

perature and competes with the Kondo effect. The competition makes the HF liquid state unstable and yields an extraordinary wide variety of possible ground states. These include a small number of paramagnets ($CeCu_6$, $CeRu_2Si_2$), small-moment antiferromagnets ($CePd_2Si_2$, $CeAl_3$, Ce_7Ni_3), several superconductors ($CeCu_2Si_2$, UPt_3), and Kondo insulators (SmB_6, CeNiSn) and so on.

1.1.2 Magnetic order in heavy-fermion system

Since these energy scales are quite small, most of these systems are largely sensitive to internal or external pressures, magnetic fields etc. Applying pressure is considered to enhance the hybridization between localized and conduction electrons and destroy a magnetic ordering. It is generally regarded as an outcome of the competition between the Kondo effect and the RKKY interaction, expressed by Doniach model [2]. The basic assumption of this model is that an exchange parameter between localized and conduction electrons, J, governs the strength of the Kondo effect and the RKKY interaction. With these two temperature scales the Doniach phase diagram can be derived and is schematically sketched in Fig. 1.1 (a). A similar phase diagram was reported by N. B. Brandt and V. V. Moshchalkov according to a classification of several real Kondo lattices [3] (see Fig. 1.1 (b)).

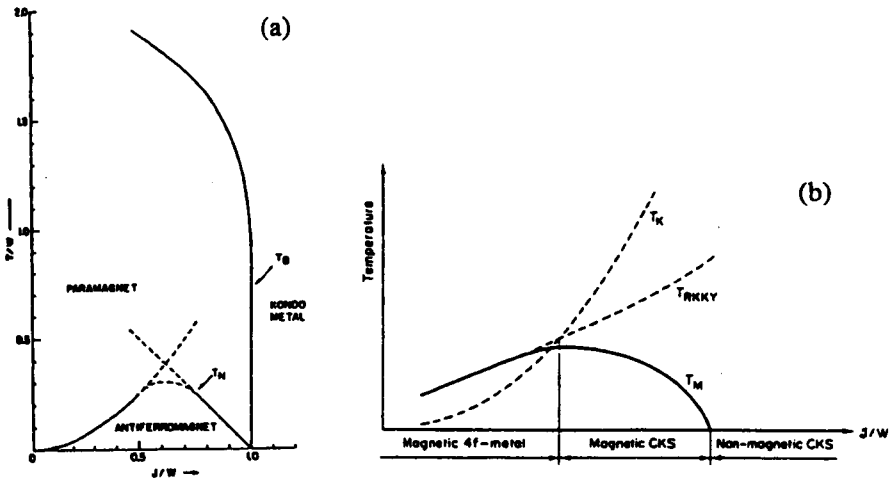

Figure 1.1 (a) Phase diagram for the one-dimensional "Kondo-necklace" model by S. Doniach [2] and (b) phase diagram according to a classification of a concentrated Kondo system (CKS) by N. B. Brandt and V. V. Moshchalkov [3].

As long as $k_B T_{RKKY}$ exceeds $k_B T_K$, the dominant RKKY interaction leads to a long-range magnetic order, which is consistent with a local moment picture. The magnetic ordering temperature is primarily determined by T_{RKKY}. As $k_B T_K$ is larger than $k_B T_{RKKY}$, the local moment description is no longer adequate. The magnetic ordering temperature decreases with increasing J and vanishes for sufficiently strong hybridization. The Fermi

liquid theory applies under such conditions.

Actually, some series of HF compounds follow qualitatively the above diagram. The rich variety of ground state in the Kondo lattice, CeT_2X_2, where T stands for transition metals and X = Si or Ge, was intensively investigated in terms of the hybridization [3, 4, 5, 6, 7]. Most of these materials have tetragonal $ThCr_2Si_2$ structure as shown in Fig. 1.4, and the ground-state property varies from conventional magnetism to Pauli paramagnetism through HF behavior including superconductors, antiferromagnets, and paramagnets. T. Endstra *et al.* demonstrated the magnetic ordering temperature with an effective hybridization strength, $J_{d\text{-}f}$ in the series as shown in Fig. 1.2. Here $J_{d\text{-}f}$ is estimated from the combination of Ce-T atomic distance and the number of d electrons. In the case of weak hybridization as $CeAu_2Si_2$ and $CeAg_2Si_2$, the magnetic ordering between stable f moments is observed, while compounds with strong hybridization show an intermediate valence state. HF compounds are found between these regions and have the most pronounced HF characteristics near a critical region where the magnetic ordering vanishes.

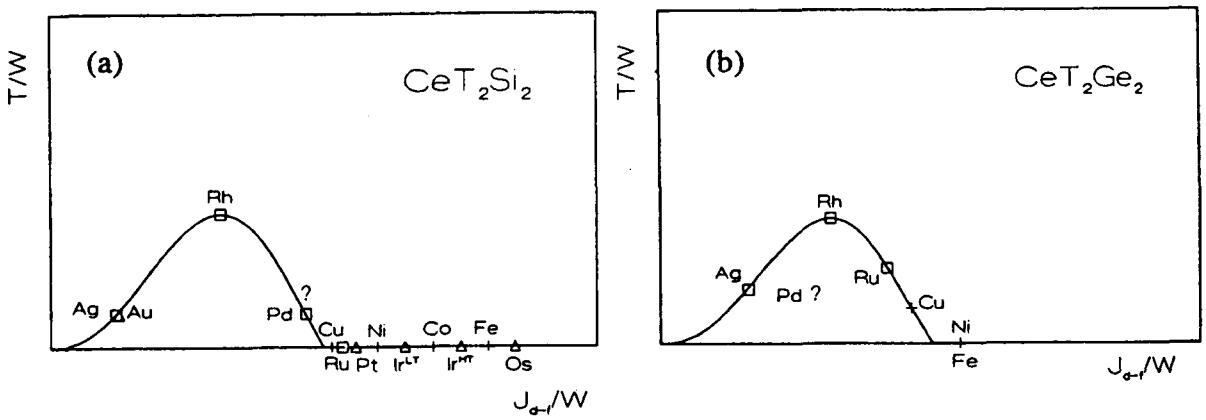

Figure 1.2 Schematic phase diagram for the Kondo lattice, with magnetic ordering temperatures of CeT_2X_2 compounds. Open crosses indicate $3d$ metals, open boxes are used for $4d$, and open triangles for $5d$ metals [4].

The typical non-magnetic HF compounds $CeRu_2Si_2$ and $CeCu_6$ are found at the non-magnetic side close to the magnetic-non-magnetic boundary in the phase diagram. Thermodynamics measurements indicate their large electronic specific-heat coefficients, $\gamma \sim$ 350 mJ/mol·K^2 in $CeRu_2Si_2$ and 1500 mJ/mol·K^2 in $CeCu_6$. A remarkable feature common to these two compounds is a pseudo-metamagnetic transition at 7.7 T in $CeRu_2Si_2$ [8] and 2 T in $CeCu_6$ at low temperature [9]. In $CeRu_2Si_2$ a rapid increase of a magnetization occurs without discontinuity. This crossover seems to be related to a collapse of the itinerant character of heavy quasi-particles by the external magnetic field. The study of the crossover behavior in $CeRu_2Si_2$ probed by Ru NMR and NQR will be presented in Chapter 5.

1.1.3 Heavy-fermion superconductivity

The study of HF superconductivity began with the discovery of superconductivity in $CeCu_2Si_2$ [10]. Since then the HF superconductivity was found in five uranium-based compounds at ambient pressures [11, 12, 13, 14, 15] and several rare-earth-based compounds at elevated pressures. Almost all HF superconductors show anomalous normal states and anisotropic natures in the superconducting state [16], indicating the new pairing state and pairing mechanism of superconductivity characterized by a proximity to a magnetic instability.

Up to now it has been established that the cerium-based HF superconductivity appears close to the magnetic instability. $CeCu_2Si_2$, showing superconductivity at ambient pressure, are considered to be located in the critical region where the magnetic order vanishes, since the magnetic order is induced by tiny amount of non-magnetic impurities such as Ge [17, 18, 19]. Correspondingly, HF antiferromagnet $CeCu_2Ge_2$, isostructural to $CeCu_2Si_2$, exhibits a pressure-induced superconducting transition by an application of pressure [20], which compensates the volume increase due to replacing Si by Ge. The phase diagram shows nearly identical pressure dependence if they are transposed so that $P = 0$ for $CeCu_2Si_2$ coincides with $P = 7.6$ GPa for $CeCu_2Ge_2$ (see Fig. 1.3) [21].

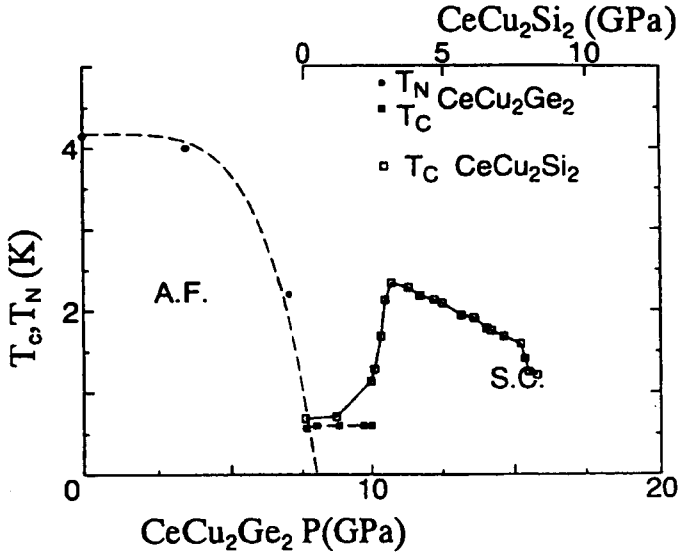

Figure 1.3 Combined phase diagram for superconductivity (SC) and antiferromagnetism (AF) in $CeCu_2Ge_2$ and $CeCu_2Si_2$ as a function of pressure [21]. Both enhancement of T_c and pressure-induced superconductivity were confirmed in $CeCu_{2.05}Si_2$ [22] and $CeCu_2Ge_2$ [20, 23, 24].

The pressure-induced superconductivity was also found in several HF antiferromagnets as $CeRh_2Si_2$ [25], $CePd_2Si_2$, $CeIn_3$ [26], $CeCu_2$ [27], and so on, although the existence of the superconducting transition strongly depends on the quality of sample. Thus the

superconductivity may occur quite generally around the critical pressure where some kind of antiferromagnetic order is suppressed, in samples of sufficiently high quality.

The superconductivity in $CePd_2Si_2$ occurs near the critical pressure, $\sim$ 27 kbar, from an anomalous normal state which has a quasi-linear temperature variation over two orders of magnitude in resistivity [28]. This non-Fermi liquid form of $\rho(T)$ extends down to the onset of superconductivity. Quite recently, the superconductivity has also been observed in $CeNi_2Ge_2$ at ambient pressure [29, 30], which has the same lattice and electronic structures as $CePd_2Si_2$. A pronounced non-Fermi liquid behavior in thermodynamic and transport properties is found in a high-quality $CeNi_2Ge_2$. There seems to be a relation between the superconductivity and the non-Fermi liquid behavior, which reminds us of one observed in some high-T_c cuprate superconductors.

1.1.4 Outline

This thesis treats several HF compounds with different ground state, $CeCu_2Si_2$, $CePd_2Si_2$, $CeRh_2Si_2$ and $CeRu_2Si_2$, which all crystallize tetragonal $ThCr_2Si_2$-type structure as shown in Fig. 1.4. These samples can be divided into three groups by their ground state.

(i) In $CeCu_2Si_2$, the HF superconductor, we have investigated magnetic properties at the crossover region from magnetic to superconducting phases and some interplay between them. In this study Cu-NQR experiments under hydrostatic pressures were carried out on nominally off-stoichimetoric $Ce_{1+x}Cu_{2+y}Si_2$. (ii) HF antiferromagnets $CePd_2Si_2$ and $CeRh_2Si_2$ are considered to be located near the magnetic to nonmagnetic phase boundary, since these magnetic orders are easily suppressed by the application of small pressure. In order to investigate the magnetic and electronic properties in the vicinity of the boundary, we have performed Si-NMR experiments at ambient pressures. (iii) The typical nonmagnetic HF compound $CeRu_2Si_2$ shows the pseudo-metamagnetic transition at $H_M \sim$ 7.7 T. The crossover behavior of HF state was studied by Ru NMR and NQR in the magnetic field from 0 to 15.5 T across H_M.

Before further descriptions on each sample, we introduce concepts of NMR technique briefly in following section and describe experimental arrangements and procedures in next chapter.

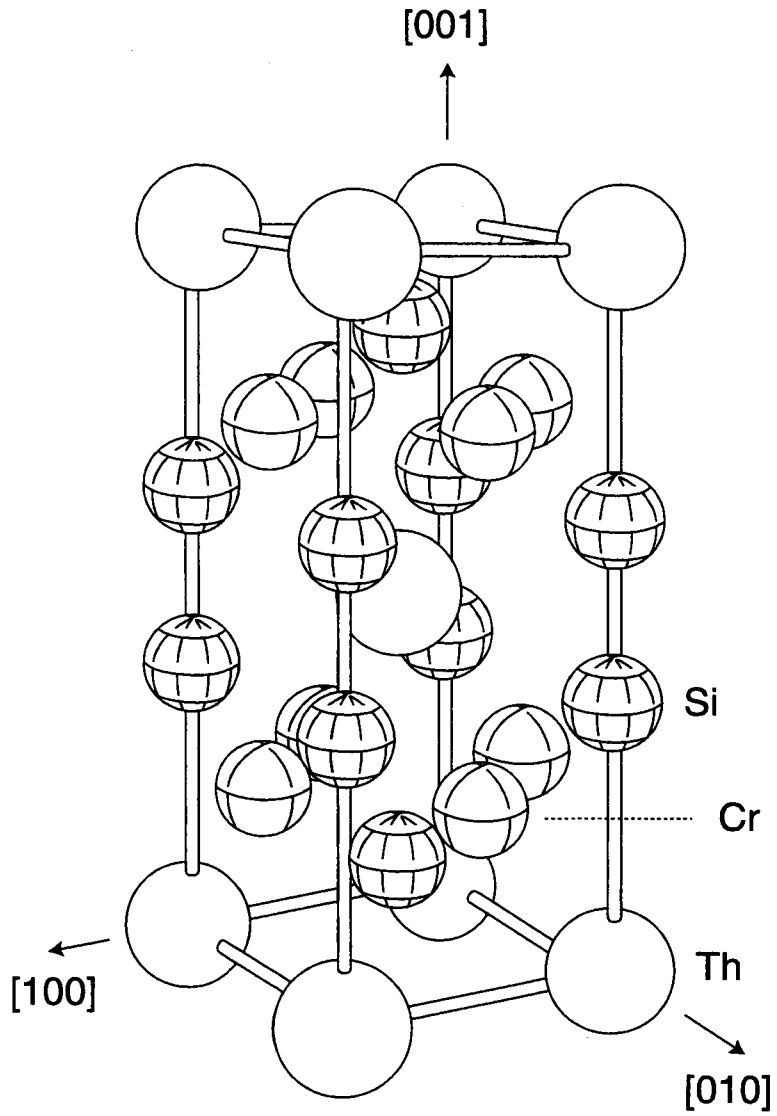

Figure 1.4 Tetragonal $ThCr_2Si_2$-type structure. The Th atoms are on the corners and at the center of the tetragonal unit cell, and the Cr atoms are on the cell faces.

1.2 NMR in heavy-fermion system

Nuclear magnetic resonance (NMR) has made a great contribution to understandings of HF compounds. This experimental technique probes the local environment of one particular nucleus and the wave-vector average of a dynamical response function with a small energy transfer. In this section we describe the experimental aspects of NMR. For more detailed descriptions on NMR, we refer to standard textbooks [31, 32].

1.2.1 Static hyperfine interaction

Most NMR experiments in HF systems have been carried out for nuclei of non-lanthanide constituents except a small number of Yb and U compounds such as $YbAl_2$ [33] and UO_2 [34]. Since the lanthanide carrying f electrons is considered to play a central role in determining the magnetic nature, we usually discuss the electronic state of f electrons through the hyperfine interaction between non-lanthanide nuclei and f electrons.

Magnetic hyperfine interactions originate in several processes; (i) the Fermi contact interaction due to s electrons, (ii) the spin-dipolar interaction due to only unpaired non s-electrons, (iii) the orbital interaction due to the orbital current of non s-electrons and (iv) the indirect interaction due to core polarization effect where closed inner s-electrons are polarized by unpaired non s-electrons through exchange polarization effects.

These hyperfine interactions cause a magnetic field at the nuclear position to deviate from an external one H_0. The additional field causes a energy shift and then the resonance condition and Knight shift. The Knight shift is expressed as the fractional displacement of the frequency in the fixed field H_0 from its value in a nonmetallic, nonmagnetic environment, ω_0,

$$K = \frac{\omega_{\rm res} - \omega_0}{\omega_0}, \tag{1.1}$$

where $\omega_{\rm res}$ is the resonance frequency. The Knight shift consists of the spin part $K_{\rm s}$ and the orbital (Van Vleck) part $K_{\rm orb}$, which are connected to the spin susceptibility, $\chi_{\rm s}$ and the Van Vleck orbital susceptibility, $\chi_{\rm VV}$, respectively.

$$K = K_{\rm s} + K_{\rm VV}, \tag{1.2}$$

where, $K_{\rm s}$ and $K_{\rm VV}$ are the spin and Van Vleck parts of Knight shifts, respectively. One can extract the hyperfine coupling constant by plotting the Knight shift vs the susceptibility with temperature as an implicit parameter.

In HF systems like Ce and U compounds, the spin-orbit interaction is so strong that the electronic state of an ion is characterized by the total angular momentum as $\vec{J} = \vec{L} + \vec{S}$ and the magnetic moment $-g_J\mu_{\rm B}\vec{J}$. The lowest $\vec{J}$ manifold is furthermore split into several sublevels by the crystal electric field. In this case, we should pay attention that the temperature dependence of both K and χ is arising from fictitious spin $\vec{J}$, *i.e.*, not only $\vec{S}$ but also $\vec{L}$.

The nucleus with $I \geq 1$ has an aspherical charge distribution and therefore an electric quadrupole moment. The electric quadrupolar interaction between electrons and nucleus splits the nuclear spin levels into several degenerate doublets. The transition between them causes a resonant absorption of radio-frequency, the nuclear quadrupole resonance (NQR). The NQR experiment is particularly advantageous in investigation low energy excitations in the superconducting state at zero magnetic field.

1.2.2 Dynamic hyperfine interaction

While the Knight shift is the measure of the time average value of the hyperfine field, the relaxation time T_1 is the measure of fluctuating components of the hyperfine field. The nuclear spin-lattice relaxation rate, $1/T_1$ probes the q-averaged imaginary part of the dynamical susceptibility, expressed as

$$\frac{1}{T_1} = \frac{2\gamma_n^2 k_B T}{(\gamma_e \hbar)^2} \sum_q A_q A_{-q} \frac{\chi''_\perp(q, \omega_0)}{\omega_0}, \tag{1.3}$$

where A_q is the hyperfine coupling constant between the nuclear spin and the q component of the electron spin density [35].

Local moment system

In the case of localized f electrons, we neglect any q dependences under the most naive assumption. In this case eq. (1.3) can be replaced by

$$\frac{1}{T_1} \propto \frac{k_B T}{\omega_0} \chi''(\omega_0). \tag{1.4}$$

Furthermore we assume the dynamic susceptibility as

$$\chi''(\omega) = \chi_0 \cdot \frac{\omega \Gamma}{\omega^2 + \Gamma^2}, \tag{1.5}$$

where Γ is a magnetic relaxation rate and χ_0 is a static susceptibility. Taking into account that the nuclear Larmor frequency $\omega_0 \ll \Gamma$, we can write

$$\frac{1}{T_1} \propto k_B T \cdot \frac{\chi_0}{\Gamma}. \tag{1.6}$$

In this case, χ_0 is a static susceptibility of a Curie-Weiss type. Γ consists of two processes, i.e., the spin exchange interaction with conduction electrons and that among local moments. The former exhibits a linear temperature dependence, whereas the latter is independent of temperature. Since spin correlation among local moments can be ignored at high temperature, $1/T_1$ decreases as upon heating. In the temperature range where the RKKY interaction can not be ignored, the latter mechanism leads to the temperature-independent $1/T_1$ [36].

Itinerant electron system

For itinerant electrons at low temperatures, we have the universal relation of

$$\frac{1}{T_1} = \frac{\pi}{\hbar} A^2 N(E_F)^2 k_B T, \tag{1.7}$$

where $A^2 = \gamma_n^2 \hbar^2 \langle A_q A_{-q} \rangle$, $N(E_F)$ is the renormalized density of states at Fermi energy [37]. We often call the constant behavior of $1/T_1T$ as the Korringa law for convenience. The characteristic temperature, below which the constant behavior of $1/T_1T$ is valid, is sometimes called the coherence temperature.

In NMR measurement we can observe the crossover from the localized to itinerant f electrons in HF systems upon cooling as shown in Fig. 1.5.

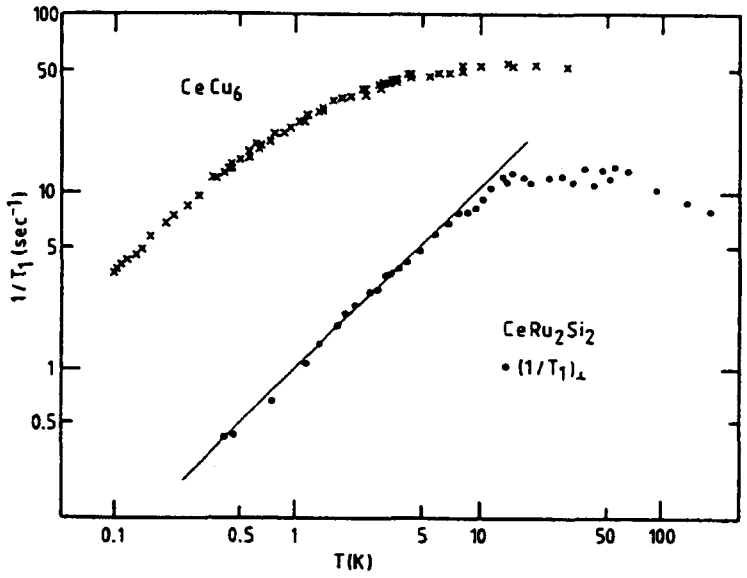

Figure 1.5 Temperature variations of $^{63}(1/T_1)$ in $CeCu_6$ (crosses) and $^{29}(1/T_1)$ in $CeRu_2Si_2$ (closed circles) [38]. The solid line represents the relation of $1/T_1T$ = constant.

References

[1] See *e.g.*, Z. Fisk, D. W. Hess, C. J. Pethick, D. Pines, J. L. Smith, J. D. Thompson, and J. O. Willis, Science **239**, 33 (1988).

[2] S. Doniach, Physica **91B**, 231 (1997); *Valence Instabilities and Related Narrow-Band Phenomena*, edited by R. D. Parks, Plenum, New York, p. 169, 1977.

[3] N. B. Brandt and V. V. Moshchalkov, Adv. Phys. **33**, 373 (1984).

[4] T. Endstra, G. J. Nieuwenhuys, and J. A. Mydosh, Phys. Rev. B **48**, 9595 (1993).

[5] B. H. Grier, J. M. Lawrence, S. Horn, and J. D. Thompson, J. Phys. C: Solid State Phys. **21**, 1099 (1988).

[6] A. Severing, E. Holland-Moritz, B. D. Rainford, S. R. Culverhouse, and B. Frick, Phys. Rev. B **39**, 2557 (1989).

[7] A. Loidl, K. Knorr, G. Knopp, A. Krimmel, R. Caspary, A. Böhm, G. Sparn, C. Geibel, and A. P. Murani, Phys. Rev. B **46**, 9341 (1992).

[8] P. Haen, J. Flouquet, P. Lapierre, P. Lejay, and G. Remenyi, J. Low. Temp. Phys. **67**, 391 (1987).

[9] A. de Visser, J. J. M. Franse, and J. Flouquet, Physica **B161**, 324 (1989).

[10] F. Steglich, J. Aarts, C. D. Bredl, W. Lieke, D. Meschede, W. Franz, and H. Schafer, Phys. Rev. Lett. **43**, 1892 (1979).

[11] G. R. Stewart, Rev. Mod. Phys. **56**, 755 (1984).

[12] H. R. Ott, H. Rudiger, Z. Fisk, and J. L. Smith, Phys. Rev. Lett. **52**, 679 (1984).

[13] M. B. Maple, J. W. Chen, Y. Dalichanouch, T. Kohara, C. Rossel, M. S. Torikachvili, M. W. McElfresh, and J. D. Thompson, Phys. Rev. Lett. **56**, 185 (1986).

[14] C. Geibel, S. Thies, D. Kaczorowski, A. Mehner, A. Grauel, B. Seidel, R. Hefrich, K. Petersen, C. D. Bedl, and F. Steglich, Z Phys. **B83**, 305 (1991).

[15] C. Geibel, C. Schank, S. Thies, H. Kitazawa, C. D. Bedl, A. Bohm, M. Rau, A. Grauel, R. Caspary, R. Helfrich, U. Ahlheim, G. Weber, and F. Steglich, Z Phys. **B84**, 1 (1991).

[16] See *e.g.*, R. H. Heffner, and M. R. Norman, Comments Condens. Matter Phys. (UK), vol.17, no.6, 361-408, 1996.

[17] G. Knebel, C. Eggert, D. Engelmann, R. Viana, A. Krimmel, M. Dressel, and A. Loidl, Phys. Rev. B **53**, 11586 (1996).

[18] O. Trovarelli, M. Weiden, R. Müller-Reisener, M. Gómez-Berisso, P. Gegenwart, M. Deppe, C. Geibel, J. G. Sereni, and F. Steglich, Phys. Rev. B **56**, 678 (1997).

[19] K. Ishida *et al.*, in preparation.

[20] D. Jaccard, K. Behnia, and J. Sierro, Phys. Rev. Lett. A **163**, 475 (1992).

[21] Y. Kitaoka, H. Tou, G. -q. Zheng, K. Ishida, K. Asayama, T. C. Kobayashi, A. Kohda, N. Takashita, K. Amaya, C. Geibel, C. Schank, and F. Steglich, Physica **B206-207**, 55 (1995).

[22] F. Thomas, J. Thomasson, C. Ayache, C. Geibel, and F. Steglich, Physica **B186-188**, 303 (1993).

[23] D. Jaccard, P. Link, E. Vargoz, and K. Alami-Yadri, Rev. High Pressure Sci. Technol. **7**, (1998); D. Jaccard, H. Wilhelm, K. Alami-Yadri, and E. Vargoz, Physica B **259-261**, 1 (1999).

[24] T. C. Kobayashi, T. Miyazu, N. Takeshita, K. Shimizu, K. Amaya, Y. Kitaoka, and Y. Ōnuki, J. Phys. Soc. Jpn. **67**, 996, (1998).

[25] R. Movshovich, T. Graf, D. Mandrus, J. D. Thompson, J. L. Smith, and Z. Fisk, Phys. Rev. B **53**, 8241 (1996).

[26] N. D. Mathur, F. M. Grosche, S. R. Julian, I. R. Walker, D. M. Freye, R. K. W. Haselwimmer, and G. G. Lonzarich, Nature **394**, 39 (1998).

[27] E. Vargoz, P. Link, and D. Jaccard, Physica B **230**, 182 (1997).

[28] F. M. Grosche, S. R. Julian, N. D. Mathur, F. V. Carter, and G. G. Lonzarich, Physica B **237-238**, 197 (1997).

[29] F. M. Grosche, P. Agarwal, S. R. Julian, N. J. Wilson, R. K. W. Haselwimmer, S. J. S. Lister, N. D. Mathur, F. V. Carter, S. S. Saxena, and G. G. Lonzarich, cond-mat/9812133.

[30] P. Gegenwart, F. Kromer, M. Lang, G. Sparn, C. Geibel, and F. Steglich, Phys. Rev. Lett. **82**, 1293 (1999).

[31] A. Abragam, *the Principles of Nuclear Magnetism*, Oxford Press, London, 1961; C. P. Slichter, *Principles of Magnetic Resonance*, Springer Series in Solid State Science, New York, 1990.

[32] G. C. Carter, L. H. Bennet, and D. J. Kahan, *Metallic Shifts in NMR*, eds. by B. Chalmers, J. W. Christian, and T. B. Massalski, Pergamon Press, Oxford, New York, Toront, Sydney, Paris, Frankfurt, vol. 20.

[33] T. Shimizu, M. Takigawa, H. Yasuoka, and J. H. Wernick, J. Magn. Magn. Mat. **52**, 187 (1985).

[34] K. Ikushima, H. Yasuoka, S. Tsutsui, M. Saeki, S. Nasu, and M. Date, J. Phys. Soc. Jpn, **67**, 69 (1998).

[35] T. Moriya, J. Phys. Soc. Jpn. **18**, 516, (1963).

[36] T. Moriya, Prog. Theort. Phys. (Kyoto), **16**, 23 (1956), **16**, 641 (1956).

[37] J. Korringa, Physica **16**, 601 (1950).

[38] Nuclear Magnetic Resonance in Heavy Fermion systems: Theoretical and Experimental Aspects of Valence Fluctuations and Heavy Fermions, eds. L. C. Gupta and S. K. Malik (Plenum, 1987) 297, Y. Kitaoka, K. Ueda, T. Kohara, Y. Kohori, and K. Asayama.

Chapter 2

Experiments

The experiments described in this chapter involve NMR and NQR measurements at temperatures range from 0.012 K to 300 K, at magnetic fields up to 16 tesla and at pressures up to 26 kbar.

In the NMR/NQR experiments on $CePd_2Si_2$, $CeRh_2Si_2$ and $CeRu_2Si_2$, we used three metal ^{4}He cryostats with the superconducting magnets (7 T, 12 T and 16 T) and a glass dewar with an electromagnet (1.7 T), while the dilution refrigerator (System I) was carried out for measurements of $CeRu_2Si_2$ below 1 K. The experiments on $Ce_{1+x}Cu_{2+y}Si_2$ system at ambient pressures were performed with the dilution refrigerator (System III), after initial measurements above 1.4 K in the glass dewar. High pressure measurements were done in a piston-and-cylinder clamp cell, immersed directly in the metal cryostat above 1.4 K and amounted to the bottom of the mixing chamber of the dilution refrigerator (System II) to cool down below 0.1 K.

The overview of the experimental procedures is presented in following sections.

2.1 Low temperatures and magnetic fields

2.1.1 Low temperatures

The glass ^{4}He dewar has been suspended into the glass nitrogen dewar. Temperatures above 4.2 K are kept by controlling a heating and the flow of liquid helium as the source of the required cooling power. Temperatures below 4 K are achieved by pumping on the ^{4}He bath. They are connected to manifold rotary pumps, which give the base temperature of 1.35 K. These temperatures are monitored by Pt thin-film thermometers (Tama Electric Co. Ltd.) above 30 K, carbon glass and Cernox thermometers (Lakeshore) below the temperature.

For the experiments at lower temperatures we used three ^{3}He-^{4}He dilution refrigerators. A dilution system offers very low temperature and high cooling power on a long time-scale, which is suitable for NMR measurements.

System I ; the high field dilution refrigerator (9 T) designed by Oxford Instruments reaches temperature down to 12 mK, the lowest temperature we can attain in our group up to now. The rough sketches of the refrigerator and the mixing chamber are shown in Fig. 2.1. System II ; the old dilution refrigerator made by Oxford Instruments early 1980's was modified for the pressure measurements. The base temperature is about 65 mK with sufficient cooling power, $\sim 150\ \mu$W at 0.1 K. System III ; the compact dilution refrigerator was recently developed [1] and designed by SANN to fit in the variable temperature insert of the superconducting magnets. We can attain the temperature down to 85 mK under high magnetic field by this refrigerator.

These temperatures are measured by RuO_2 and carbon resistor thermometers. They were calibrated by the measurements of nuclear spin-lattice relaxation time, T_1 in Pt of Johnson-Matthey product with the relation $T_1T = 30 \times 10^{-3}$ sec·K in advance.

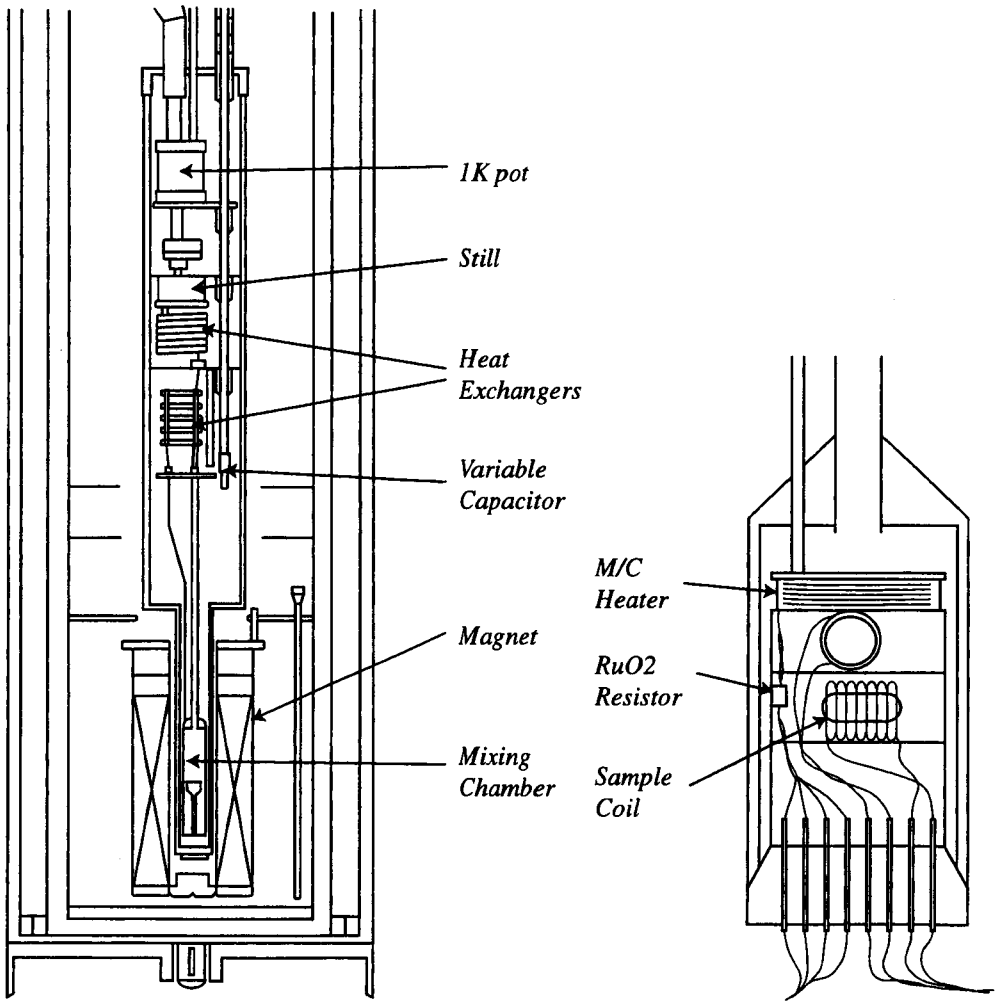

Figure 2.1 (Left) ^{3}He-^{4}He dilution refrigerator with the superconducting magnet. (Right) Mixing chamber in the dilution refrigerator.

2.1.2 Magnetic fields

For the low-field measurements the usual Helmholtz type of electromagnet was used to generate magnetic fields up to 1.7 T. The high-field measurements were performed in the cryostats with the solenoid type superconducting magnets made by Oxford Instruments (see Fig. 2.2). Inhomogeneity of the magnetic field at the center of the superconducting magnet is less than 10^{-5}, which guarantees the precise Knight shift measurement.

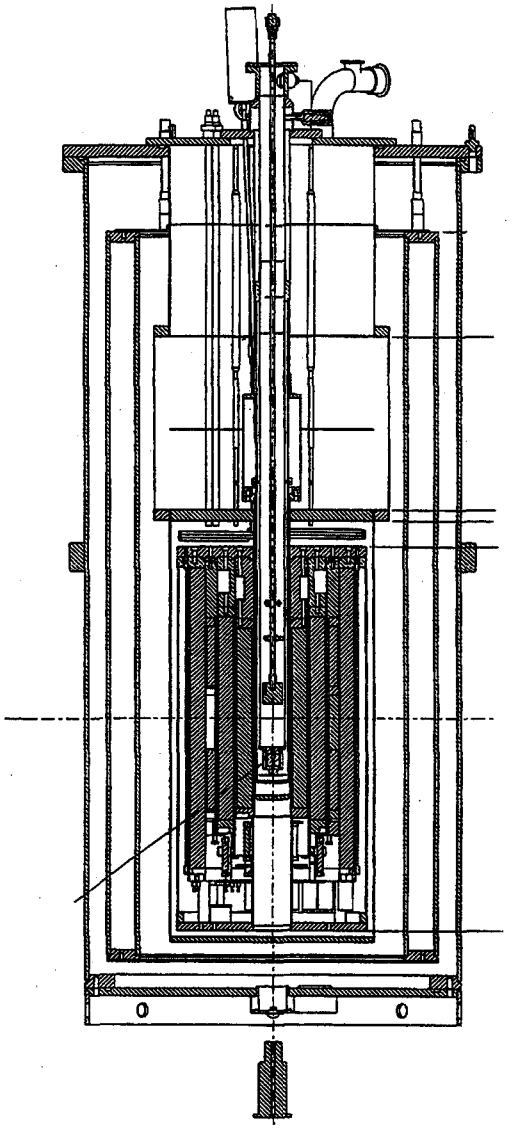

Figure 2.2 Cryostat for high field NMR experiments with the solenoid type superconducting magnet.

2.2 High pressures

2.2.1 Design

The high pressure measurements were performed in a piston-cylinder self clamping pressure cell. The main advantage of this type of design is the relatively large sample volume. A hydrostatic pressure environment is created by compressing a pressure-transmitting medium inside a cylinder by pistons on either side. In this study we used a mixture of Fluorinert FC70 and FC77 as the pressure-transmitting medium. The liquid is contained with in a Teflon cap, which fits tightly to the cylinder. A sketch of the pressure cell and the Teflon cap with adjunctive parts for the pressure range $P < 20$ kbar are shown in Fig. 2.3. The body of the pressure cell was constructed from hardened beryllium-copper alloy. We employed a kind of ceramic as a material of a piston for NMR studies by taking advantage of its hardness and nonmagnetism. At room temperature, force was applied by a conventional press and then clamped in by tightening a beryllium-copper bolt against the piston.

2.2.2 Pressure measurement

The pressure can be measured both at room temperature and below 4 K. At room temperature the resistivity of manganin wire is known to depend strongly and reproducibly on pressure, at low temperatures the shift in the superconducting transition temperature of tin is used for a pressure gauge [2].

The resistivity of manganin wire is measured by a four-terminal probe method. The pressure dependence in T_c of tin can be determined by ac susceptibility measurement which can be obtained by variation of the ac impedance of the in-situ NQR coil containing small amount of tin. If one describes the inductance as

$$L = L_0(1 + 4\pi f_0 \chi), \tag{2.1}$$

where L_0 is the inductance of the empty coil and f_0 is the filling factor of the coil, then a change in the susceptibility, χ, causes a proportional change in ΔL in the inductance of the coil. A frequency counter device measures the resonance frequency f of the circuit containing a coil (L) and a capacity (C), where

$$2\pi f = 1/\sqrt{LC}. \tag{2.2}$$

It is known that the frequency begins to increase due to the Meissner effect at the temperature where the value of electrical resistivity becomes zero upon cooling [3].

Fig. 2.4 shows the temperature dependence of the resonance frequency in the circuit with the NQR coil containing sample and tin. T_c of tin under pressure could be clearly determined, and the reduction of T_c by pressure, $\delta T_c = T_c(0) - T_c(P)$ was used to estimate pressure.

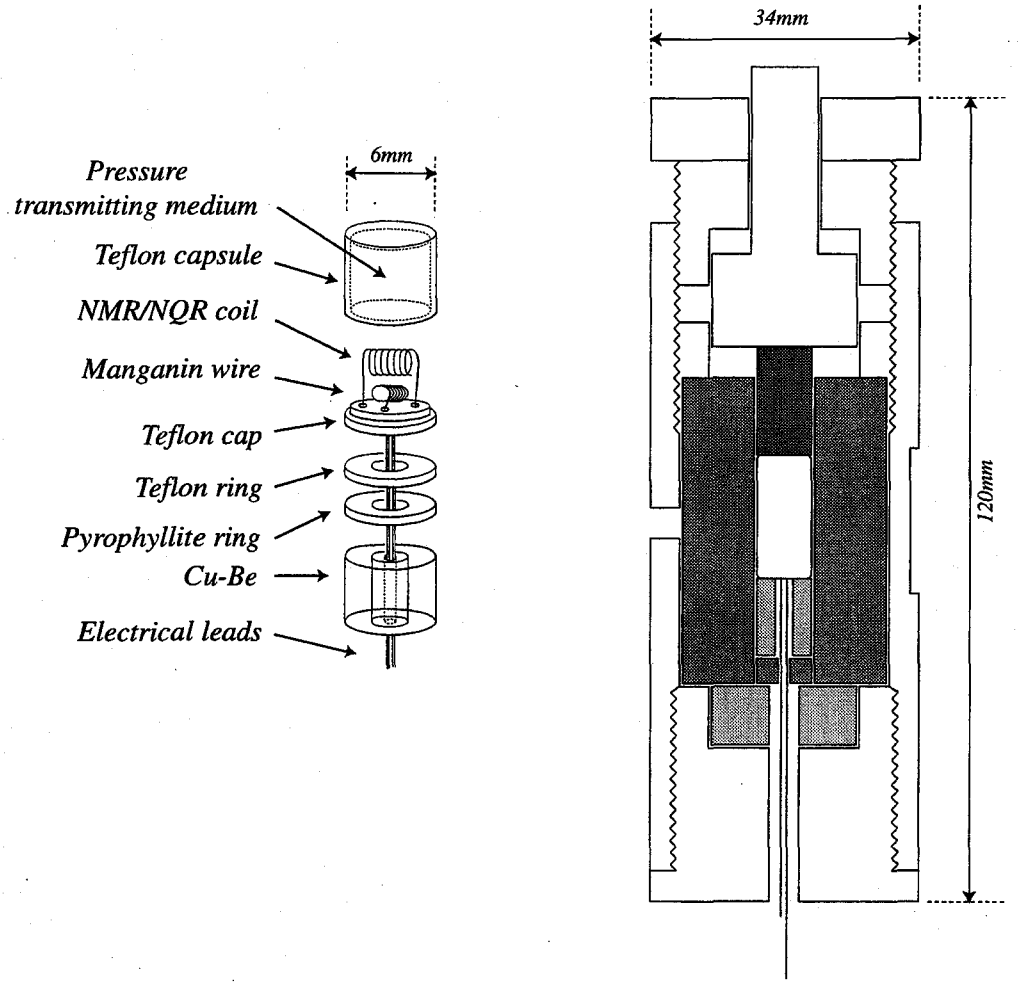

Figure 2.3 (Left) Sketch of the Teflon cell and adjunctive parts. (Right) Piston-cylinder, self-clamping pressure cell.

2.2.3 Cooling pressure cell

In order to cool down the pressure cell below 0.1 K, it was amounted to the bottom of the mixing chamber in the dilution refrigerator (System II) as shown in Fig. 2.5. To get good heat contact, the pressure cell and the mixing chamber were covered by a Cu shield. Three thermometers were attached to them as seen in Fig. 2.5 to monitor the temperature at respective points.

There is no thermometer inside the pressure cell, but only on the pressure cell. It is, therefore, important to know the thermal gradients between the thermometers and the inside of the pressure cell. Here we note that a rf pulse for NMR measurement induces heating effect due to a eddy current loss. Our preliminary measurements at ambient pressure revealed that the temperature difference between outside and inside the pressure cell was less than 10 mK at 100 mK even in exciting rf pulse on practical condition as

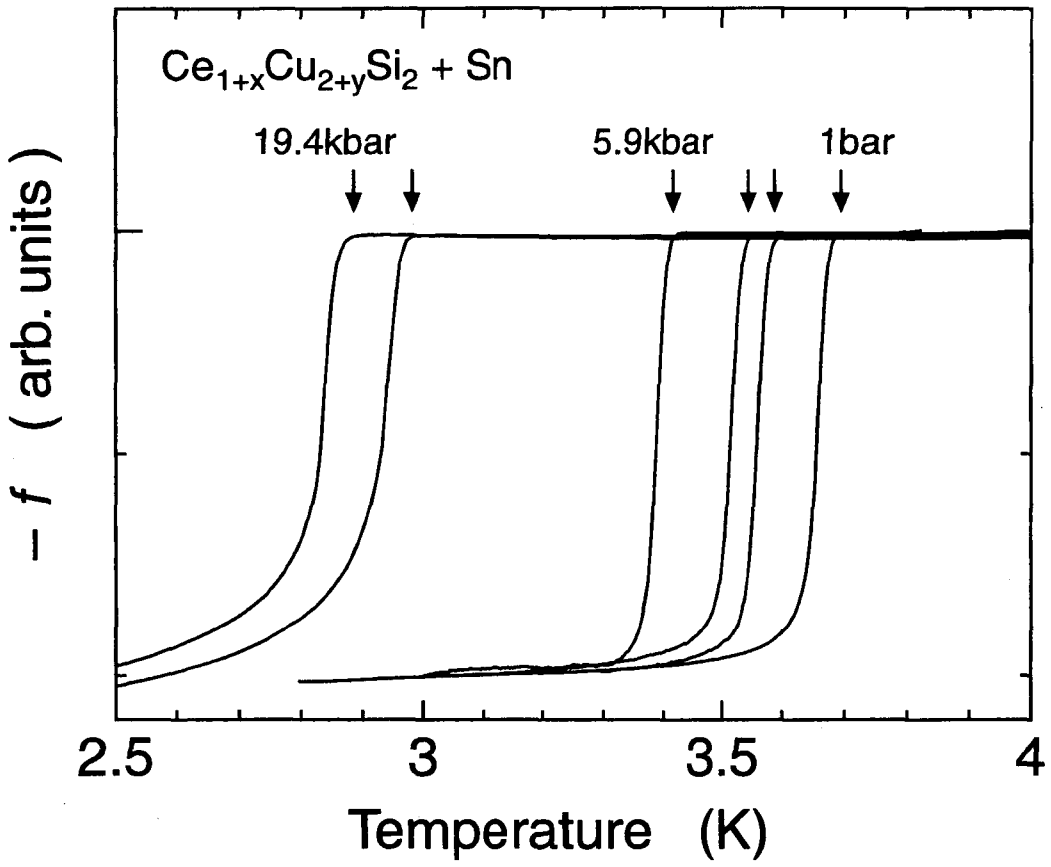

Figure 2.4 Temperature dependence of the inductance change of the NQR coil containing sample and tin under various pressures.

described in the following.

We measured nuclear spin-lattice relaxation rate, $1/T_1$ by ^{63}Cu NQR on $CeCu_6$ (ν_Q = 3.9 MHz) and $Ce_{0.975}Cu_2Si_2$ (ν_Q = 3.435 MHz) inside and outside the pressure cell, after waiting enough time so that a temperature stabilized over the pressure cell and the mixing chamber. Fig. 2.6 shows the temperature variations of $1/T_1$ in (a) $CeCu_6$ and (b) $Ce_{0.975}Cu_2Si_2$. Here closed and open circles indicate the results inside the pressure cell and outside the cell, respectively. We used the Fluorinert and a Si-based organic liquid as the pressure-transmitting medium in run 1 and run 2, respectively. The result on $CeCu_6$ outside the cell was obtained from Ref. [4]. Both sets of data are almost the same within the experimental error over the temperature range measured, indicating that the temperature gradient is negligible.

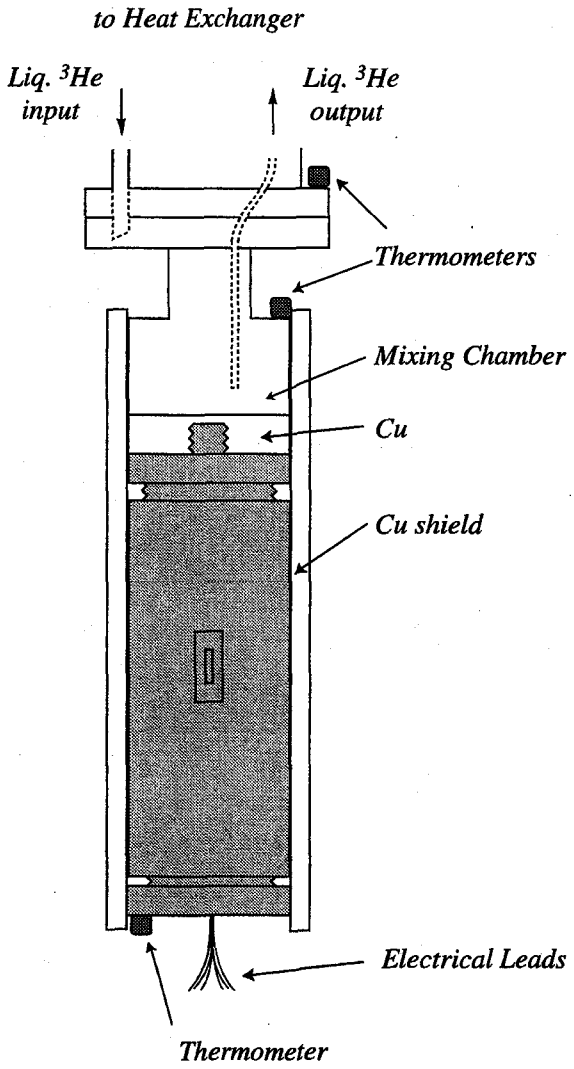

Figure 2.5 Sketch of the pressure cell connected to the mixing chamber.

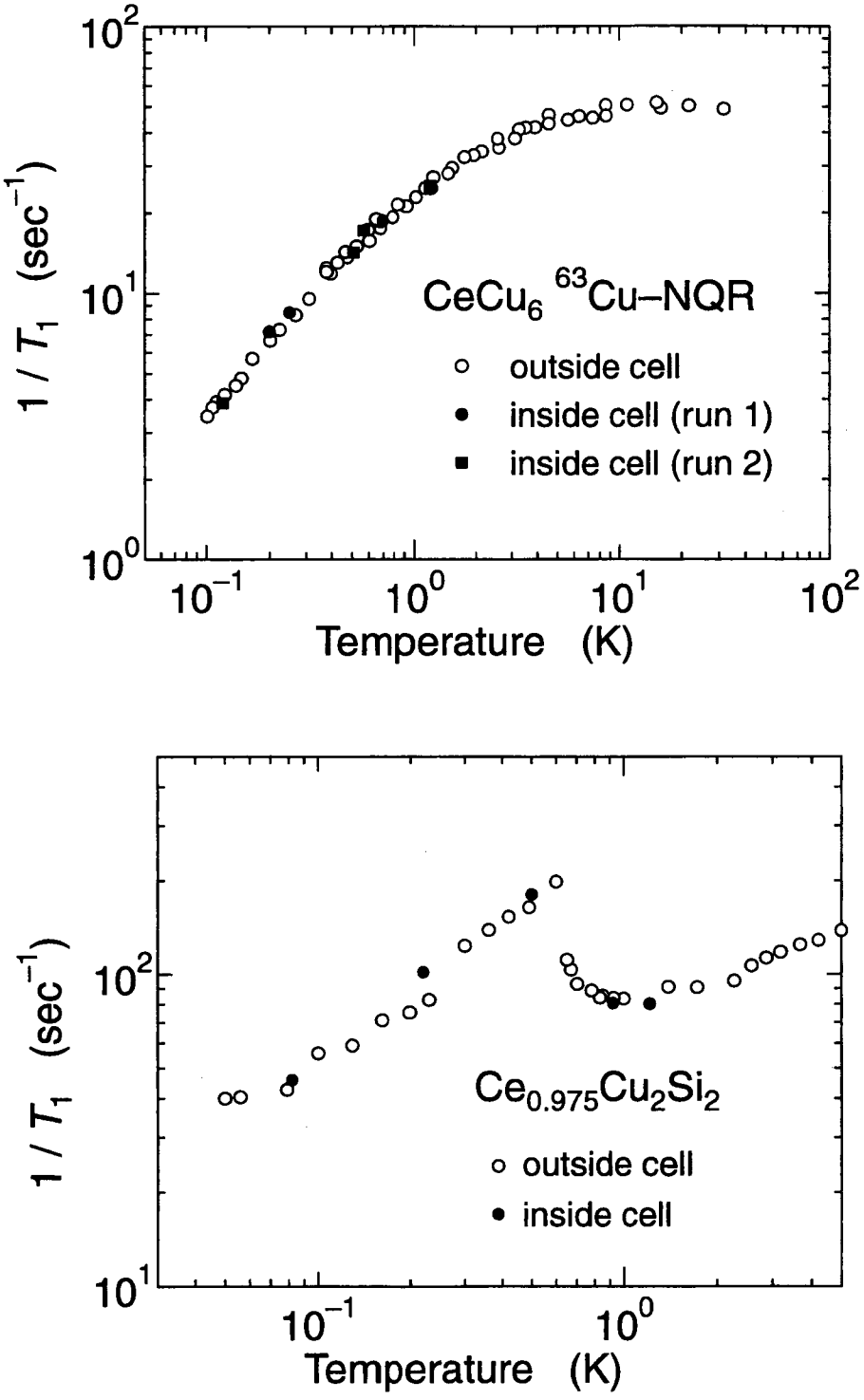

Figure 2.6 The temperature variations of $1/T_1$ in (a) $CeCu_6$ and (b) $Ce_{0.975}Cu_2Si_2$. Closed and open circles indicate the results inside the pressure cell and outside the cell, respectively. The data on $CeCu_6$ outside the cell was obtained from Ref. [4].

2.3 NMR spectrometer

The spin-echo NMR and NQR measurements were performed with a phase-coherent type laboratory-built spectrometer. The block diagram of the typical NMR spectrometer is shown in Fig. 2.7. We measured NMR spectrum by tracing the spin-echo intensity at fixed frequency as a function of external field. NQR spectrum was obtained by measuring the spin-echo intensity as a function of frequency or the Fourier transform (FT) technique of the spin-echo signals. Since the magnitude of the exciting rf field is about 50–150 Oe, the FT technique was utilized for the spectrum whose line width is narrower than 50 kHz. The nuclear spin-lattice relaxation time, T_1 was obtained from fitting the longitudinal nuclear magnetization recovery after saturating pulse to theoretical curves.

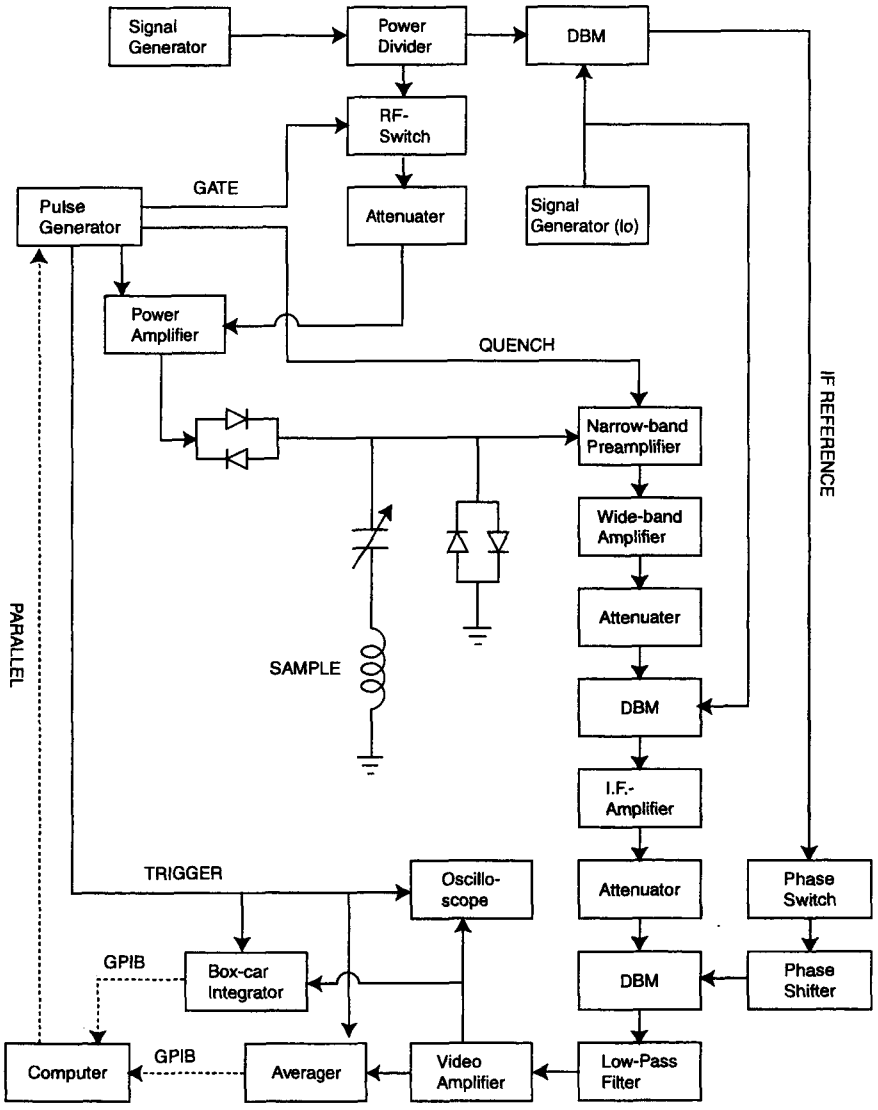

Figure 2.7 The block diagram of a phase-coherent pulsed spectrometer.

References

[1] S. Yoshida, S. Mori, T. Umeno, Y. Kamioka, M. Watanabe, and Y. Ootuka, the Proceedings of 16th International Cryogenic Engineering Conference / International Cryogenic Materials Conference and Industrial Exhibition 1996.

[2] See *e.g.*, M. I. Eremets, *High Pressure Experimental Methods*, Oxford University Press, Oxford, New York, Tokyo, 1996.

[3] T. Mito, Ph. D. Thesis, Osaka University, 1998.

[4] Nuclear Magnetic Resonance in Heavy Fermion systems: Theoretical and Experimental Aspects of Valence Fluctuations and Heavy Fermions, eds. L. C. Gupta and S. K. Malik (Plenum, 1987) 297, Y. Kitaoka, K. Ueda, T. Kohara, Y. Kohori, and K. Asayama.

Chapter 3

Magnetism and superconductivity in pressurized $Ce_{1+x}Cu_{2+y}Si_2$

3.1 Introduction

It has been established that in some cerium-based heavy-fermion (HF) compounds, superconducting phase is located close to a magnetic instability and might thus be related to new pairing state and pairing mechanism [1]. An intimate interplay between magnetism and superconductivity (SC) is to be resolved for a full understanding of possible mechanism of unconventional SC. In most of these compounds, the SC is attained by applying pressure to HF antiferromagnetic ground state, e.g. in $CeCu_2Ge_2$ [2], $CeRh_2Si_2$ [3], $CePd_2Si_2$, $CeIn_3$ [1], and so on. The underlying compound, $CeCu_2Si_2$, showing the SC at ambient pressure, itself has been considered to be located in the critical region between a static magnetic order (SMO) and the SC, since the superconducting phase is embedded in an unusual magnetic phase denoted as A-phase in the H-T phase diagram (see Fig. 3.1) [4], and the SMO is induced by tiny amount of non-magnetic impurities such as Ge [5, 6, 7].

The A-phase has unusual magnetic properties as probed first by NMR [8] and μSR [9, 10] measurements on high-quality polycrystals, and then by elastic and thermal expansion experiments on a high-quality single crystal [4]. On the basis of the NMR and NQR studies [8, 11, 12], it was suggested that the A-phase should be distinguished from the SMO but characterized by the magnetic fluctuations with low frequency comparable to NMR and NQR frequency, $\omega_N \sim 3$ MHz, since a spectral broadening associated with spontaneous magnetic moment has never been observed even at lowest temperature (T). This dynamical character of the A-phase is consistent with recent μSR experiments [13].

A series of polycrystalline $Ce_{1+x}Cu_{2+y}Si_2$ in the vicinity of stoichiometric composition together with a high-quality single crystal have been studied thoroughly by means of resistivity, specific heat, μSR, NQR, elastic constant and dilatation measurements [4, 12, 13, 14, 15, 16, 17]. It was found that both the A- and SC phases are extremely sensitive to sample preparation and that these two phases are nearly degenerate [4]. The A-phase was furthermore suggested to be expelled below T_c under zero field due to the onset of SC in

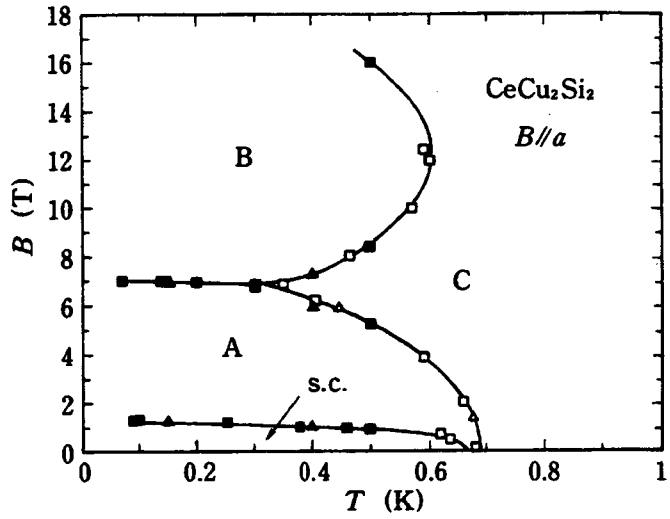

Figure 3.1 Magnetic field vs temperature phase diagram of $CeCu_2Si_2$. Superconducting to A-phase and A- to B-phase boundaries are determined from elastic constant, magnetostriction and thermal expansion anomalies [4].

both the high-quality single [4] and polycrystal samples [16]. Quite recently, macroscopic measurements have revealed that $CeCu_2Si_2$ is located in the vicinity of a quantum critical point [17].

From recent Cu-NQR study on the series of $Ce_{1+x}Cu_{2+y}Si_2$ at ambient pressure [12], it was suggested that the magnetic fluctuations in the A-phase may be referred to as the critical state between the SMO and the SC, since $Ce_{0.99}Cu_{2.02}Si_2$ (Ce0.99) located at the crossover point between $Ce_{0.975}Cu_2Si_2$ (Ce0.975) with SMO and $Ce_{1.025}Cu_2Si_2$ (Ce1.025) showing SC has the ground state dominated by this magnetic fluctuations down to lowest T. The study of the crossover from magnetism to superconductivity in $Ce_{1+x}Cu_{2+y}Si_2$ with varying the Ce-nominal content x is described in Section 3.3.

However, a disorder effect associated with a nominal Ce deficiency should be taken into account in this system, as well as the change of the strength of the hybridization between $4f$ and conduction electrons by the Ce-content, since the extent of the microscopic disorder is different in each compound, and the disorder effect tends to stabilize the SMO if the SMO-SC transition is of first order in a clean system [18]. It has been convinced that the best way to study how SMO evolves to SC, and whether or not there exists a quantum ($T \rightarrow 0$ K) phase transition between them is measurement under pressure. Hence, we have performed Cu-NQR studies under hydrostatic pressure on Ce0.99 dominated by the magnetic A-phase fluctuations and Ce0.975 showing the SMO. We present the results of the pressure effects on Ce0.99 and Ce0.975 in Section 3.4 and 3.5, respectively.

3.2 Sample and characterization

We used four samples with different Ce-nominal content; $Ce_{1.025}Cu_2Si_2$ (Ce1.025) with $T_c \sim 0.65$ K, $CeCu_{2.05}Si_2$ (Ce1.00) with $T_c \sim 0.7$ K, $Ce_{0.99}Cu_{2.02}Si_2$ (Ce0.99) with a minor part of SC, and non-superconducting $Ce_{0.975}Cu_2Si_2$ (Ce0.975) These characteristics are summarized in Table 3.1. These samples have been prepared at Institute für Festkorperohysik, Technishe Hochschule, Darmstadt. The detailed preparation and the characterization are reviewed in their report [13, 16].

The X-ray diffraction experiments indicate that the lattice parameters [$a = 4.4002(4)$ Å, $c = 9.919(1)$ Å at ambient T] are nearly the same in these samples [13, 19]. EPMA (electron probe microanalysis) results show that although there exist small amount of secondary phase $\sim 5\%$ in Ce1.025, $< 5\%$ in Ce1.00, and $< 3\%$ in Ce0.99, the main phase exhibits the ideal Ce:Cu:Si stoichiometry of 1:2:2, within which the inhomogeneity of the composition is $\leq 1\%$ [13].

Table 3.1 Compositions of the polycrystalline samples under investigation. ^{63}Cu-NQR linewidths (FWHM) for Ce1.00 and Ce0.99 are comparable to that for the single crystal [20], ensuring the high quality of these samples in a microscopic level. The small anomalies of the specific heat and the thermal expansion at T_c in Ce0.99 are indicative of its non-bulk nature in superconductivity.

Sample	Batch number	Type	FWHM (kHz)	T_c (K)
$Ce_{1.025}Cu_2Si_2$ (Ce1.025)	♯29004	S	26	0.65
$CeCu_{2.05}Si_2$ (Ce1.00)	♯30075	A/S	13	0.7
$Ce_{0.99}Cu_{2.02}Si_2$ (Ce0.99)	♯30031	A	14	(0.6)
$Ce_{0.975}Cu_2Si_2$ (Ce0.975)	♯29038	X	35	—

These samples are the same as used in the previous experiments of specific heat, thermal expansion [16], μSR [13], and NQR [21]. Ce1.00, Ce1.025 and Ce0.99 correspond to the samples number ♯1, ♯3 and ♯4 in Ref. [16] and [13], respectively. According to these results, Ce1.025 shows mainly superconducting and only minor A-phase signal (S-type). In Ce1.00, the A-phase starts to develop upon cooling below 1 K and is replaced by the SC phase below T_c (A/S-type). Ce0.99 presents mainly A-phase at the low T and a small diamagnetic signal (A-type). The absence of significant anomalies at T_c in the specific heat and the thermal expansion are indicative of its non-bulk nature in superconductivity. In addition to these samples, more Ce-deficient sample than Ce0.99, Ce0.975 is also investigated, which was reported to have more magnetic character than Ce0.99 (X-type) [16, 24].

These samples were moderately crashed into rough powder with a diameter larger than 100 μm in order to avoid some crystal distortion.

NQR spectrum

In Fig. 3.2 are shown ^{63}Cu-NQR spectra at 4.2 K in the series of $Ce_{1+x}Cu_{2+y}Si_2$. The NQR frequency $\nu_Q = \omega_N/2\pi$ ($\sim$ 3.435 MHz) is confirmed to be independent of the nominal composition. The full width at the half maximum (FWHM) in Ce0.99, $\sim$ 14 kHz, is comparable to those for a single crystal and $CeCu_{2.05}Si_2$ (Ce1.00), ensuring the high quality in a microscopic level [12, 21]. FWHM in Ce0.975 was 35 kHz much larger than that in Ce0.99, indicating that some crystal inhomogeneity is introduced by a slight Ce deficiency. The value of the FWHM in Ce0.975, however, is even smaller than $\sim$ 40 kHz and $\sim$ 150 kHz reported in Ref. [22] and [23], respectively.

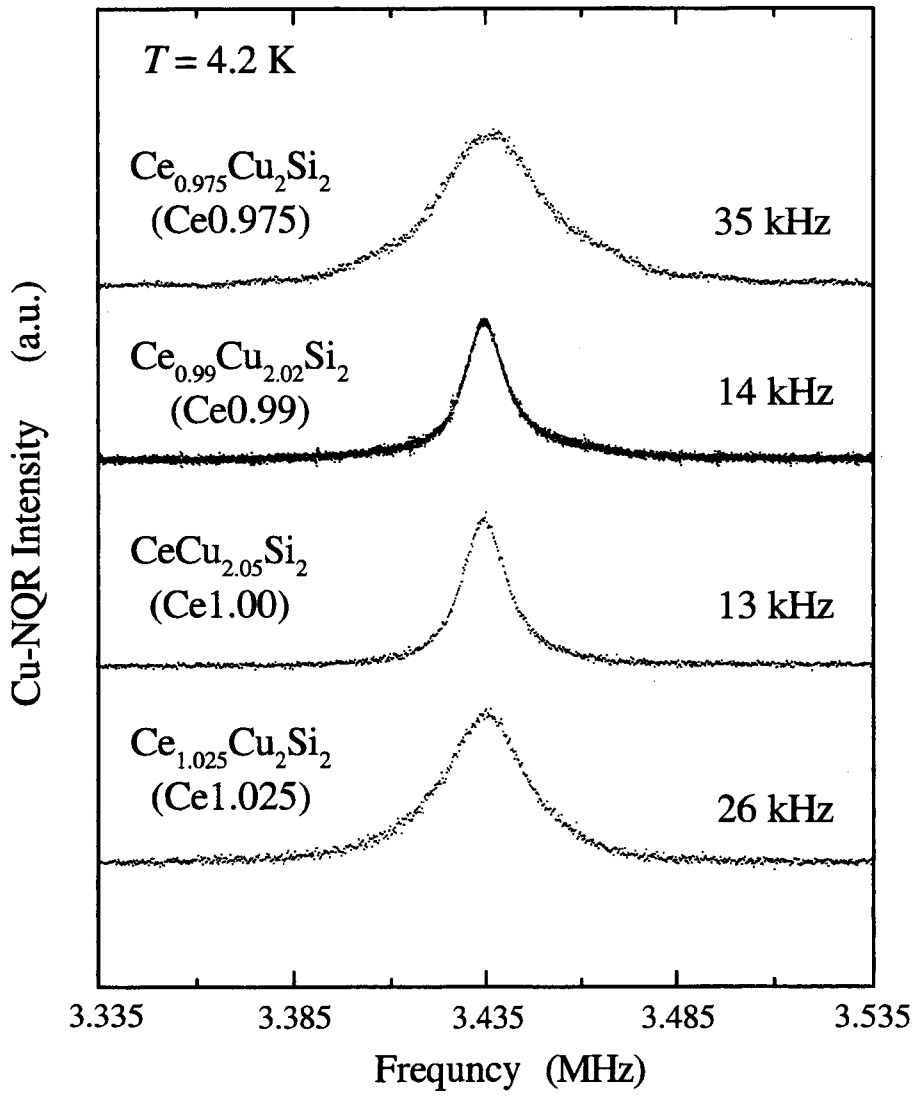

Figure 3.2 ^{63}Cu-NQR spectra in $Ce_{0.975}Cu_2Si_2$ (Ce0.975), $Ce_{0.99}Cu_{2.02}Si_2$ (Ce0.99), $CeCu_{2.02}Si_2$ (Ce1.00), and $Ce_{1.025}Cu_2Si_2$ (Ce1.025) at 4.2 K.

3.3 Cu-NQR study of $Ce_{1+x}Cu_{2+y}Si_2$ system at ambient pressure

3.3.1 Spin-echo intensity and NQR spectrum

Spin-echo intensity

The anomalies relevant to the A-phase were observed in the T-dependence of NQR intensities. Figure 3.3 displays the T dependence of NQR intensity (I) multiplied by T, $I \times T$ normalized by $I \times T$ at 4.2 K for all the samples. $I \times T$ decreases rapidly below T_c due to the SC diamagnetic shielding of rf field, whereas it is also clear that $I \times T$ starts to decrease below T_m far above T_c. Since $I(\tau)$ depends on a pulse interval (τ) between two pulses by means of the spin-echo method, $I(0)$ is evaluated through the relation of $I(\tau) = I(0)\exp(-2\tau/T_2)$ where $1/T_2$ is the spin-echo decay rate. T_m is estimated as 0.8 K, 1 K, 1.2 K and 1 K for Ce1.025, Ce1.00, Ce0.99 and Ce0.975, respectively.

The μSR measurements on the same samples detected the A-phase below T_m dominated by very slow magnetic fluctuations ($\sim$ 3 MHz) close to the NQR frequency and a coexistence with the paramagnetic region where frequencies of magnetic fluctuations remain over a higher frequency range [13]. The marked reduction in $I \times T$ without any spectral broadening is therefore due to the emergence of the A-phase. Note that the decrease in $I \times T$ upon cooling is ascribed to an extraordinary short T_1 and/or T_2 in the A-phase, which are estimated to be $\sim$ 0.14 μsec from the very slow fluctuations ($\sim$ 3 MHz).

The emergence of A-phase is also deduced from the specific measurements. The gradual increase of C/T in the specific heat [16] upon cooling to T_c for Ce1.00 and Ce0.99 is intimately related to the decrease of the NQR intensity, $I \times T$, whereas the T invariant behavior of C/T in Ce1.025 corresponds to the constant of $I \times T$. It should be noted that the crystal imperfection or inhomogeneity is not a main origin of the emergence of the magnetic fluctuations, since Ce1.00 and Ce0.99 are considered to be the best quality in all samples from the narrowest width of the Cu-NQR spectra.

NQR spectrum

Figure 3.4 shows the T-dependence of the Cu-NQR spectra in Ce0.975. Both ^{63}Cu- and ^{65}Cu-NQR spectral widths increase below 0.6 K, which gives evidence for an onset of the SMO. Provided that possible magnetic structure in Ce0.975 is of antiferromagnetic type with a wave vector $q = (1/2, 1/2, c)$ in $CePd_2Si_2$ [25, 26] and $CeRh_2Si_2$ [25, 27] or with $q = (0, 0, 1/2)$ in URu_2Si_2 [28, 29], hyperfine fields are canceled out at the Cu sites occupying a magnetically symmetric position. Therefore either such a helical structure as in $CeCu_2Ge_2$ or some spin-density wave (SDW) may be realized [30]. The increase of FWHM proportional to spontaneous moment M_s is close to a mean-field type below T_N

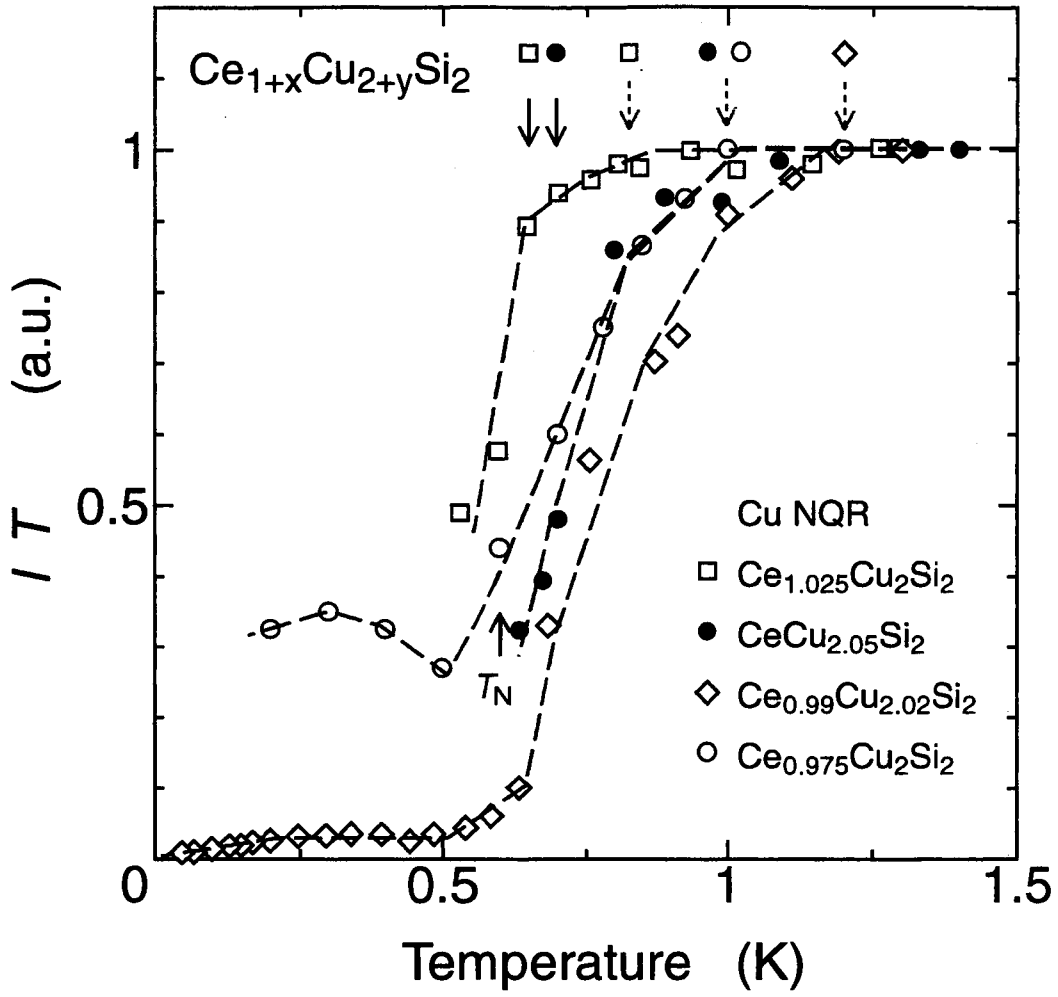

Figure 3.3 T dependence of the Cu-NQR intensity multiplied by temperature, $I \times T$ normalized by $I \times T$ at 4.2 K. Dotted and solid arrows indicate T_m and T_c, respectively.

= 0.6 K (see the bottom figure in Fig. 3.4). A rough estimate of M_s from the FWHM at low T gives rise to 0.05 μ_B per Ce ion by assuming the hyperfine coupling constant $A_{hf}^{\parallel} = -4.6$ kOe/μ_B [31].

On the other hand, FWHM in Ce0.99 does not show T-dependence at all down to 12 mK. An absence of broadening of the Cu-NQR spectrum was also found in Ce1.00, indicating no SMO in Ce0.99 and Ce1.00. From these results, the ground state in Ce0.975 is clearly distinguished from those in Ce0.99 and Ce1.00. We note that this SMO coexists with the A-phase below $T_N \sim 0.6$ K, because the value of $I \times T$ below T_m remains reduced as seen in Fig. 3.3.

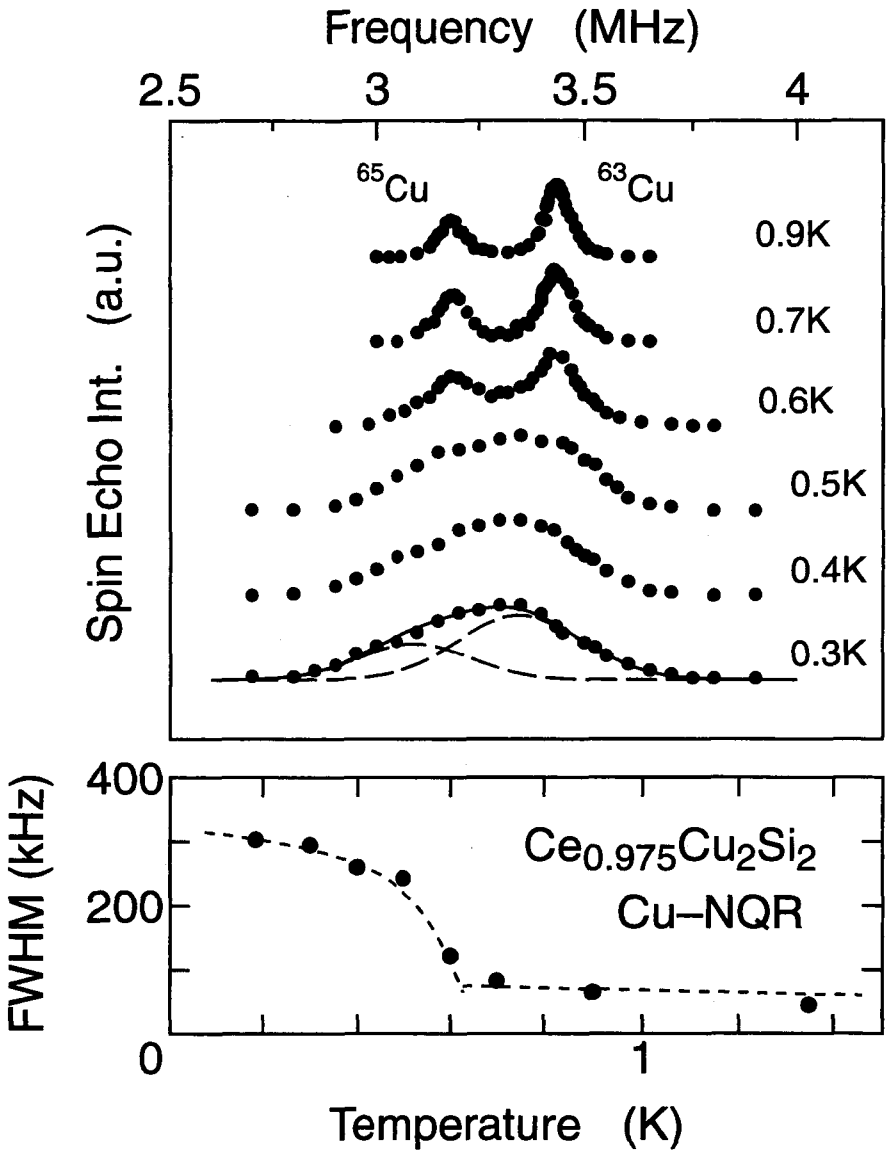

Figure 3.4 T dependence of ^{63,65}Cu-NQR spectrum in $Ce_{0.975}Cu_2Si_2$. The bottom figure shows the T dependence of the FWHM for the ^{63}Cu-NQR spectrum.

3.3.2 Nuclear spin-lattice relaxation rate, $1/T_1$

Next in order to demonstrate an evolution of the ground state from the magnetically ordered to the SC state in the series of $Ce_{1+x}Cu_{2+y}Si_2$, we show the T-dependence of $1/T_1$ of ^{63}Cu under zero field for all the samples in Fig. 3.5. $1/T_1$ is determined by a single component except for the T_1 data below 1 K in Ce0.975 where long (T_{1L}) and short (T_{1S}) components are estimated tentatively (see Fig. 3.16). Above 3 K, $1/T_1$'s for all the samples fall on a same curve regardless of varying x. It is experimentally known that a constant value of $1/T_1$ starts to decrease below T_K. $T_K \sim 10$ K is hence nearly independent of x. Below 2 K, the T dependence of $1/T_1$ reflects the difference in the ground state of each compound. A clear peak in $1/T_{1S}$ for Ce0.975 is observed at $T_N = 0.6$ K due to critical magnetic fluctuations towards the SMO.

By contrast, the $1/T_1$ for Ce1.025 exhibits a linear-T decrease below 1.2 K (denoted as T_F), probing the formation of HF band. It is confirmed from the present NQR, the μSR [13] and the specific heat [14, 16] measurements that the anomalies relevant to the A-phase below T_m is much more pronounced for Ce1.00 than for Ce1.025. It should, however, be noted that $1/T_1$'s in the SC state for Ce1.025 and Ce1.00 follow a T^3 dependence in the T range of 0.6 – 0.1 K, falling on a single line. This result suggests that the A-phase is expelled below T_c by the onset of SC phase, which is consistent with the result by the elastic measurement on the high-quality single crystal [4].

In Ce0.99, as seen in Fig. 3.3, the $I \times T$ at 0.012 K reduces to $\sim$ 5% of the value at 4.2 K without any trace of SMO. This proves that the A-phase remains dominated by slow magnetic fluctuations comparable to ω_N down to 0.012 K. In this context, the A-phase should be characterized as"critical magnetic phase" (CMP). The fact that the NQR spectrum is yet visible below T_m demonstrates a contamination of "paramagnetic domain" (PD) characterized by magnetic fluctuations with much higher frequencies than ω_N. $1/T_1$ for the PD state decreases gradually with decreasing T, followed by a small hump at around 0.6 K. With further decreasing T below 0.6 K, the small SC diamagnetization emerges associated with an onset of SC in the PD. Correspondingly, $1/T_1$ decreases steeply below 0.6 K and exhibits a similar T variation to ($1/T_{1L}$) in Ce0.975 below 0.3 K. Thus *the SC characteristics for the PD are not the same as those in the bulk SC phase for Ce1.00 and Ce1.025.* We note that the SC phase contained in Ce0.99 is significantly affected by the low-lying magnetic excitations of thermally excited quasi-particles. The sample of Ce0.99 reveals the magnetic criticality at the border to both the magnetic and SC phases.

3.3.3 Discussion

On the basis of these rich outcomes from the resent NQR study, we may propose a schematic view on dynamical magnetic response function in Fig. 3.6. In the figure, the q

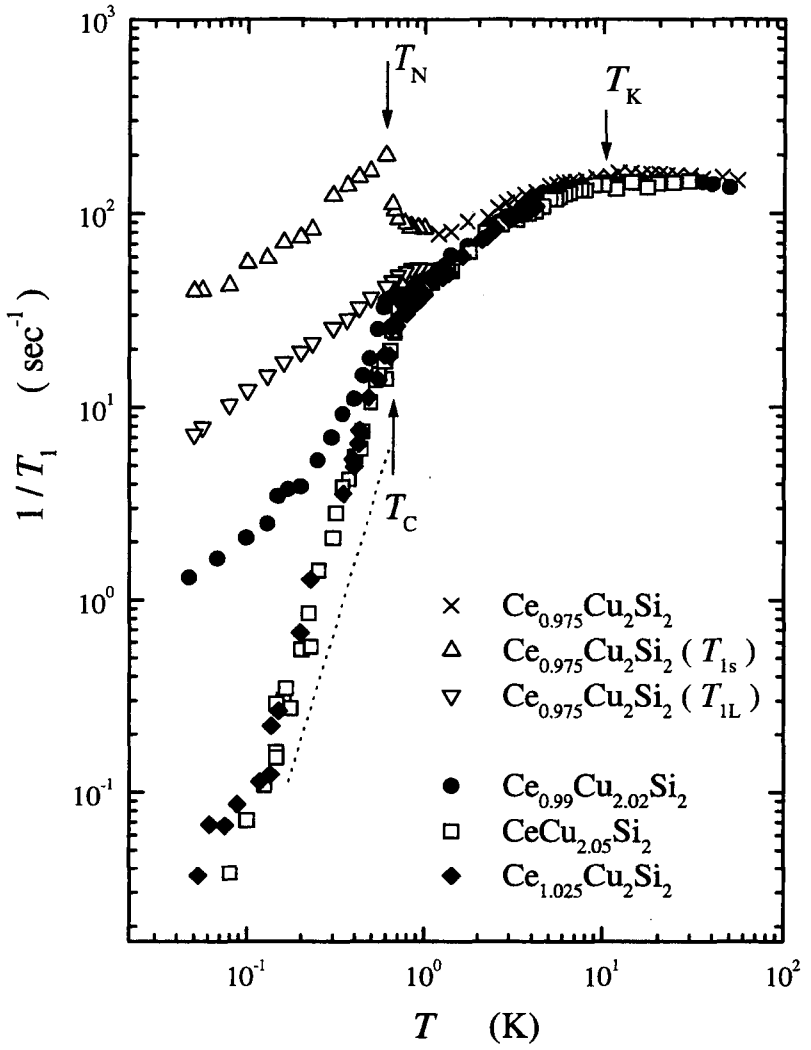

Figure 3.5 T dependence of $1/T_1$ in $Ce_{1+x}Cu_{2+y}Si_2$. Above 1 K, the T_1 in $Ce_{0.975}Cu_2Si_2$ is determined by a single component. Below 1 K, short (T_{1S}) and long (T_{1L}) components of $1/T_1$ are presented.

averaged imaginary part of dynamical susceptibility $\sum_q \chi''(q,\omega) \equiv \chi''(\omega)$ is schematically depicted as the function of frequency of magnetic correlations ω. Around 3 K, the spectral weight (SPW) of $\chi''(\omega)$ is distributed over ω from 0 to $\omega_K = k_B T_K/\hbar$ ($T_K \sim 10$ K) for all the samples as in Fig. 3.6 (a). We note that the SPW for the CMP develops around $\omega_Q \sim \omega_N$ below T_m. In Ce1.025 and Ce1.00, as shown in Fig. 3.6 (b) and (c), once these SPW's develop below T_m, but they are totally transferred into a frequency range above $\omega_s = \Delta_s/\hbar$ at $T \rightarrow 0$. Here Δ_s is the SC energy gap. Note that an intensity of SPW around $\omega_Q \sim \omega_N$ reflects a fraction of the CMP. A larger intensity of SPW in Ce1.00 than in Ce1.025 is because $I \times T$ proportional to a fraction of the PD is smaller for the former than for the latter. In Ce0.99, the SPW for the CMP around $\omega_Q \sim \omega_N$ grows markedly below $T_m \sim 1.2$ K and remains dominant down to 0.012 K. A small fraction of the PD

gives rise to the minor SC phase below 0.6 K. Therefore, a tiny SPW (5% of the total) is present in a frequency range higher than ω_Q as in Fig. 3.6 (d). Thus the dominant CMP coexists with the SC phase. In Ce0.975, a tiny saturation moment $M_s \sim 0.05\ \mu_B$ in the SMO below $T_N = 0.6$ K means that the small SPW peaks at $\omega = 0$ as indicated in Fig. 3.6 (e). In addition, considerable SPW remains finite around $\omega_Q \sim \omega_N$.

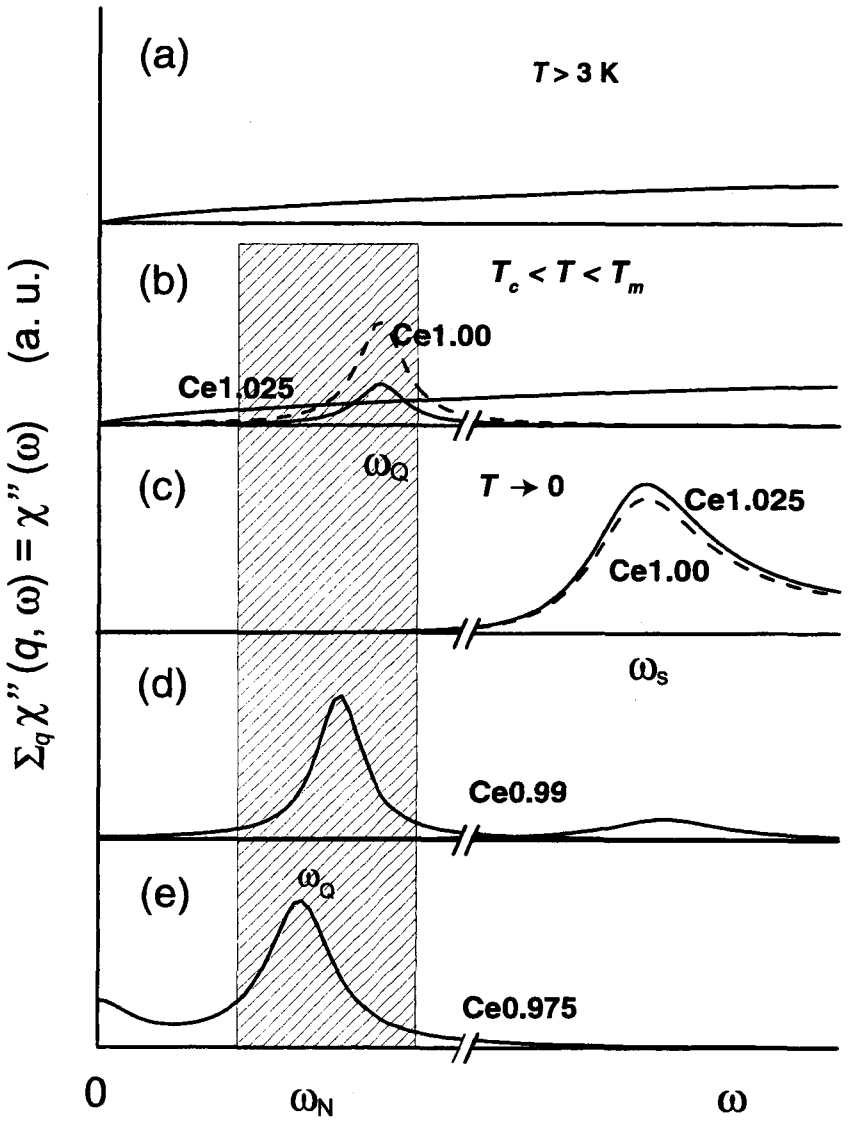

Figure 3.6 Schematic figures of the frequency dependence of the q averaged imaginary part of dynamical susceptibility in $Ce_{1+x}Cu_{2+y}Si_2$.

3.3.4 Summary in $Ce_{1+x}Cu_{2+y}Si_2$ system

Cu-NQR studies have been performed to clarify the ground-state characteristics in a series of $Ce_{1+x}Cu_{2+y}Si_2$ system at ambient pressure. $Ce_{1.025}Cu_2Si_2$ (Ce1.025) with $T_c \sim$ 0.6 K, $CeCu_{2.05}Si_2$ (Ce1.00) with $T_c \sim 0.7$ K, $Ce_{0.99}Cu_{2.02}Si_2$ (Ce0.99) with a minor part of superconductivity with $T_c \sim 0.65$ K, and non-superconducting $Ce_{0.975}Cu_2Si_2$ (Ce0.975) were examined. We present the phase diagram in a series of $Ce_{1+x}Cu_{2+y}Si_2$ compounds with varying the Ce nominal content x in Fig. 3.7.

In these samples, the Ce rich sample, Ce1.025 shows the typical property of the HF superconductivity with the anisotropic d-wave character. On the other hand, the Ce poor sample, Ce0.975 shows the static magnetic-order from the broadening of the Cu-NQR spectrum. At the border between the two phases, the ground state in Ce0.99 is dominated down to 0.012 K by slow magnetic fluctuations comparable to the NQR frequency ω_N. This state referred as the "critical magnetic phase" (CMP) in place of the A-phase coexists with the SC phase of a tiny fraction.

However, $Ce_{1+x}Cu_{2+y}Si_2$ system has the disorder effect associated with a crystal imperfection. In order to investigate the origin of the CMP seen in Ce0.99 and how the CMP evolves to SC, we have performed Cu-NQR measurements under pressure in Ce0.99 and Ce0.975. The results are presented in the following sections.

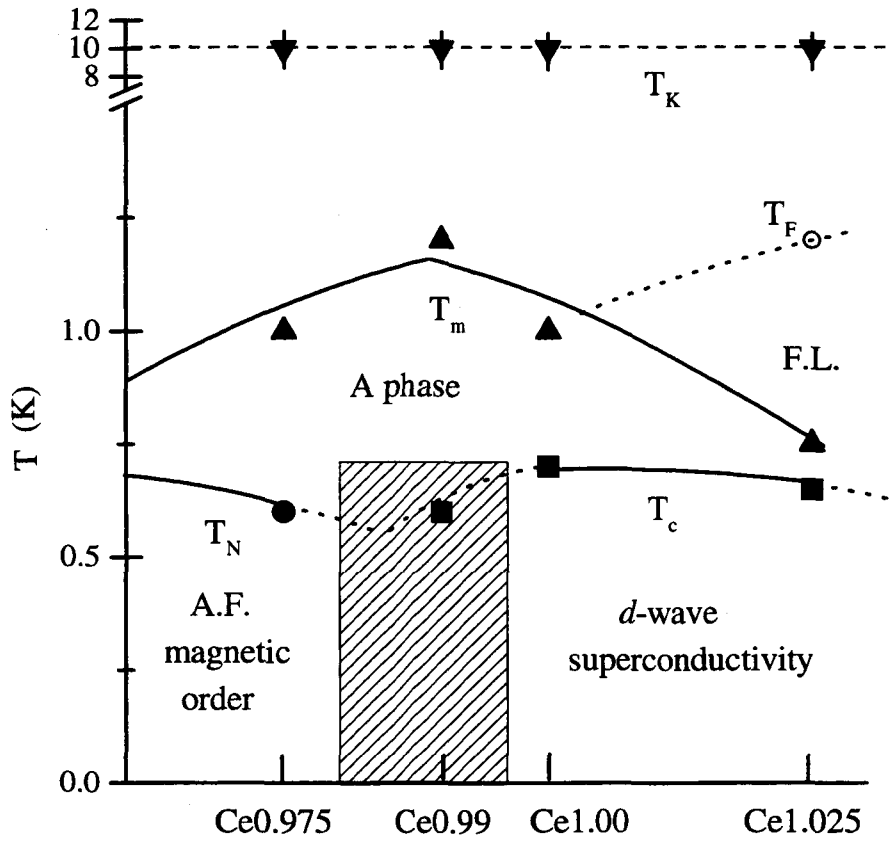

Figure 3.7 Schematic phase diagram in $Ce_{1+x}Cu_{2+y}Si_2$. T_K is the Kondo temperature. T_N and T_c are the magnetic and SC transition temperatures, respectively. T_m is the temperature below which $I \times T$ starts to decrease. T_F is the temperature below which T_1T = const. relation holds. The region denoted by slant lines is the critical region where the static magnetic order crossover to the unconventional superconductivity.

3.4 Results and discussion on $Ce_{0.99}Cu_{2.02}Si_2$ under pressure

3.4.1 NQR spectrum

We show ^{63}Cu-NQR spectra in Ce0.99 at 4.2 K under various pressures in Fig. 3.8. With increasing pressure, NQR resonance frequency, ν_Q increases linearly towards a higher frequency side, reflecting an increase of the electric gradient. In Fig. 3.9 we show the pressure dependences of ν_Q in Ce0.99 (open circles) as well as Ce0.975 (closed circles). Vertical error bars correspond to the value of linewidth or pressure distribution under each pressure. The pressure coefficient of the NQR frequency, $d\nu_Q/dp = 9.52$ Hz/bar is in good agreement with the previous study [22]. A gradual increase of linewidth with applying pressure is mainly owing to a pressure distribution, which can be estimated to be about $\pm$ 0.6 kbar at 25.8 kbar in Ce0.99, indicating the pressure inhomogeneity is relatively small.

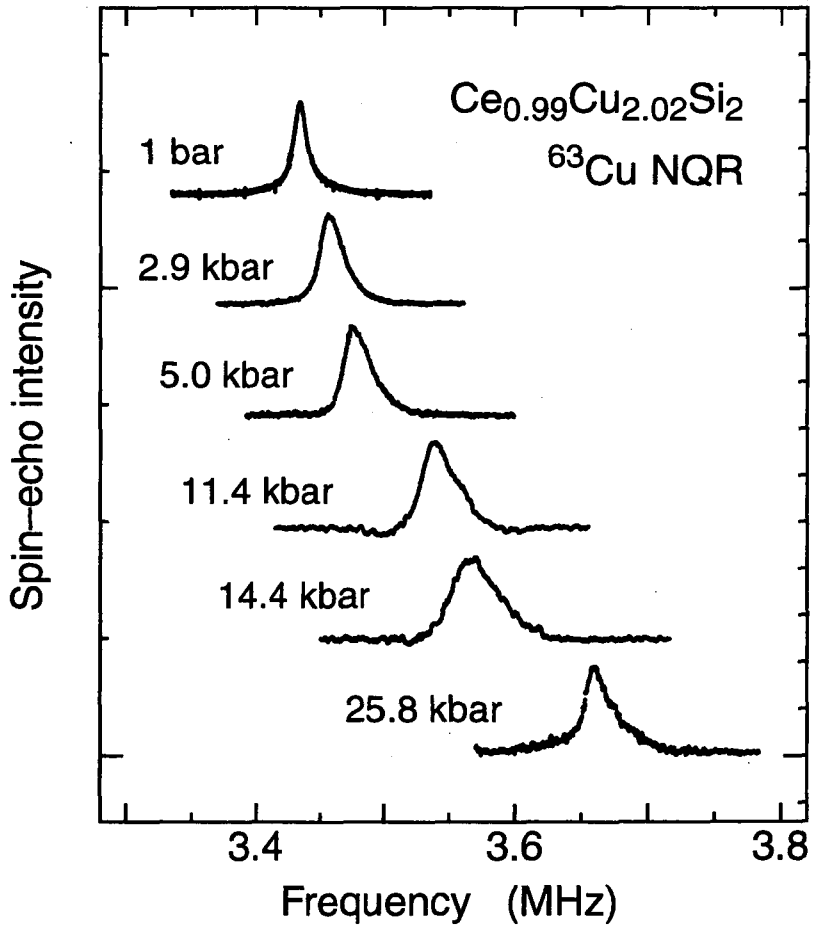

Figure 3.8 ^{63}Cu-NQR spectra in $Ce_{0.99}Cu_{2.02}Si_2$ (Ce0.99) at 4.2 K under various pressures.

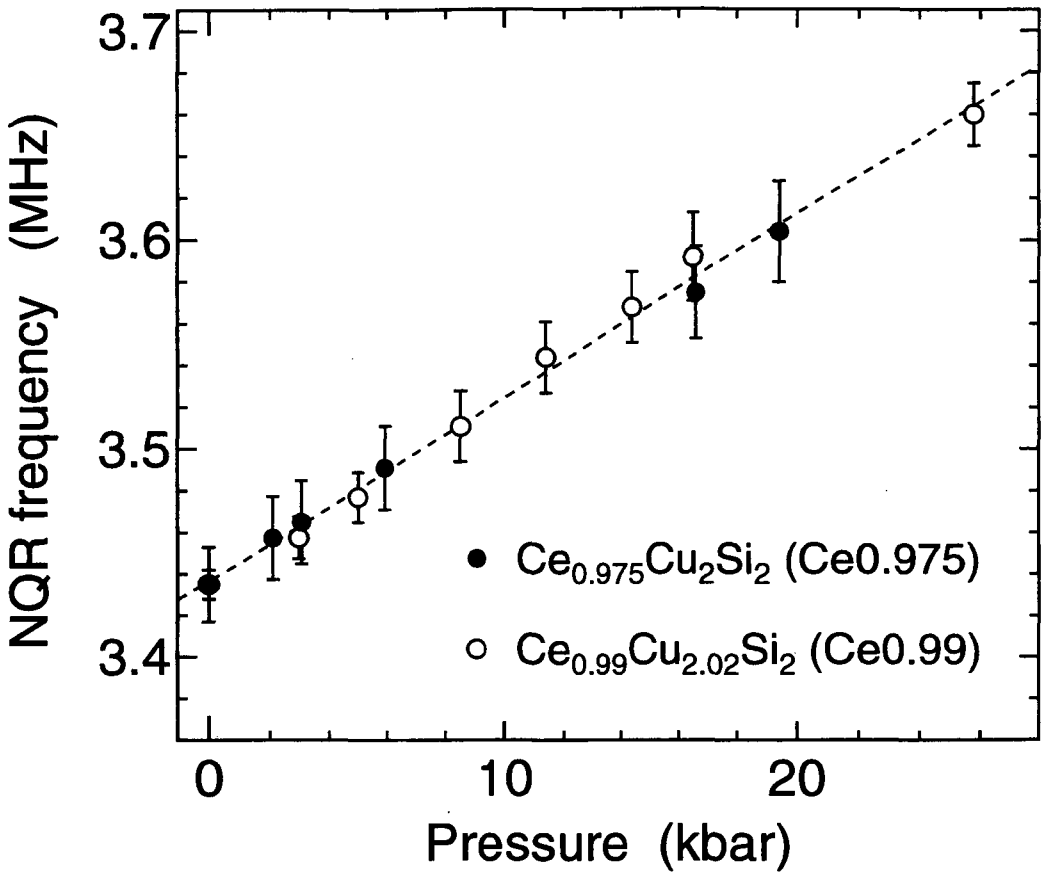

Figure 3.9 The pressure dependences of NQR resonance frequency, $^{63}\nu_Q$ in Ce0.975 (closed circles) and Ce0.99 (open circles). Vertical error bars correspond to the value of linewidth or pressure distribution under each pressure.

3.4.2 Spin-echo intensity

Fig. 3.10 displays the temperature dependence of the NQR intensity (I) of Ce0.99 multiplied by temperature, $I \times T$ normalized by $I \times T$ at 4.2 K. It should be noted that $T_c \sim 0.65$ K shown by a dotted line, monitored by the distinct change of the NQR-coil inductance, does not shift by the pressure at all. $I \times T$ at ambient pressure starts to decrease below T_m far above T_c and is reduced to less than 10%. This decrease is ascribed to the development of A-phase magnetic fluctuations with the low energy comparable to ω_N, and then the missing fraction in $I \times T$ is proportional to A-phase volume fraction.

With increasing pressure, the decreasing rate of $I \times T$ becomes weak and $I \times T$ at T_c increases significantly, indicating that the application of the pressure suppresses the development of the A-phase. $I \times T$ under 14.4 kbar below T_c decreases sharply due to the superconducting diamagnetic shielding of rf field as in Ce1.025. These results indicate

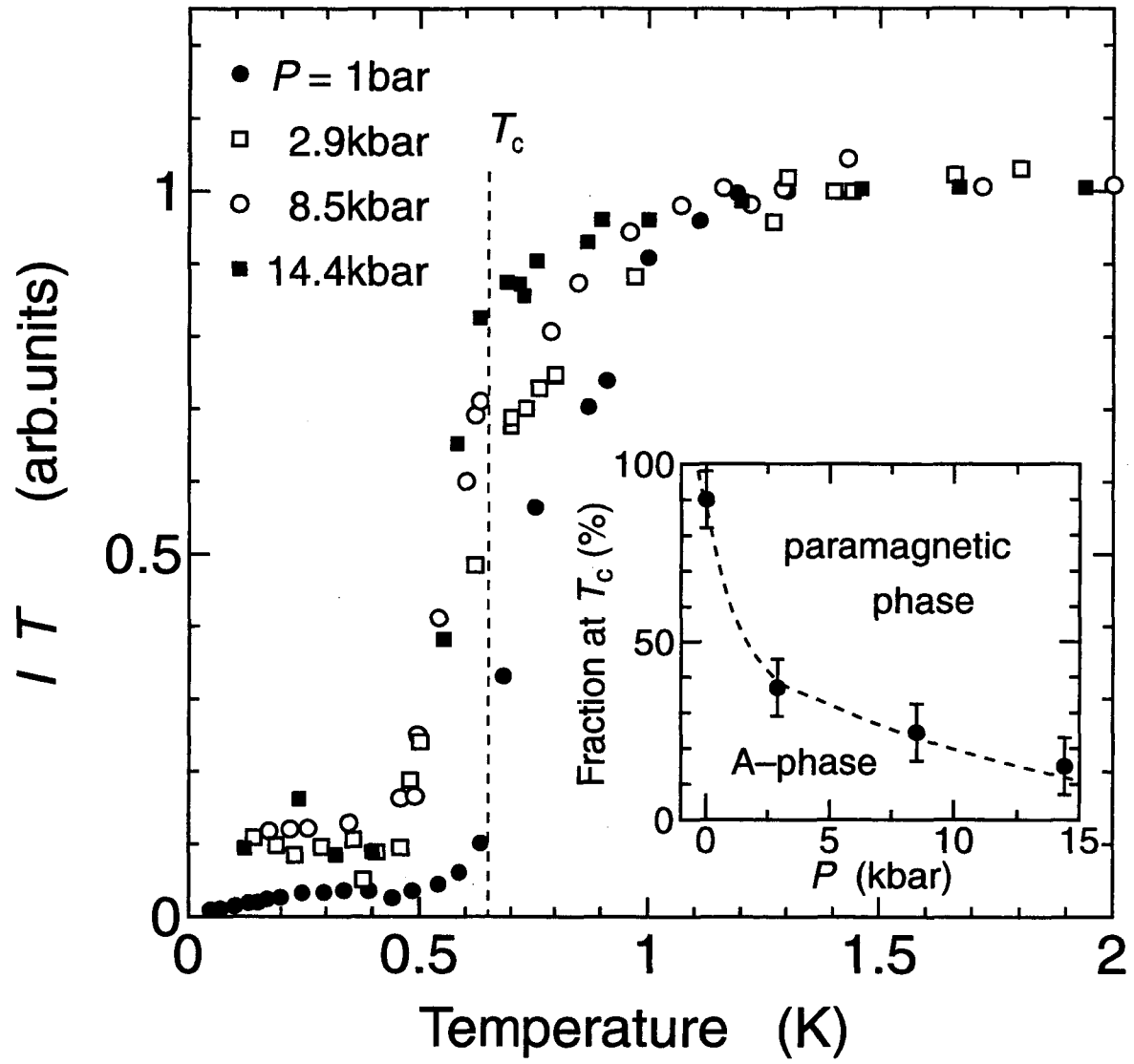

Figure 3.10 Temperature dependence of the spin-echo intensity $I \times T$ under various pressures. The inset shows the pressure dependence of A-phase fraction at T_c obtained from the missing fraction of $I \times T$.

clearly that by applying pressure the magnetic A-phase changes to the paramagnetic phase turning to SC below T_c, which is also supported by the result of $1/T_1$ below T_c as shown later. In an inset of Fig. 3.10 is shown the pressure dependence of the A-phase fraction at T_c proportional to the missing fraction of $I \times T$ at T_c. The A-phase is rapidly reduced from 90% at ambient pressure to 15% at 14.4 kbar. If this reduction of the A-phase fraction at T_c by pressure is compared with that in the $Ce_{1+x}Cu_{2+y}Si_2$ system, application of 10 kbar pressure is almost the same effect as excess Ce-doping observed in Ce1.025, consistent with the results from the specific heat measurements under pressure [14].

3.4.3 Nuclear spin-lattice relaxation rate, $1/T_1$

In Fig. 3.11 are shown the nuclear relaxation behaviors for the determination of $1/T_1$ at various temperatures and pressures. The nuclear relaxation for NQR transition $\pm 1/2 \leftrightarrow \pm 3/2$ of Cu nucleus ($I = 3/2$) is given by

$$m(t) \equiv \frac{M(\infty) - M(t)}{M(\infty)} = \exp(-t/T_1), \tag{3.1}$$

where $M(\infty)$ and $M(t)$ are the nuclear magnetization in the thermal equilibrium and at a time t after saturating pulses, respectively. $1/T_1$ is determined by a single component for whole measured range of temperature and pressure. The solid lines in the figures are the best fitting of the single exponential curves to the experimental points by the least square method. The result indicates that $1/T_1$'s were measured not at Cu site in A-phase but at the only observable Cu site in the paramagnetic phase turning to SC, since $1/T_1$ in the A-phase is quite shorter than that in the paramagnetic phase.

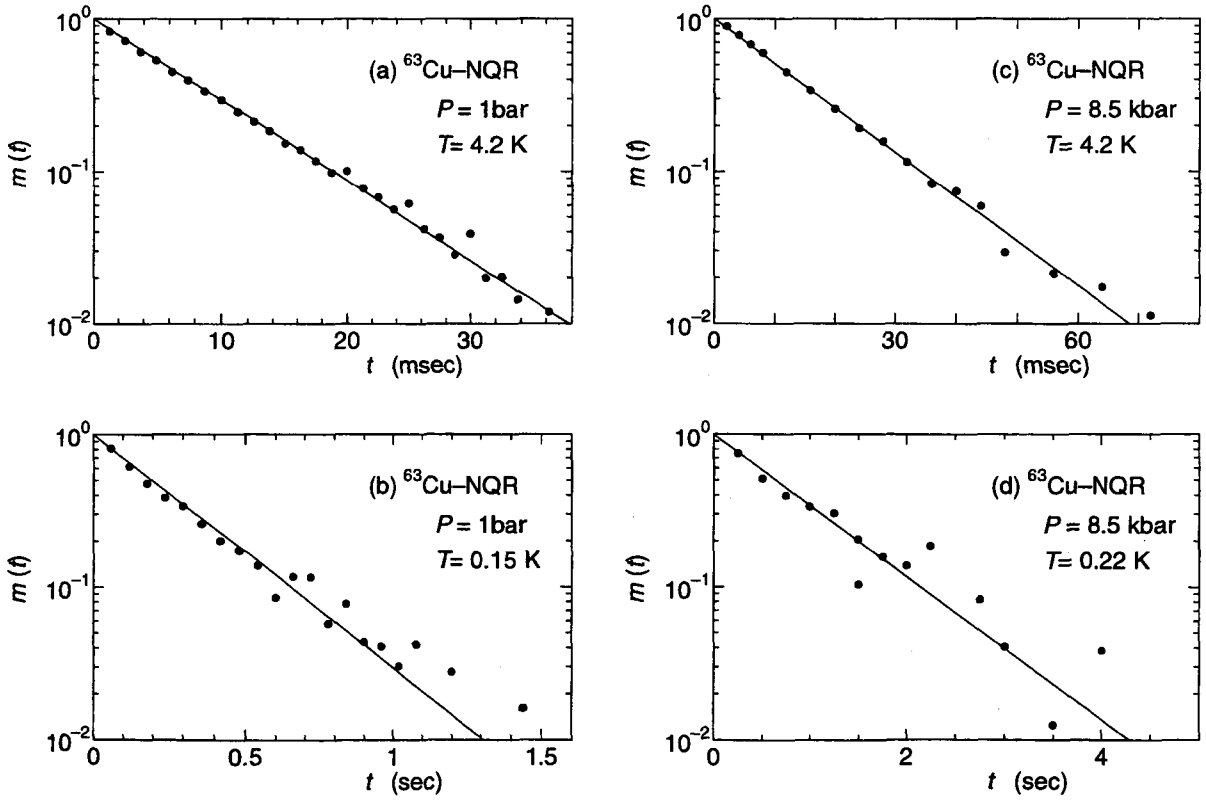

Figure 3.11 Typical magnetization recovery of ^{63}Cu NQR for the $\pm 1/2 \leftrightarrow \pm 3/2$ transition at ambient pressures and 8.5 kbar in Ce0.99. Here $m(t)$ stands for $(M(\infty) - M(t))/M(\infty)$. $1/T_1$ is determined by a single component for measured range of temperature and pressure.

In Fig. 3.12, we display the temperature variations of $1/T_1$ of Cu in Ce0.99 under various pressures. The rapid suppression of A-phase by pressure is also seen in results of $1/T_1$ in both the superconducting and the normal state as discussed following.

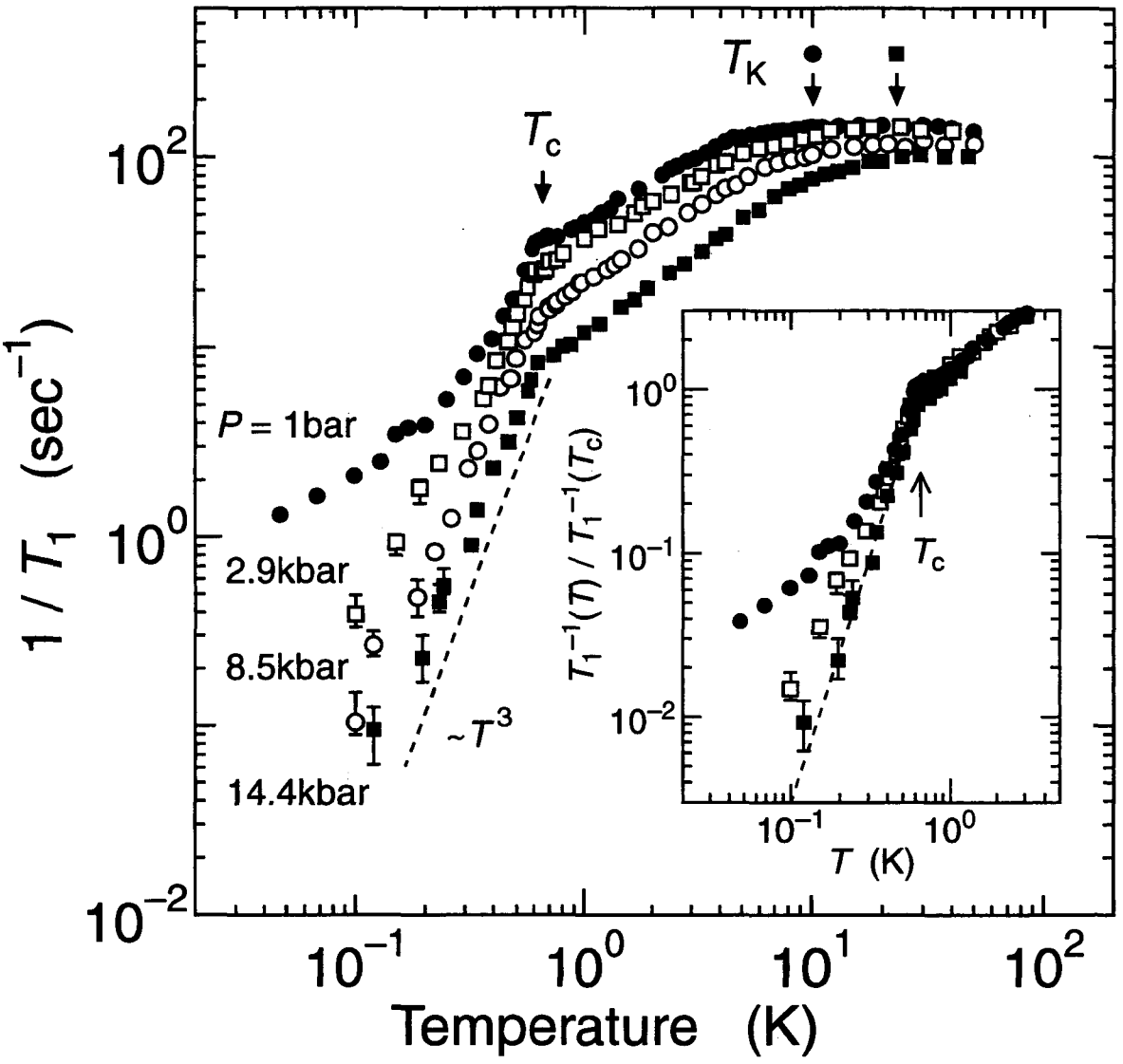

Figure 3.12 $1/T_1$ versus temperature at different pressures. The inset shows the temperature dependence of $1/T_1$ normalized by $1/T_1$ at T_c. The dash line indicates the result of $Ce_{1.025}Cu_2Si_2$ (Ce1.025).

Superconducting state

First, we discuss the behaviors of $1/T_1$ in the superconducting state. With decreasing temperature below 0.65 K, $1/T_1$ at ambient pressure becomes deviating from the T^3-dependence seen in the HF superconductors, indicating that the paramagnetic phase is significantly affected by the low-lying magnetic excitations related with the A-phase. The enhancement of $1/T_1$ in low temperature at ambient pressure is suppressed by applying small pressure such as 2.9 kbar.

In order to see the evolution of $1/T_1$ in the superconducting state by pressure, $1/T_1$ normalized by the value at T_c, $T_1^{-1}(T)/T_1^{-1}(T_c)$ is plotted against temperature, together with that in Ce1.025 at ambient pressure shown by a dash line. It may be instructive that the superconductivity occurs at nearly the same temperature ($\sim$ 0.65 K) in various samples and under pressures, especially, the invariant T_c by applying pressure strongly suggests that there does not exist the quantum phase transition between magnetic and superconducting phases in $CeCu_2Si_2$. Alternatively, if it is taken into account that volume fraction of each phase is only changed by pressure without the shift in T_c, it can be concluded that the transition between these phases may be of first order. Since the hysteresis behaviors, however, have never been reported in the development of the A-phase volume upon cooling, and the application of tiny pressure makes the magnetic phase change to the superconducting phase, it is suggested that an energy difference between these phases is very small and/or that these phases are nearly degenerate.

Normal state

Next we discuss an evolution of the spin fluctuations in the normal state, which is relevant to the change of the ground states. In the high-temperature region, $1/T_1$ shows T-independent behavior and deviates from the T-independent behavior below 10 K at ambient pressure. With increasing pressure the constant values in $1/T_1$ become suppressed and the temperature, below which $1/T_1$ starts to deviate from the T-independent behavior, increases. In the high-temperature region where the $4f$ electrons is regarded as local moments, T-independent $1/T_1$ is proportional to the square of the effective moments, $p_{\rm eff}^2$ and to the inverse of the exchange interaction between local moments, $J_{\rm ex}$ by means of the RKKY interaction. The suppression of the value in the T-independent $1/T_1$ by pressure implies the increase of the interaction between $4f$ local moments and conduction electrons, $J_{\rm cf}$ and the decrease of $p_{\rm eff}$, since $J_{\rm ex}$ is proportional to $J_{\rm cf}^2/W$ with W being the width of the conduction band, and the increase of $J_{\rm cf}$ suppresses $p_{\rm eff}$. In addition the temperature below which $1/T_1$ starts to decrease is known experimentally as the Kondo temperature T_K from a comparison with neutron experiments, therefore application of pressure makes T_K increase (see Fig. 3.13), indicating also the increase of $J_{\rm cf}$, since T_K can be expressed as $T_K \propto \exp(-W/J_{\rm cf})$.

Far below T_K, $4f$ electrons have an itinerant character, resultantly the renormalized

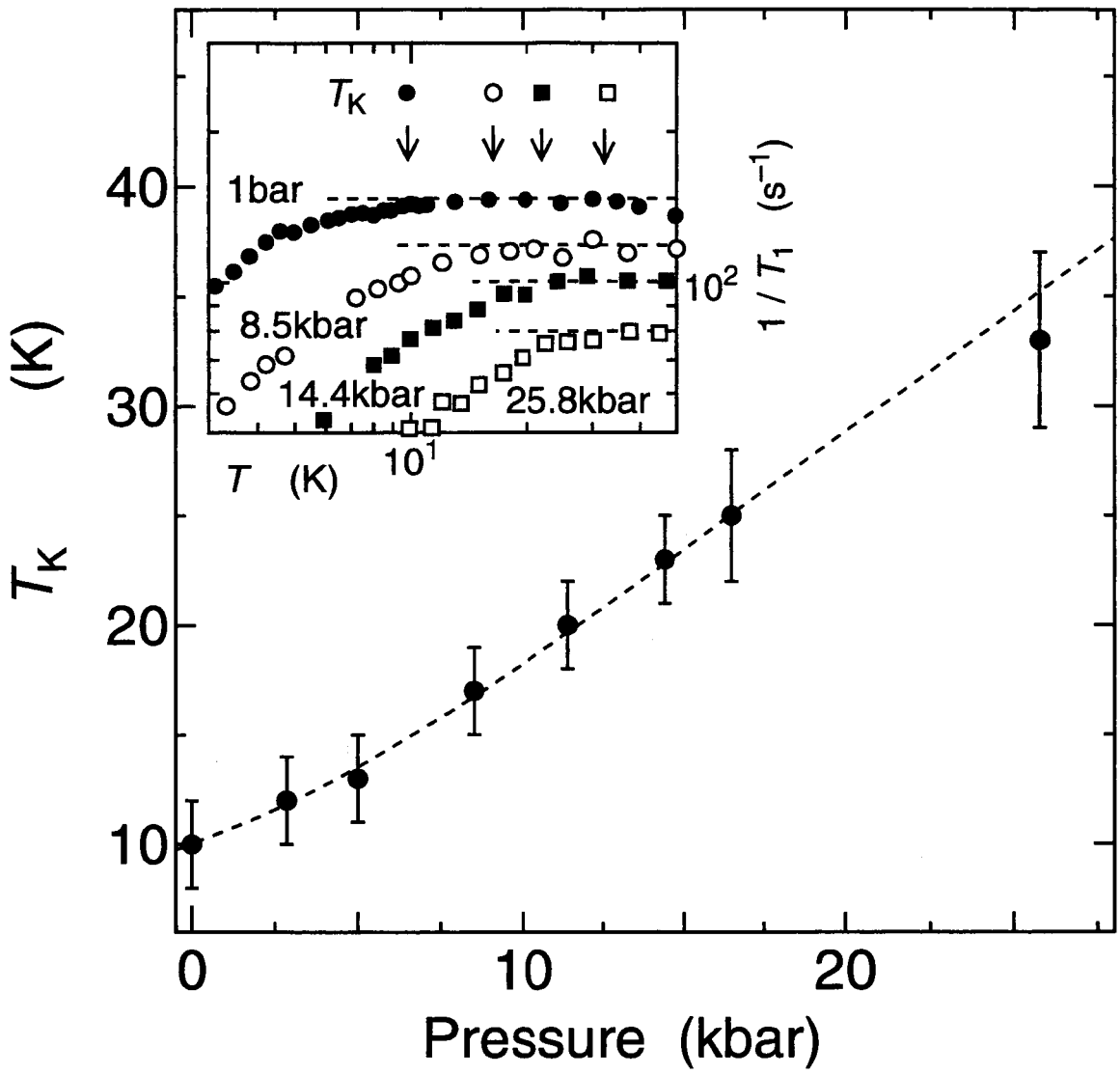

Figure 3.13 The pressure dependence of Kondo temperature, T_K. T_K is estimated from the temperature at which $1/T_1$ starts to decrease from the $1/T_1$ = constant as shown in the inset.

system may be considered to evolve to the Fermi-liquid (FL) state with small characteristic energy. The SCR theory developed by Moriya *et al.* is probably helpful for the understanding of the evolution in $1/T_1$ by pressure [32], since it has been reported that the crossover from a magnetic-ordered state to a FL state can be described by the SCR theory of the spin fluctuations in some compounds [33, 34]. Here we apply the SCR theory to the results of $1/T_1$ only above 8.5 kbar, where the volume fraction of the A-phase is largely suppressed. Since the SCR theory is not appropriate for a system, in which two phases coexist, such as Ce0.99 at the low pressure range. Since the parameter of T_0 characterizing the energy width of the dynamical spin-fluctuation (SF) spectrum may be considered to be approximately the same as T_K [32], $1/T_1$ divided by the reduced temperature t $(= T/T_K)$, $1/T_1t$ is plotted against t as shown in Fig. 3.14.

The t variation in $1/T_1t$ can be reproduced by calculations of $1/T_1t$ from the SCR theory shown by dotted lines, in which $1/T_1t$ is expressed,

$$\frac{1}{T_1t} = \frac{\hbar\gamma_n^2 A_{hf}^2}{2\pi T_A} \frac{3\pi}{4\sqrt{y(y_0, y_1, t)}} \tag{3.2}$$

with parameters of T_A, y_0 and y_1 for three dimensional system close to an antiferromagnetic instability [35]. Here γ_n is the geomagnetic ratio of ^{63}Cu nucleus and A_{hf} is the hyperfine coupling constant perpendicular to c-axis, ~ 1.6 kOe/μ_B in this compound [31]. T_A is the characteristic SF energy in the momentum space and y_0 is inversely proportional to the staggered susceptibility at $T = 0$, then $y_0 = 0$ at the magnetic critical point. Here we take $y_1 = 4$ from the result of specific heat measurement under pressure [17]. A good agreement is seen between the experimental results and the calculated lines in the temperature region between T_c and $0.5t$. The value of y_0, plotted in Fig. 3.15 (b), increases monotonically by pressure from $y_0 \sim 0.035$ at 8.5 kbar to 0.1 at 26 kbar, suggesting strongly that the application of pressure makes the SF character apart from the quantum critical behavior.

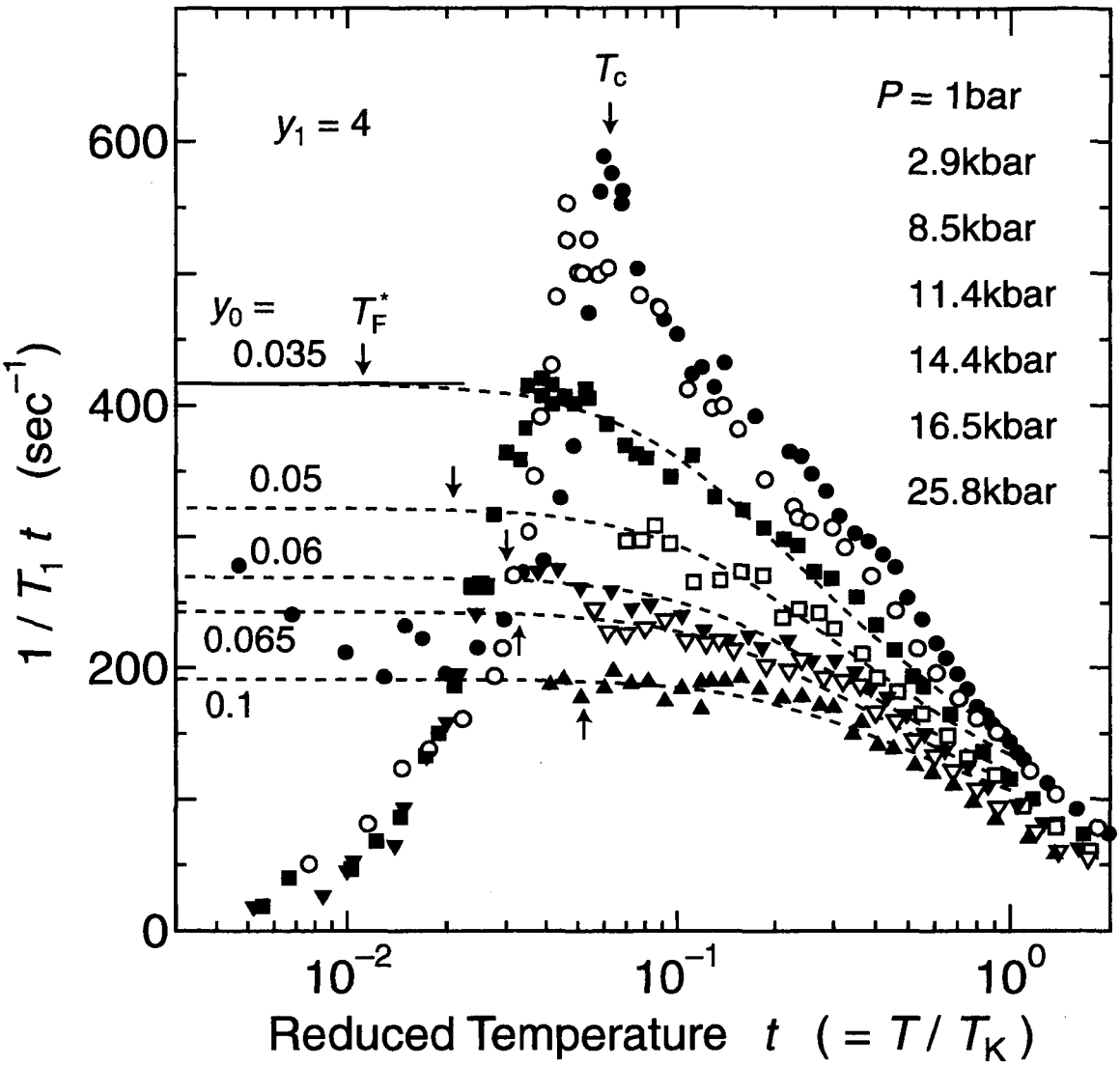

Figure 3.14 The reduced temperature t ($= T/T_K$) dependence of $1/T_1t$ at different pressures. The solid lines are the calculated ones using the SCR theory with $y_1 = 4$.

3.4.4 Discussion

To discuss the relation between SF character and SC in this region, we show pressure variations of T_K, T_c and an effective Fermi liquid temperature, T_F^*, in Fig. 3.15 (c). We tentatively take T_F^* from the temperature below which $1/T_1t$ stays constant on the calculated line by SCR theory as indicated by arrow in Fig. 3.14. At low pressure T_F^* is much lower than T_c, showing the development of SF down to T_c with decreasing temperature. It should be noted that SC emerges initially in the non-Fermi-liquid behavior in $1/T_1t$ as in underdoped LSCO ($La_{2-x}Sr_xCuO_4$ with $0.05 < x < 0.10$) [36]. This indicates clearly that SC appears before the formation of HF band, resulting in that the SC nature is of a strong coupling. Above 15 kbar T_F^* exceeds T_c. Here the enhancement of $1/T_1t$ becomes suppressed with decreasing temperature and $1/T_1t$ shows a saturated behavior above T_c, as is often the case with uranium-based HF superconductors such as UPt_3 [37].

Although the SF characters are much affected by pressures, T_c is almost independent of pressure below 15 kbar and gradually increases above this pressure as reported already [38]. The slight increase of T_c above 15 kbar, where T_F^* is higher than T_c, might be understood in the framework of the SCR theory [39], since in this theory the value of T_c is roughly proportional to T_0 for a fixed value of y_0 and almost independent of y_0 for a fixed value of T_0. By contrast, T_c stays nearly constant from 0 to 15 kbar, although the system is dominated by the magnetic A-phase which largely affects the normal and SC state. This predominant A-phase at low pressure region might play an important role to sustain the SC, since the volume fraction of the A-phase almost vanishes above this pressure.

It may be worthwhile pointing to the following results: SC coexists with the magnetic A-phase turning to the superconducting phase by a tiny pressure and only 1% Ge-doped samples, $CeCu_2(Si_{0.99}Ge_{0.01})_2$ with $T_K \sim 9$ K, shows the A-phase anomaly and the SMO below 0.65 K [7]. It is evidenced experimentally that A-phase fluctuations seen in pure Ce0.99 at ambient pressure possesses the quantum critical character. We propose that low-energy spin-fluctuations observed in the A-phase may be regarded as the intermediate state between SMO and SC. Recently, S. C. Zhang proposed SO(5) theory to deal with the close proximity between the SC and the antiferromagnetic (AF) phase [40]. In this theory, d-wave SC and AF phase are treated on equal footing, and d-wave SC is regarded as AF state viewed in the SO(5) coordinates. We point out that the SO(5) theory is one of the most promising candidates to explain the novel relation between SMO and SC.

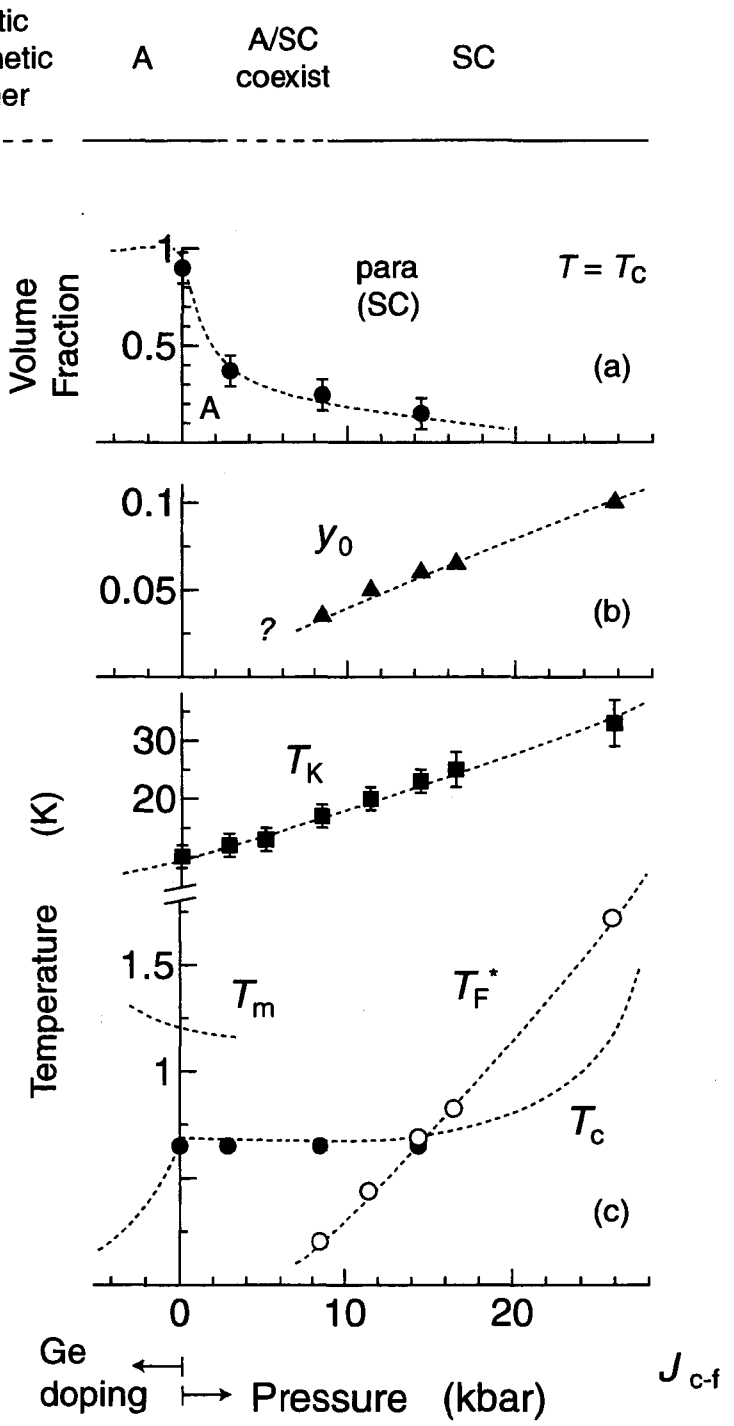

Figure 3.15 (a) Pressure dependence of the volume fraction of the A-phase at T_c. (b) Pressure dependence of y_0, which is inversely proportional to the staggered susceptibility at $T = 0$. (c) Pressure variations of T_K (closed boxes), T_c (closed circles), and the effective Fermi temperature, T_F^* (open circles). Below T_m, the A-phase starts to develop upon cooling. The pressure dependence of T_c (dash line) was obtained from Ref. [6, 38].

3.5 Results and discussion on $Ce_{0.975}Cu_2Si_2$ under pressure

In this section we discuss the pressure effect of magnetic properties in Ce0.975, exhibiting the SMO below $T_N \sim 0.6$ K at ambient pressure. It is considered that a helical structure as in $CeCu_2Ge_2$ [30] or some SDW are realized in the ordered state as described in Section 3.3.1.

The nuclear relaxation behaviors for the determination of T_1 at various temperatures and pressures are shown in Fig. 3.16. The solid lines in the figures are calculated by the least square fitting to eq. (3.1). While T_1 can be determined uniquely above T_N, the nuclear relaxation does not have unique single solution on the fitting below T_N at every pressure.

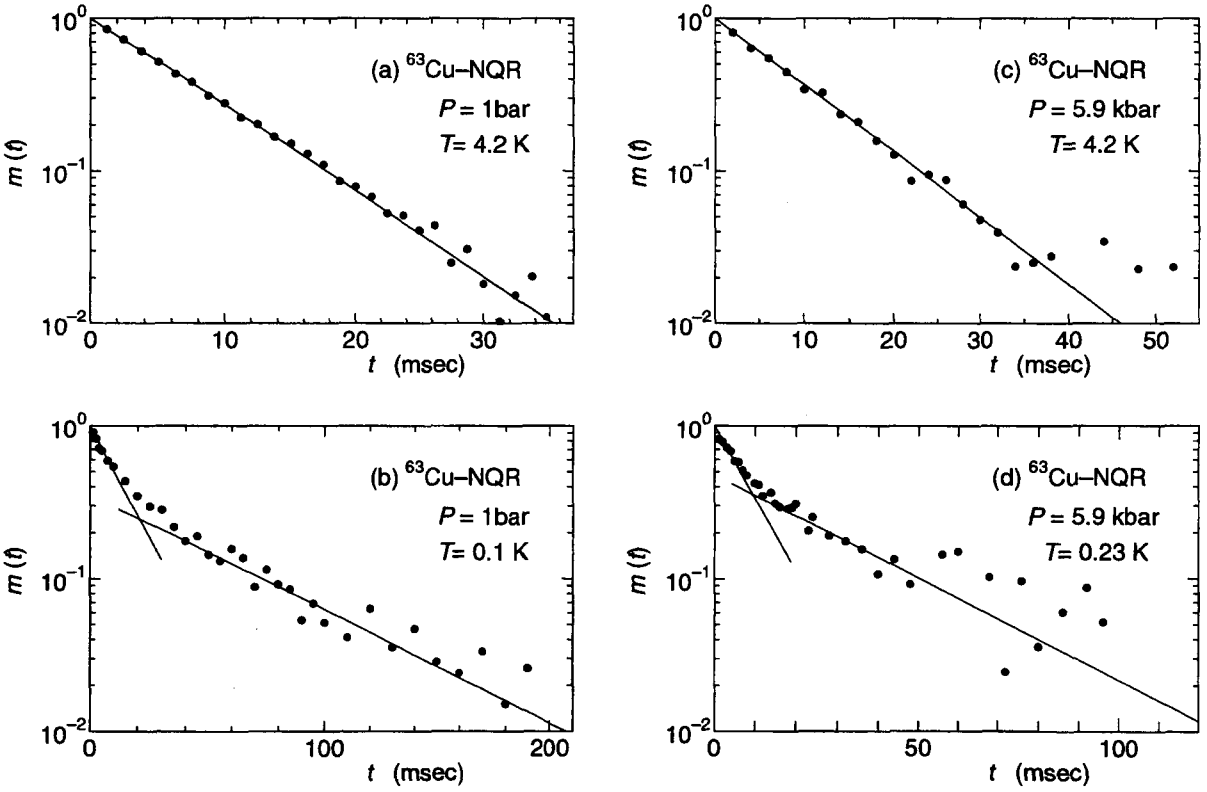

Figure 3.16 Typical magnetization recovery of ^{63}Cu NQR for the $\pm 1/2 \leftrightarrow \pm 3/2$ transition at ambient pressures and 5.9 kbar in Ce0.975. $m(t)$ stands for $(M(\infty) - M(t))/M(\infty)$. An appreciable distribution of T_1 appears below T_N (0.6 K at ambient pressure and 0.3 K at 5.9 kbar) at every pressure.

The onset of the SMO is detected both by the peak in $1/T_1$ and the rapid increase of NQR spectral width below T_N. Fig. 3.17 and Fig. 3.18 show the temperature variations of $1/T_1$ and the ^{63}Cu-NQR spectral width for various pressures. Since $1/T_1$ is not a single component below T_N, only short component is shown for comparison. The onset of SMO

is indicated by arrows in the figures. The application of pressure decreases both T_N and spectral width at the lowest temperature. The increase of spectral width proportional to spontaneous moment M_s are close to a mean-field type below T_N for all pressures. We could roughly estimate M_s from the spectral width at low temperature, assuming the hyperfine coupling constant $A_{hf}^{\parallel} = -4.6$ kOe/μ_B [31]. In Fig. 3.19, we show the pressure dependences of T_N and M_s, indicating M_s is roughly proportional to T_N. The proportionality between M_s and T_N is not expected for well localized magnetic electrons but is rather characteristic of the itinerant electron magnets.

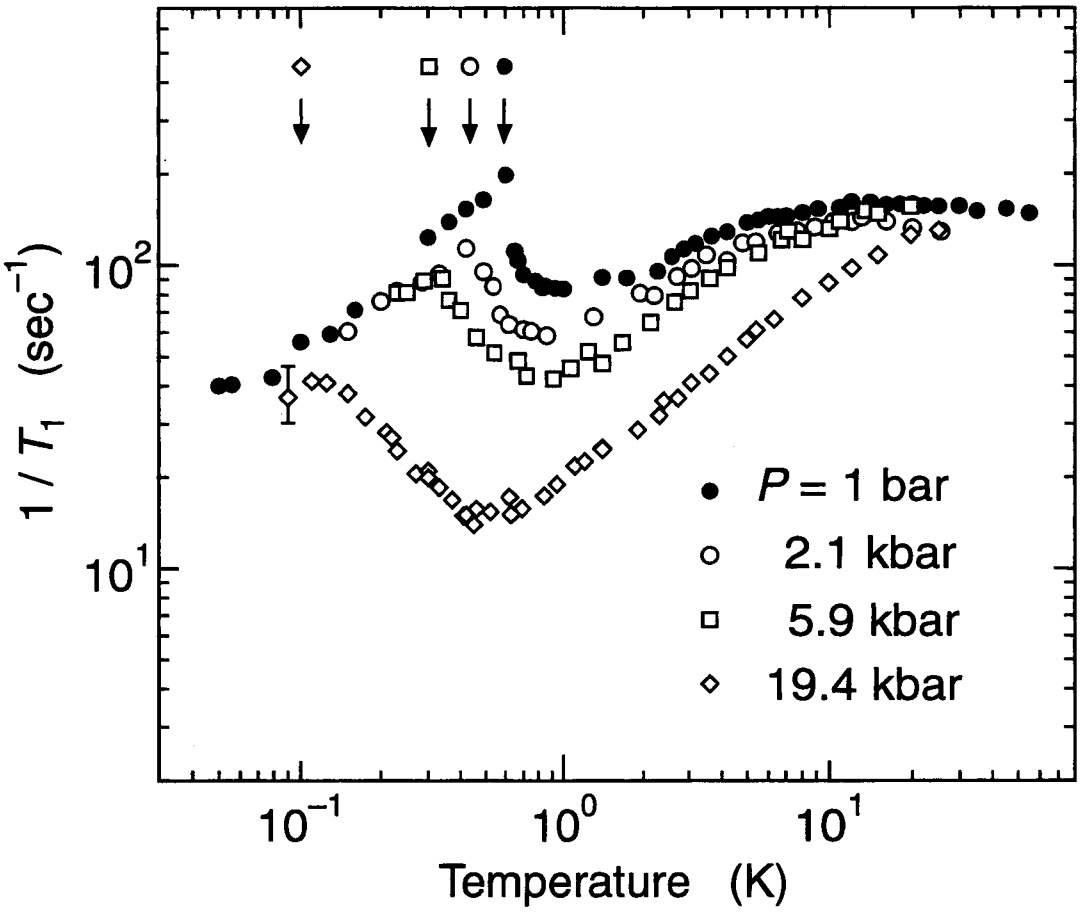

Figure 3.17 The temperature variations of $1/T_1$ in Ce0.975 at various pressures. Since $1/T_1$ is not a single component below T_N indicated by arrows, only short component is shown for comparison.

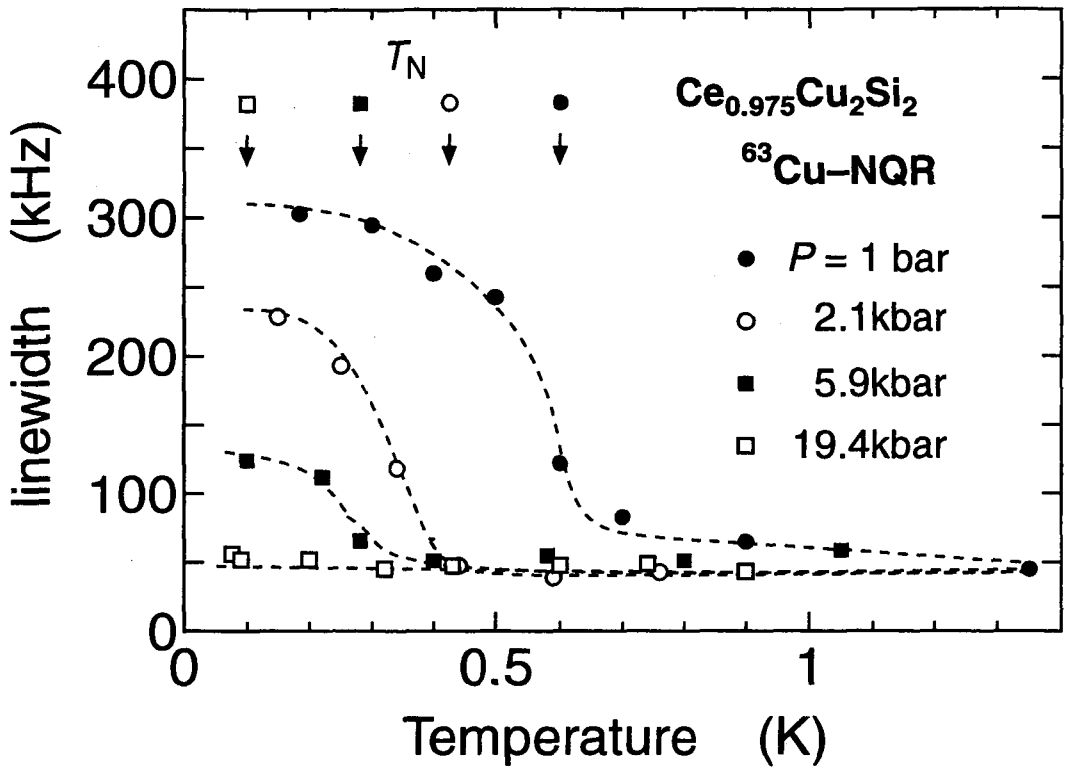

Figure 3.18 The temperature variations of NQR spectral width for various pressures in Ce0.975. T_N at each pressure is indicated by arrows. The dash lines are guide for eye.

We next show the pressure effect in the high-temperature region. As seen in Fig. 3.17, the $1/T_1$ = constant value decreases with pressure and the temperature T^* at which $1/T_1$ starts to decrease from the $1/T_1$ = constant increases with applying pressure. Since T^* empirically corresponds to the Kondo temperature, T_K, it is indicated that T_K is enhanced with increasing pressure as shown in Fig. 3.20, and hence the hybridization between $4f$ and conduction electrons becomes stronger. The increasing rate of T_K against pressure is almost the same as that in Ce0.99.

The SMO remains up to P = 19.4 kbar with T_N lower than 0.1 K. T_K goes up to 25 K, whereas no superconductivity is detected even at P = 19.4 kbar. From the fact the spectral linewidth is much larger for Ce0.975, $\sim$ 35 kHz, than for Ce0.99, $\sim$ 14 kHz as indicated in Fig. 3.2, it is considered that some kind of crystal inhomogeneity or spin defect prevents a possible pressure induced phase change in Ce0.975. This reminds us of the previous results from resistivity measurements under pressure that no superconductivity has been observed in samples with large residual resistivity above several $\mu\Omega$ in $CePd_2Si_2$ and $CeIn_3$ [1].

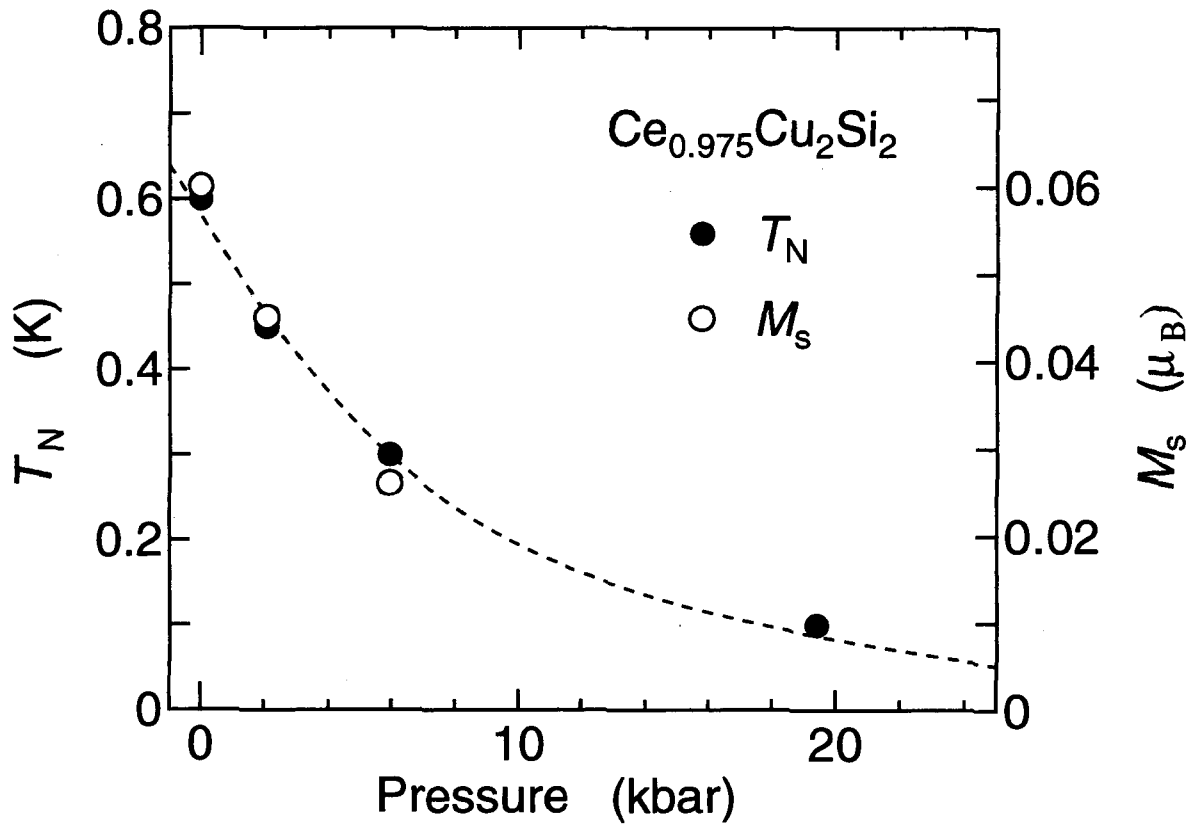

Figure 3.19 The pressure variations of T_N and spontaneous moment M_s, indicating M_s is roughly proportional to T_N. The dash lines are guide for eye.

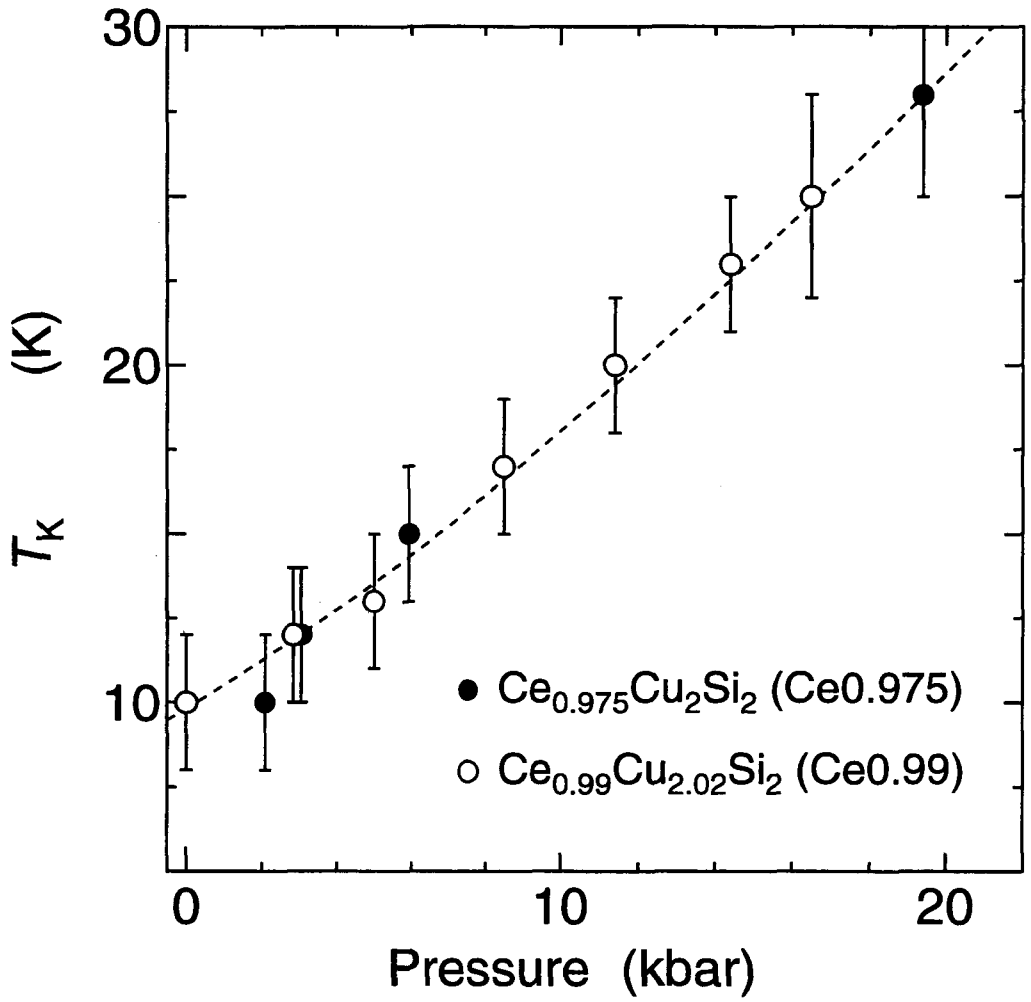

Figure 3.20 The pressure dependences of Kondo temperature, T_K for Ce0.975 (closed circles) and Ce0.99 (open circles). T_K was estimated from the temperature below which $1/T_1$ starts to deviate from the constant behavior on cooling. The dash line is guide for eye.

3.6 Conclusion

In order to study magnetic properties at the region where the ground state changes from magnetism to SC, we have performed Cu-NQR measurements under hydrostatic pressure on two off-stoichiometric $Ce_{1+x}Cu_{2+y}Si_2$; $Ce_{0.99}Cu_{2.02}Si_2$ (Ce0.99) exhibits the anomalous ground state so-called A-phase dominated by critical magnetic correlations and $Ce_{0.975}Cu_2Si_2$ (Ce0.975) shows the SMO at ambient pressure.

In Ce0.99, the magnetic A-phase by low-energy magnetic fluctuations changes to the superconductivity by application of small pressure without passing through the quantum critical point, while T_c is almost unchanged below 15 kbar. The transition from the magnetic A-phase to the SC is of a first-order type, and occurred close to an antiferromagnetic instability. However, it is suggested that the energy difference between these states may be very small, since any hysteresis behavior in the A-phase development can not seen at all by the cooling process. We propose that low-energy spin-fluctuations observed in the A-phase magnetic state may be regarded as the intermediate state between SMO and SC.

In Ce0.975 showing SMO at ambient pressure, no superconductivity was induced up to 19.4 kbar, showing that some crystal inhomogeneity or spin defect prevents a pressure-induced superconductivity in Ce0.975. It was also shown that the pressure-induced superconductivity is quite sensitive to the sample quality as in $CePd_2Si_2$ and $CeIn_3$.

References

[1] N. D. Mathur, F. M. Grosche, S. R. Julian, I. R. Walker, D. M. Freye, R. K. W. Haselwimmer, and G. G. Lonzarich, Nature **394**, 39 (1998).

[2] D. Jaccard, K. Behnia, and J. Sierro, Phys. Rev. Lett. A **163**, 475 (1992).

[3] R. Movshovich, T. Graf, D. Mandrus, J. D. Thompson, J. L. Smith, and Z. Fisk, Phys. Rev. B **53**, 8241 (1996).

[4] G. Bruls, B. Wolf, D. Finsterbusch, P. Thalmeier, I. Kouroudis, W. Sun, W. Assmus, and B. Lüthi, Phys. Rev. Lett. **72**, 1754 (1994).

[5] G. Knebel, C. Eggert, D. Engelmann, R. Viana, A. Krimmel, M. Dressel, and A. Loidl, Phys. Rev. B **53**, 11586 (1996).

[6] O. Trovarelli, M. Weiden, R. Müller-Reisener, M. Gómez-Berisso, P. Gegenwart, M. Deppe, C. Geibel, J. G. Sereni, and F. Steglich, Phys. Rev. B **56**, 678 (1997).

[7] K. Ishida *et al.*, in preparation.

[8] H. Nakamura, Y. Kitaoka, T. Iwai, H. Yamada, and K. Asayama, J. Phys. Condens. Matter **4**, 473 (1992).

[9] Y. J. Uemura, W. J. Kossler, X. H. Yu, H. E. Schone, J. R. Kempton, C. E. Stronach, S. Barth, F. N. Gygax, B. Hitti, A. Schenck, C. Baines, W. F. Lankford, Y. Ōnuki, and T. Komatsubara, Phys. Rev. B **39**, 4726 (1989).

[10] G. M. Luke, A. Keren, K. Kojima, L. P. Le, B. J. Sternlieb, W. D. Wu, Y. J. Uemura, Y. Ōnuki, and T. Komatsubara, Phys. Rev. Lett. **59**, 1853 (1994).

[11] Y. Kitaoka, H. Nakamura, T. Iwai, K. Asayama, U. Ahlheim, C. Geibel, C. Schank, and F. Steglich, J. Phys. Soc. Jpn. **60**, 2122 (1992).

[12] K. Ishida, Y. Kawasaki, K. Tabuchi, K. Kashima, Y. Kitaoka, K. Asayama, C. Geibel, and F. Steglich, Phys. Rev. Lett. **82**, 5353 (1999).

[13] R. Feyerherm, A. Amato, C. Geibel, F. N. Gygax, P. Hellmann, R. H. Heffner, D. E. MacLaughlin, R. Müller-Reisener, G. J. Nieuwenhuys, A. Schenck, and F. Steglich, Physica B **206-207**, 596 (1995); Phys. Rev. B **56**, 699 (1997).

[14] F. Steglich, B. Buschinger, P. Gegenwart, M. Lohmann, R. Helfrich, C. Langhammer, P. Hellmann, L. Donnevert, S. Thomas, A. Link, C. Geibel, M. Lang, G. Sparn, and W. Assmus, J. Phys. Condens. Matter **8**, 9909 (1996).

[15] I. Sheikin, D. Braithwaite, J. -P. Brison, A. Buzdin, and W. Assmus, J. Phys. Condens. Matter **10**, L749 (1998).

[16] R. Modler, M. Lang, C. Geibel, C. Schank, R. Müller-Reisener, P. Hellmann, A. Link, G. Sparn, W. Assmus, and F. Steglich, Physica B **206-207**, 586 (1995).

[17] P. Gegenwart, C. Langhammer, C. Geibel, R. Helfrich, M. Lang, G. Sparn, F. Steglich, R. Horn, L. Donnevert, A. Link, and W. Assmus, Phys. Rev. Lett. **81**, 1501 (1998).

[18] H. Kohno, H. Fukuyama, and M. Sigrist, J. Phys. Soc. Jpn. **68**, 1500 (1999).

[19] C. Geibel, private communication.

[20] K. Ishida, in preparation.

[21] K. Ishida, Y. Kawasaki, K. Tabuchi, K. Kashima, Y. Kitaoka, K. Asayama, C. Geibel, and F. Steglich, Physica B **259-261**, 678 (1999).

[22] Y. Kitaoka, H. Tou, G. -q. Zheng, K. Ishida, K. Asayama, T. C. Kobayashi, A. Kohda, N. Takeshita, K. Amaya, Y. Ōnuki, C. Geibel, C. Schank, and F. Steglich, Physica B **206-207**, 55 (1995).

[23] C. Tien, Phys. Rev. B **43**, 83 (1991).

[24] R. Feyerherm *et al.*, unpublished.

[25] B. H. Grier, J. M. Lawrence, V. Muragai, and R. D. Parks, Phys. Rev. B **29**, 2664 (1984).

[26] R. A. Steeman, E. Frikkee, R. B. Helmholdt A. A. Menovsky, J. van den Berg, G. J. Nieuwenhuys, and J. A. Mydosh, Solid State Comm. **66**, 103 (1988).

[27] S. Kawarazaki, Y. Kobashi, J. A. Fernandez-Baca, S. Murayama, Y. Ōnuki, and Y. Miyako, Physica B **206-207**, 298 (1995).

[28] C. Broholm, J. K. Kjems, W. J. L. Buyers, P. Matthews, T. T. M. Palstra, A. A. Menovsky, and J. A. Mydosh, Phys. Rev. Lett. **58**, 1467 (1987).

[29] C. Broholm, H. Lin, P. Matthews, T. E. Mason, W. J. L. Buyers, M. F. Collins, A. A. Menovsky, J. A. Mydosh, and J. K. Kjems, Phys. Rev. B **43**, 12809 (1991).

[30] G. Knopp, A. Loidl, K. Knorr, L. Pawlak, M. Duczmal, R. Caspary, U. Gottwick, H. Spille, F. Steglich, and A. P. Murani, Z. Phys. B **77**, 95 (1989).

[31] K. Ueda, Y. Kitaoka, H. Yamada, Y. Kohori, T. Kohara, and K. Asayama, J. Phys. Soc. Jpn. **56**, 867 (1987).

[32] T. Moriya and T. Takimoto, J. Phys. Soc. Jpn. **60**, 2122 (1992).

[33] S. Kambe, S. Raymond, L. P. Regnault, J. Flouquet, P. Lejay, and P. Haen, J. Phys. Soc. Jpn. **65**, 3294 (1996).

[34] K. Umeo, H. Kadomatsu, and T. Takabatake, Phys. Rev. B **55**, 692 (1997).

[35] A. Ishigaki and T. Moriya, J. Phys. Soc. Jpn. **65**, 3402 (1996).

[36] S. Ohsugi, Y. Kitaoka, K. Ishida, and K. Asayama, J. Phys. Soc. Jpn. **60**, 2351 (1991).

[37] Y. Kohori, T. Kohara, H. Shibai, Y. Oda, T. Kaneko, Y. Kitaoka, and K. Asayama, J. Phys. Soc. Jpn **56**, 2263 (1987); ibid. Jpn. J. Appl. Phys. Suppl. **26**, 1239 (1987).

[38] F. Thomas, C. Ayache, I. A. Fomine, J. Thomasson, and C. Geibel, J. Phys.: Condens. Matter **8**, L51 (1996).

[39] S. Nakamura, T. Moriya, and K. Ueda, J. Phys. Soc. Jpn. **65**, 4026 (1996).

[40] S. C. Zhang, Science **275**, 1089 (1997).

Chapter 4

Si-NMR study of antiferromagnets $CePd_2Si_2$ and $CeRh_2Si_2$

4.1 Introduction

$CePd_2Si_2$ and $CeRh_2Si_2$ are isostructural compounds to the heavy-fermion (HF) superconductor $CeCu_2Si_2$ ($ThCr_2Si_2$ structure shown in Fig. 1.4). Both are known to order antiferromagnetically below a Néel temperature T_N which is about $T_N \sim 10$ K for $CePd_2Si_2$ and $T_N \sim 36$ K for $CeRh_2Si_2$ [1]. The latter compound has the highest ordering temperature of cerium-based HF systems. These compounds have been considered to be located at a magnetic side slightly off the magnetic-nonmagnetic boundary in the Doniach diagram, since these antiferromagnetic orders are easily suppressed by an application of small pressure as shown in Fig. 4.1 [2, 3, 4, 5]. These compounds show superconductivity around the critical pressure, $P_c \sim 27$ kbar in $CePd_2Si_2$ [6, 7] and ~ 9 kbar in $CeRh_2Si_2$ [8, 9], where the antiferromagnetic orders are suppressed.

The antiferromagnetic spin structure in $CePd_2Si_2$ has the wave vector of $q = (1/2, 1/2, 0)$ and its saturation moment is almost 0.7 μ_B [1, 10]. The magnetic structure is shown in Fig. 4.2. In $CeRh_2Si_2$ there exist two antiferromagnetic phases with the wave vector of $q_1 = (1/2, 1/2, 0)$ below $T_{N1} \sim 36$ K and $q_2 = (1/2, 1/2, 1/2)$ below $T_{N2} \sim 25$ K [1, 11, 12, 13]. The respective magnetic structures are indicated in Fig. 4.3 (a) and (c). In the case of $CePd_2Si_2$ the moments are pointing along the (110) direction, while in $CeRh_2Si_2$ the moments are aligned along the c axis.

$CePd_2Si_2$ and $CeRh_2Si_2$ are thus a suitable systems for the investigation of magnetic and electronic properties in the vicinity of antiferromagnetic to non-magnetic phase boundary. In this section we describe the Si-NMR studies in both compounds at ambient pressures.

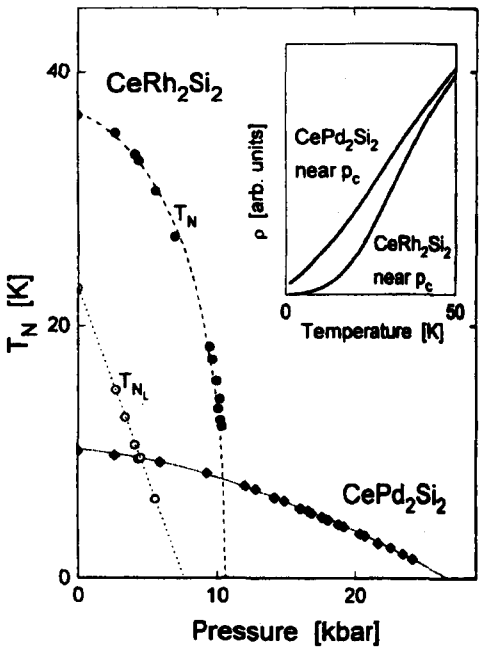

Figure 4.1 Comparison between the magnetic phase diagrams of $CePd_2Si_2$ and $CeRh_2Si_2$ as a function of hydrostatic pressure. The inset shows the temperature variations of the resistivities of the two materials, rescaled for comparison on the same diagram [6].

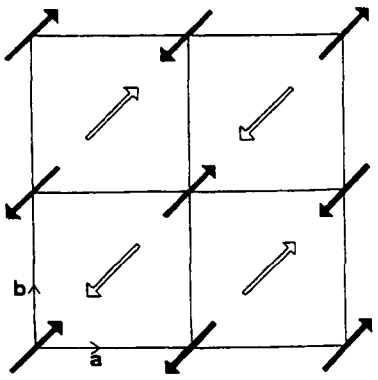

Figure 4.2 The spin configuration of $CePd_2Si_2$ below T_N shown projected into the c plane [1, 10].

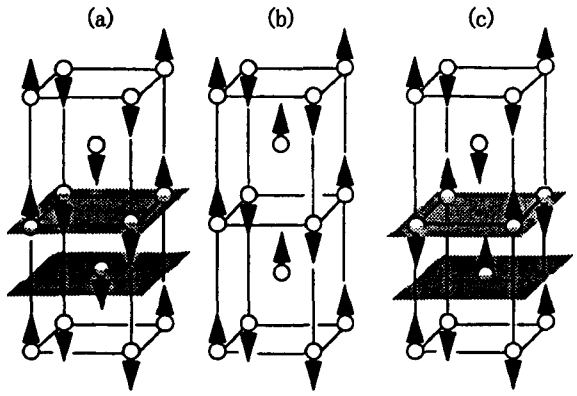

Figure 4.3 The spin structures with the wave vector of (a) $(1/2, 1/2, 0)$, (b) $(-1/2, 1/2, 0)$, and (c) $(1/2, 1/2, 1/2)$ [14].

4.2 Sample and characterization

Polycrystal ingot samples of $CePd_2Si_2$, $CeRh_2Si_2$, $LaPd_2Si_2$ and $LaRh_2Si_2$ were prepared by an argon-arc furnace. Stoichiometric quantities of Ce (3N), La (3N), Pd (3N), Rh (3N) and Si (5N) were melted in an argon atmosphere with zirconium getters, followed by annealing in vacuum for 4–5 days at 1000°C in $CePd_2Si_2$ and $LaPd_2Si_2$, and at 800°C in $CeRh_2Si_2$ and $LaRh_2Si_2$.

The X-ray diffraction experiment confirmed that all the samples are of a single phase with the $ThCr_2Si_2$-type structure. The magnetic susceptibility was measured at 1 kOe by using a SQUID magnetometer. The temperature variations of susceptibility, $\chi(T)$ in $CePd_2Si_2$ and $CeRh_2Si_2$ are indicated in Fig. 4.4. $\chi(T)$ has a sharp cusp at 10 K and 36 K for $CePd_2Si_2$ and $CeRh_2Si_2$, respectively, pointing to the onset of antiferromagnetic order. From the respective Curie-Weiss behavior in $\chi(T)$ above 60 K and 100 K in $CePd_2Si_2$ and $CeRh_2Si_2$, effective paramagnetic moments $\mu_{\rm eff}$ are estimated to be 2.61 $\mu_{\rm B}$ and 2.58 $\mu_{\rm B}$, which are close to 2.54 $\mu_{\rm B}$ for the trivalent Ce^{3+} state. These results are consistent with the previous results [10, 15].

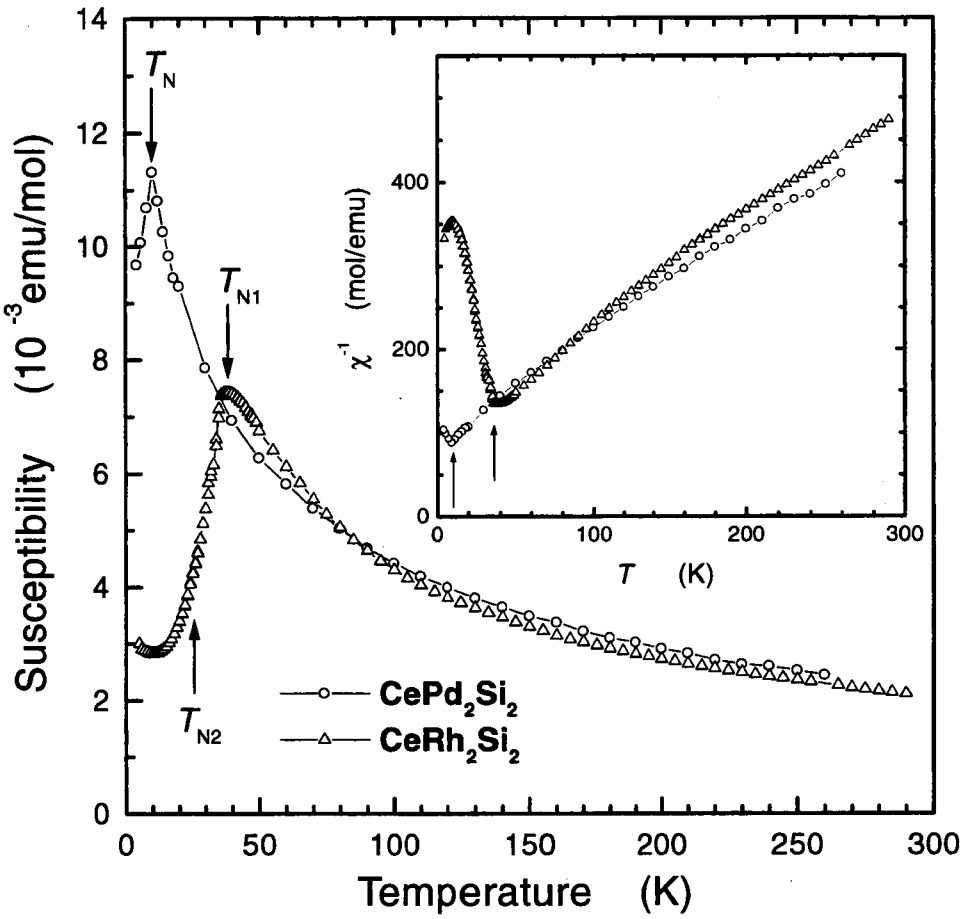

Figure 4.4 Temperature variations of the magnetic susceptibility, $\chi(T)$ of $CePd_2Si_2$ and $CeRh_2Si_2$. Inset shows the inverse susceptibility, $\chi^{-1}(T)$.

4.3 Results and discussion

4.3.1 NMR spectrum in $CePd_2Si_2$

paramagnetic state

Figure 4.5 (a) indicates the temperature dependence of Si-NMR spectrum above T_N = 10 K for partially-oriented powder $CePd_2Si_2$, where [110] direction is parallel to an external field H_0. As compared with the spectrum of unoriented powder sample at 11.4 K shown in the inset of Fig. 4.5 (a), the NMR linewidth in the oriented powder is one-third narrower than that in the unoriented one. This allows us to measure the Knight shift precisely. In Fig. 4.6 is shown the temperature dependence of the Knight shift, $K_{ab}(T)$ parallel to [110]. The inset of Fig. 4.6 indicates $K_{ab}(T)$ vs. $\chi_{ab}(T)$ plot with the temperature as an implicit parameter. The susceptibility, χ_{ab} parallel to [110] in the single crystal was used [10]. K_{ab} is nearly proportional to χ_{ab}. From a linear fit to the data, as drawn by solid line, a hyperfine-coupling constant A_{hf} = 2.84 kOe/μ_B is obtained from the relation of $K_{ab} = (A_{hf}/N\mu_B)\chi_{ab}$, where N is the Avogadro's number and μ_B is the Bohr magneton.

antiferromagnetic state

Below T_N, the spectrum is markedly affected by the appearance of the internal field H_{int} at the Si sites as seen in Fig. 4.5 (b). The spectrum forms a rectangular shape characteristic for the antiferromagnetic powder pattern for $H_0 \gg H_{int}$. The orientation of powder seems to be disturbed below T_N associated with some change in the anisotropy of susceptibility. In Fig. 4.7 is shown the temperature dependence of the half width at half maximum (HWHM) proportional to H_{int}. As seen in the figure, H_{int} increases to $\sim$ 530 Oe at 4.2 K as temperature decreases below T_N. It is evident that $H_{int}(T)$ is in good agreement with the temperature dependence of the square root of the ND intensity proportional to M_{AF} [1]. In this antiferromagnetic-spin structure with $q = (1/2, 1/2, 0)$, the direction of M_{AF} is aligned along [110] and, hence, H_{int} is produced through the transferred hyperfine interaction with one Ce antiferromagnetic moment in the five nearest neighbor Ce sites. This is because the contributions from the four Ce antiferromagnetic moments in the basal plane are canceled out at the Si sites. The isotropic transferred hyperfine-coupling constant H_{thf} per Ce 1 μ_B is estimated to be $A_{hf}/5 \sim 568$ Oe/μ_B. By using H_{int} = 532 Oe, an estimate of its size at 4.2 K gives rise to M_{AF}(NMR) $\sim$ 0.94 μ_B from the ratio of 532(Oe)/568(Oe/μ_B), which is somewhat larger than M_{AF}(ND) $\sim$ 0.7 μ_B.

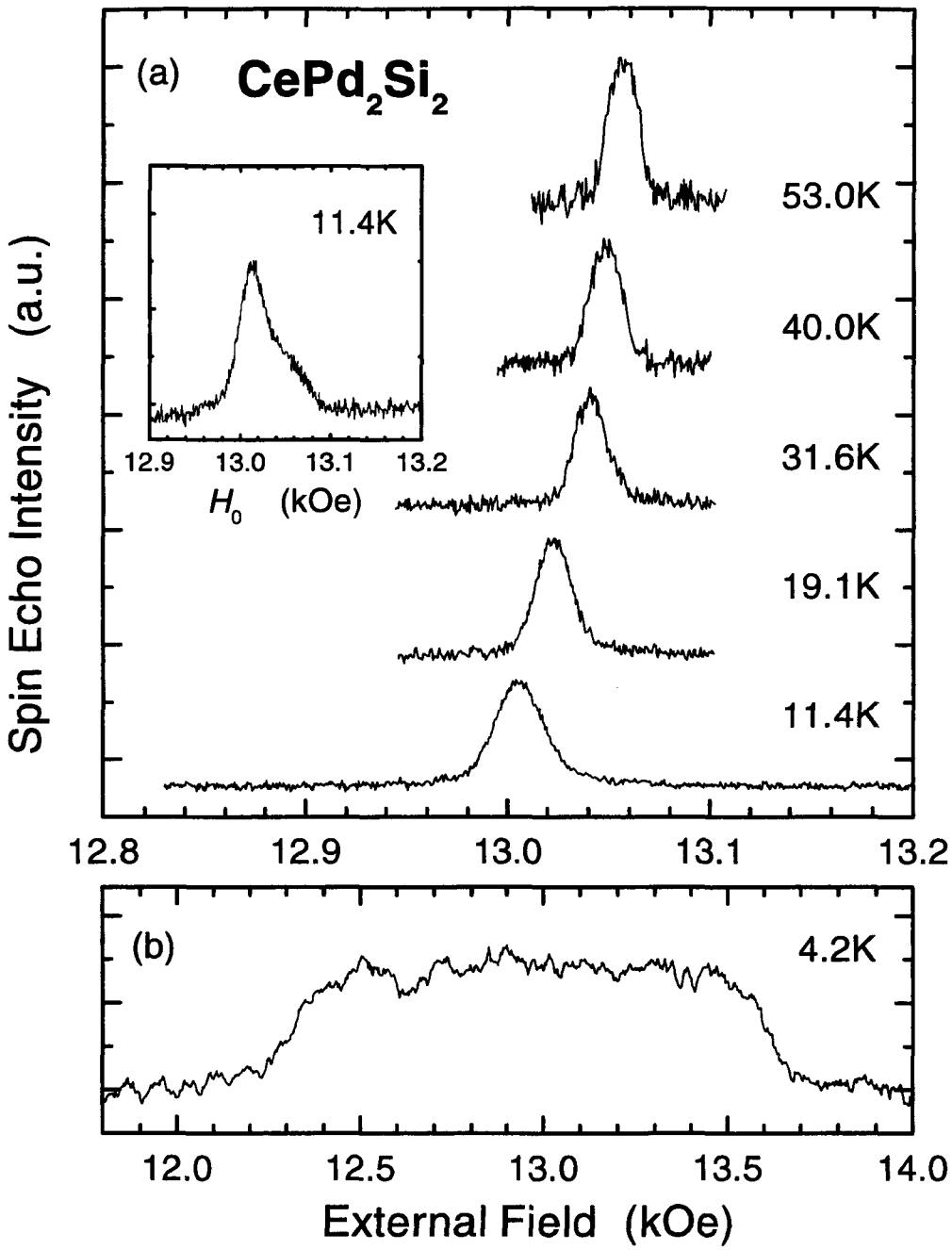

Figure 4.5 The Si-NMR spectra of oriented powder $CePd_2Si_2$ with [110] direction parallel to the external field (a) above and (b) below T_N. Inset shows the NMR spectrum for unoriented powdered sample.

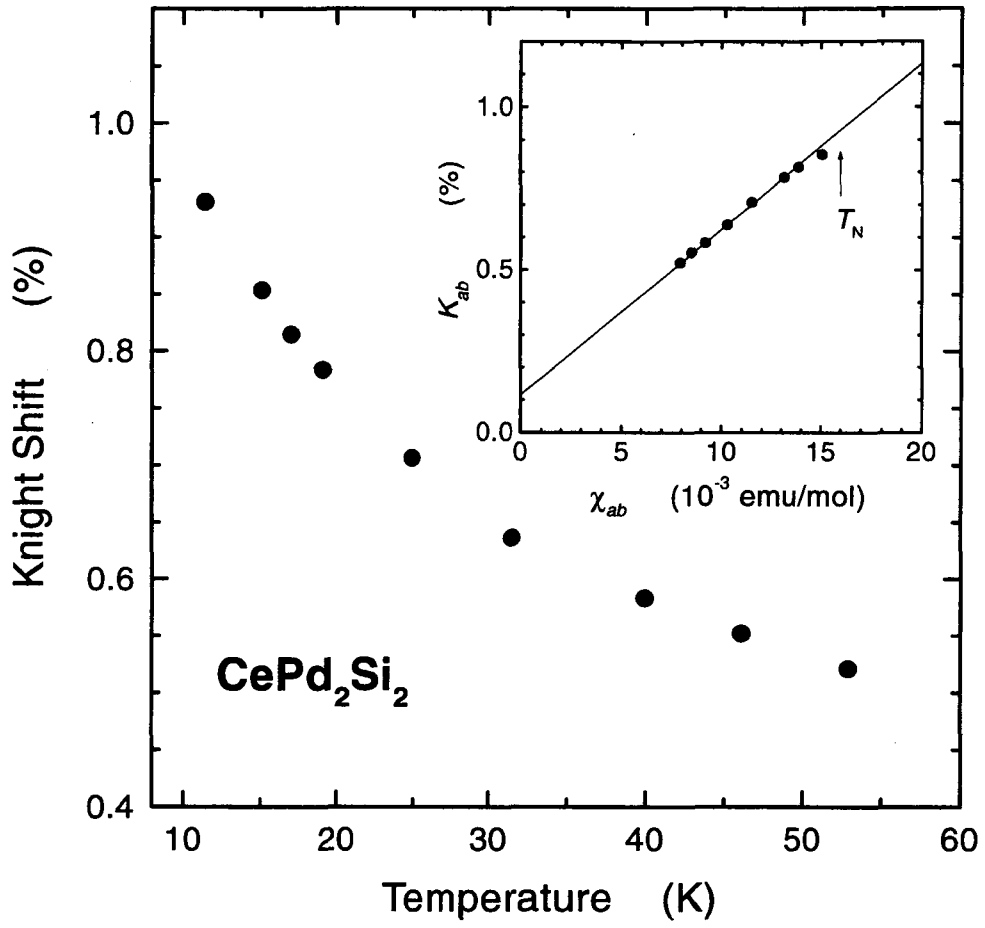

Figure 4.6 Temperature dependence of the Knight shift K_{ab} parallel to [110] direction. Inset shows the $K_{ab}(T)$ vs. $\chi_{ab}(T)$ plot for $CePd_2Si_2$. Solid line indicates a best fit to the data with $A_{\rm hf}$ =2.84 kOe/$\mu_{\rm B}$.

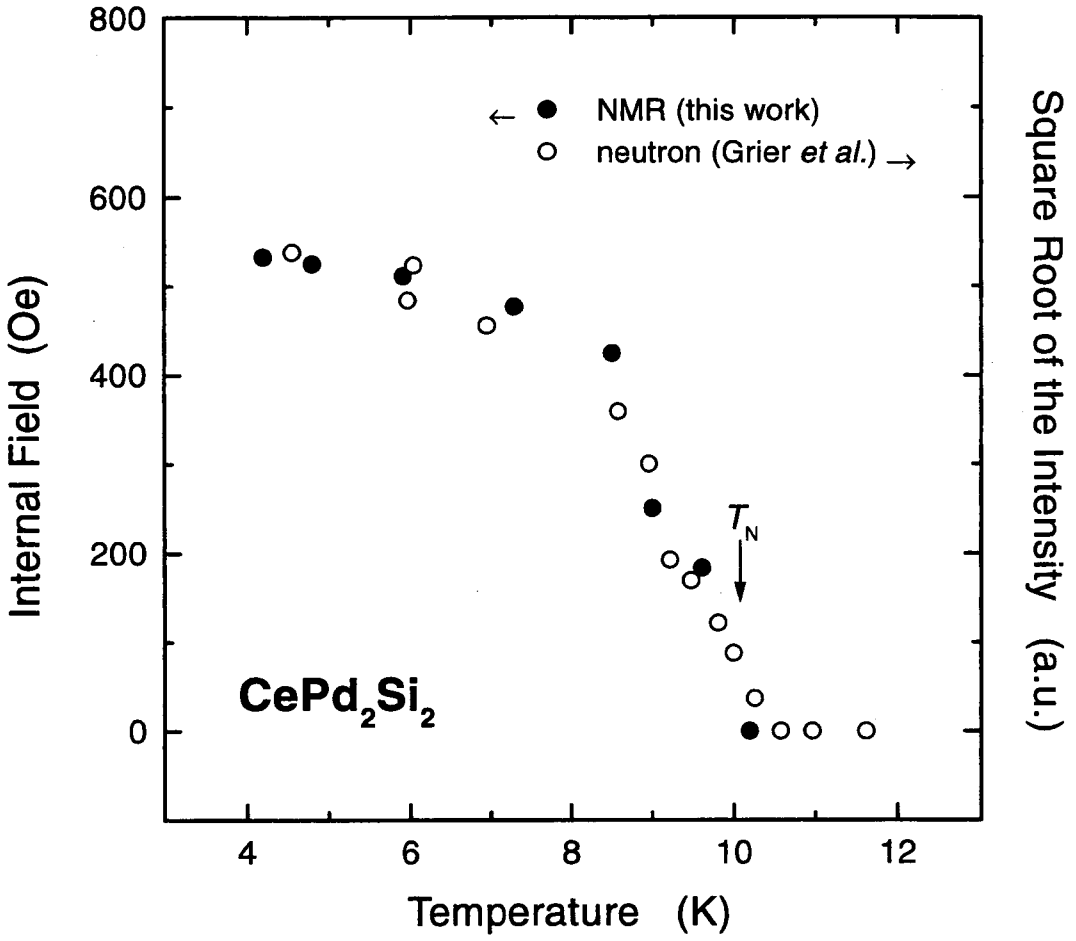

Figure 4.7 Temperature dependence of the half width at half maximum (HWHM) in the Si-NMR spectrum of $CePd_2Si_2$ below T_N. HWHM is proportional to the internal field H_{int}. Open circle shows the square root of the neutron magnetic scattering intensity [1].

4.3.2 NMR spectrum in $CeRh_2Si_2$

Figure 4.8 indicates the temperature dependence of Si-NMR spectrum at 25.14 MHz for the oriented powder $CeRh_2Si_2$ with the c-axis parallel to H_0. The NMR spectrum above T_N consists of a single peak. The Knight shift K_c increases upon cooling in proportion to susceptibility as seen in Fig. 4.9. Inset displays the K_c vs. χ_c plot with χ_c parallel to the c axis for the single crystal [16]. From a slope in the K_c vs. χ_c plot, a hyperfine-coupling constant is deduced to be $A_{hf} = 2.34$ kOe/μ_B.

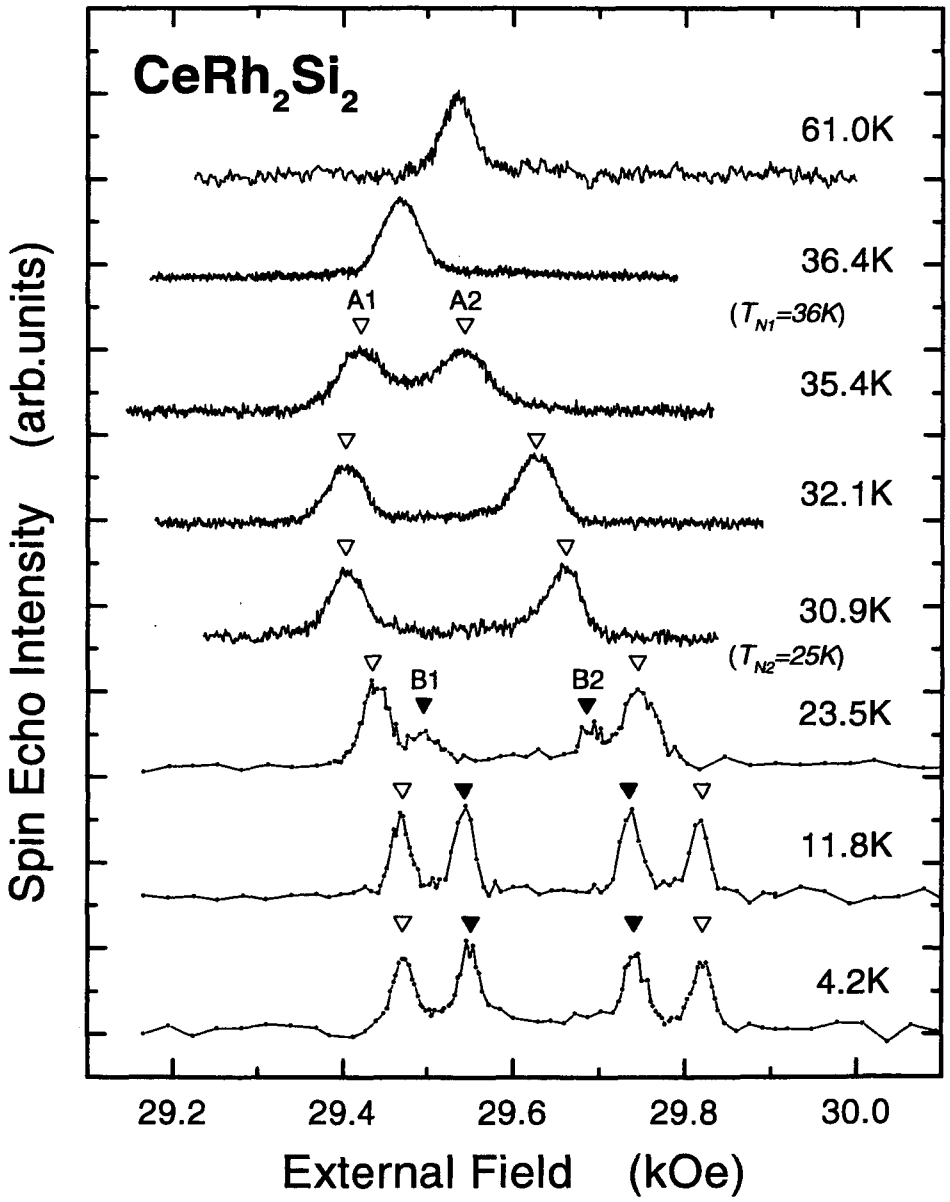

Figure 4.8 The Si-NMR spectra of $CeRh_2Si_2$ at $f = 25.14$ MHz with the c-axis parallel to the external field.

As seen in Fig. 4.8, the spectrum below $T_{N1} = 36$ K splits into two peaks (A1 and A2) due to the appearance of the first antiferromagnetic phase with $q_1 = (1/2, 1/2, 0)$. Below $T_{N2} = 25$ K where the secondary antiferromagnetic phase sets in, the two peaks (B1 and B2) newly appear. We show the spin-echo intensities of peak A (A1 and A2) and peak B (B1 and B2) as a function of temperature in Fig. 4.10. The intensities of A1 and A2 decrease rapidly below $T_{N2} = 25$ K but remain about half volume. The intensities of A1, A2, B1 and B2 are independent of the temperature below $\sim$ 23 K where both the intensities for the A and B peaks are comparable to each other. In Fig. 4.11 are shown the respective temperature variations of $H_{A,int}(T)$ and $H_{B,int}(T)$ which are obtained from a half value of separation in the A and B peaks. $H_{A,int} = 161$ Oe and $H_{B,int} = 101$ Oe stay constant below 23 K, which means that both the M_{AF}'s are totally saturated just below $T_{N2} = 25$ K.

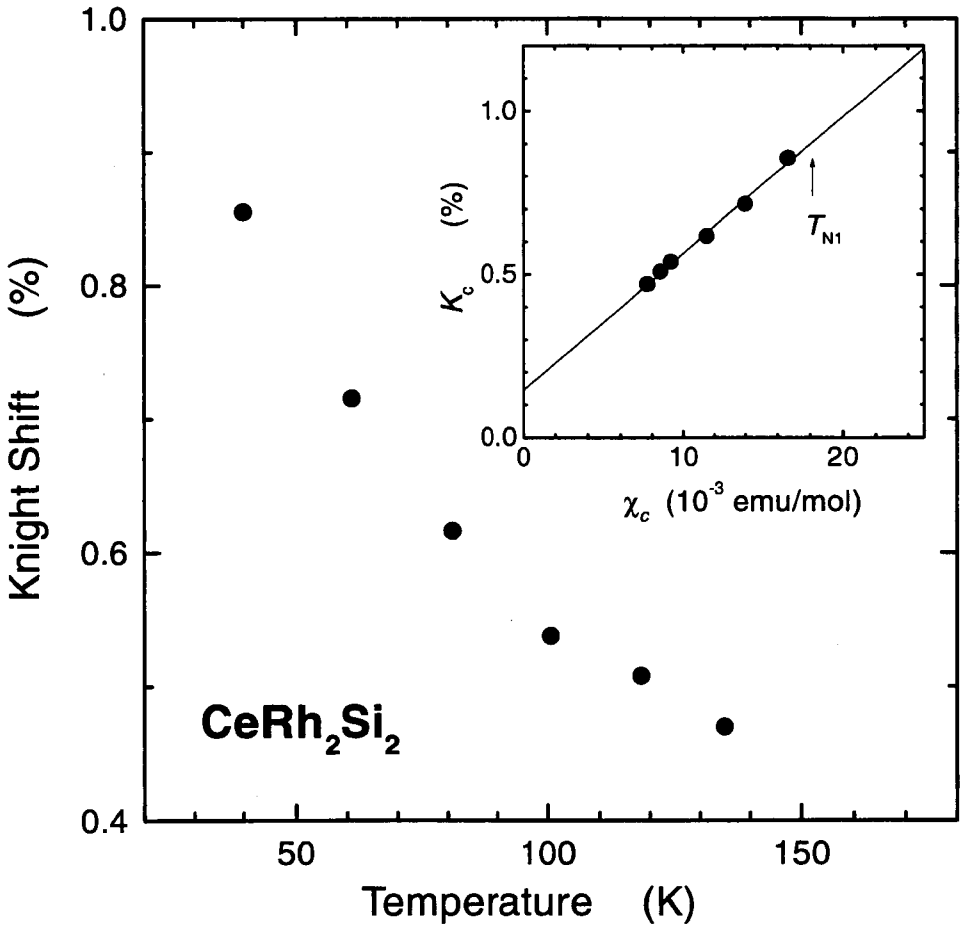

Figure 4.9 Temperature dependence of the Knight shift K_c in $CeRh_2Si_2$. Inset shows $K_c(T)$ vs. $\chi_c(T)$ plot. Solid line indicates a best fit to the data with $A_{hf\|}$ =2.34 kOe/μ_B.

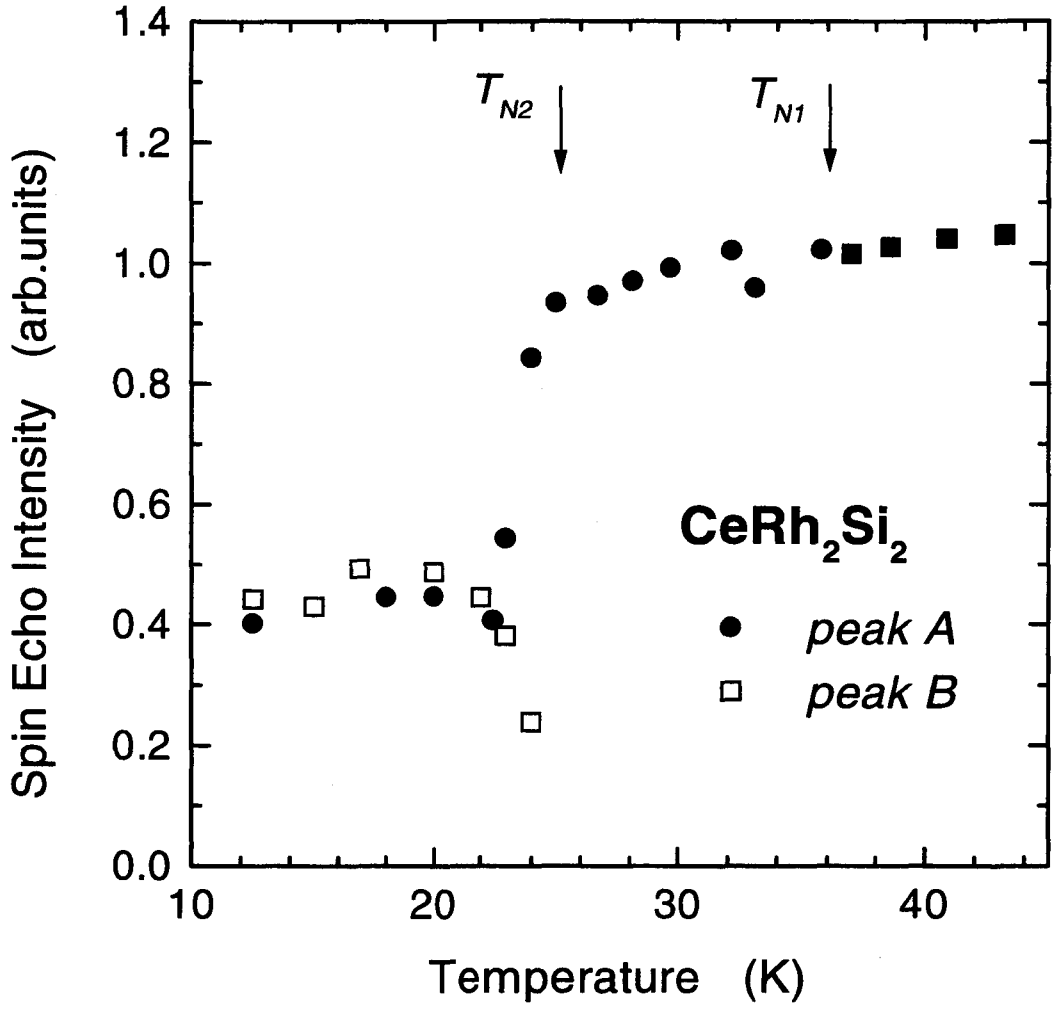

Figure 4.10 Spin-echo intensities of peak A (A1 and A2) and peak B (B1 and B2) as a function of temperature.

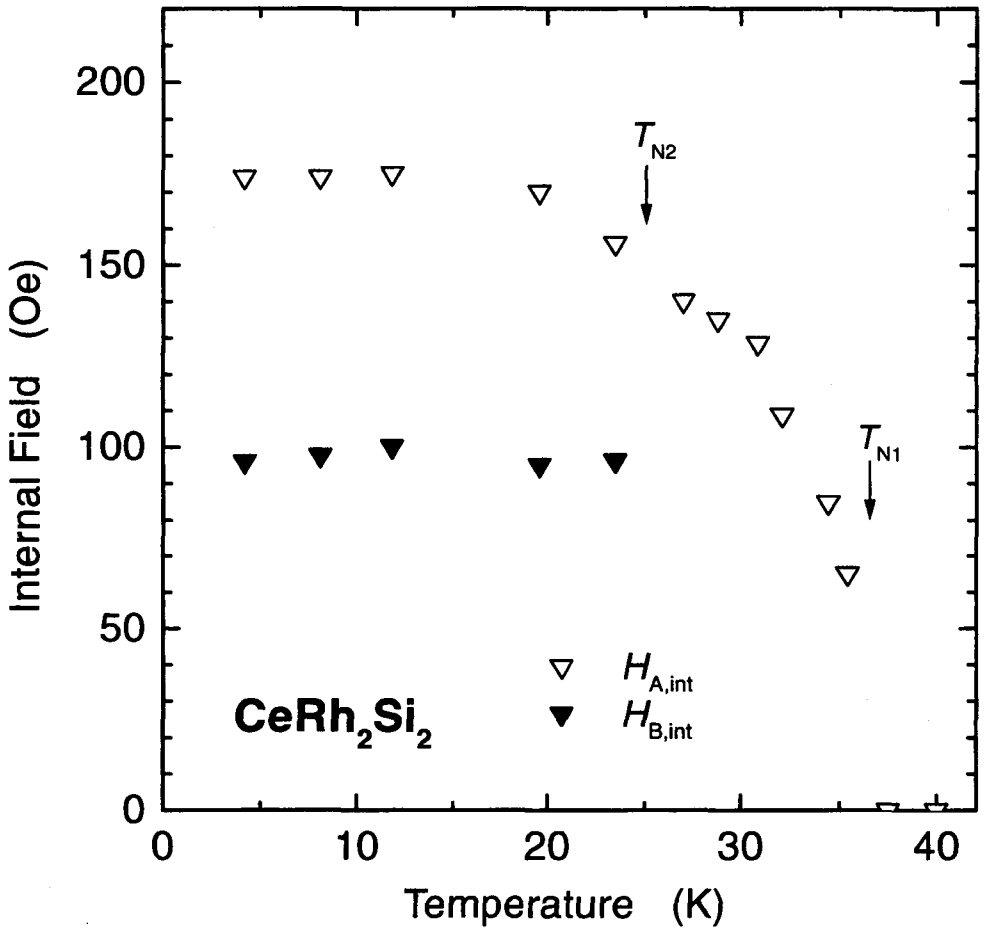

Figure 4.11 Temperature dependence of the internal fields, $H_{\mathrm{A,int}}(T)$ and $H_{\mathrm{B,int}}(T)$ which are obtained from the half value of separation in the A and B peaks in Fig. 4.8.

magnetic structure and comparison with neutron-diffraction results

The ND measurements revealed that the two independent magnetic reflections with $q_1 = (1/2, 1/2, 0)$ and $q_2 = (1/2, 1/2, 1/2)$ coexist at low temperatures, indicative of two possible magnetic structures [1, 11, 12]. A scenario is that two antiferromagnetic phases exist with different magnetic moment and antiferromagnetic wave vectors, $M_{q_1} = 1.86$ μ_B with q_1 (denoted as q_1 domain) and $M_{q_2} = 1.69$ μ_B with q_2 (denoted as q_2 domain). Another one is that two magnetic structures are superimposed in the single magnetic phase, which yields the modulated structure with the two kinds of moments 2.52 and 0.12 μ_B. For either case, the two Si sites should exist with the different H_{int}. The ratio of internal field $H_{A,int}/H_{B,int} = 161/101 \sim 1.59$ deduced from NMR is comparable to the ratio of M_{AF}, $M_{q_1}/M_{q_2} = 1.86/1.69 \sim 1.1$ for the former scenario, but far from $2.52/0.12 \sim 21$ for the latter scenario. From the NMR spectrum combined with the ND results, it is concluded that the two antiferromagnetic domains coexist below T_{N2}. The comparable NMR intensities in the A and B peaks indicate that each domain occupies half volume.

In estimating M_{AF} for each domain, we notice that one Ce moment in the five nearest neighbor Ce sites yields a dominant transferred hyperfine field, H_{thf} at the Si sites. This is because a sum of H_{thf} at the Si sites arising from the four Ce moments in the basal plane becomes zero in $CeRh_2Si_2$ as well as in $CePd_2Si_2$. From the relation of $H_{thf} = A_{hf}/5 = 467$ Oe/μ_B with $A_{hf} = 2.34$ kOe/μ_B, the M_{AF} in the q_1 and q_2 domains are estimated to be 0.36 and 0.22 μ_B, respectively. A novel result is that $M_{AF}(NMR) = 0.36$ and 0.22 μ_B are significantly reduced than $M_{AF}(ND) = 1.86$ and 1.69 μ_B in the q_1 and q_2 domain, respectively. This is in a striking contrast with the result in $CePd_2Si_2$ where $M_{AF}(NMR) \sim 0.9$ μ_B is comparable with $M_{AF}(ND) \sim 0.7$ μ_B. The fact that M_{AF} is apparently probe-dependent in $CeRh_2Si_2$ shows that the correlation time in fluctuations of f-electron moments is longer than the characteristic time of observation for thermal neutrons but shorter than for NMR.

The probe-dependence of M_{AF} was reported in the uranium HF compounds UPt_3[17, 18, 19, 20] and URu_2Si_2 [21, 22, 23]. In these compounds the saturation moments are as small as $\sim 10^{-2}$ μ_B from ND, but no indication of H_{int} from NMR was observed. The antiferromagnetic saturation moments in $CeRh_2Si_2$, which are two orders of magnitude larger than those in UPt_3 and URu_2Si_2, may make it easy to detect the reduced magnetic moments in $CeRh_2Si_2$ by NMR. Such the probe-dependent aspect of M_{AF} in $CeRh_2Si_2$ may be explored from the μSR experiment as well.

The recent ND result on the single crystal [14], which is consistent with the previous ND results by Grier *et al.* [1], has revealed that the q_1 domain involves two structures with crystallographically equivalent wave numbers of $q_1^+ = (1/2, 1/2, 0)$ and $q_1^- = (-1/2, 1/2, 0)$. These magnetic structures are indicated in Fig. 4.2. Combined with the NMR results, they concluded that the three phases form antiferromagnetic domain-superlattice structure with 1.42 μ_B for the q_1^+ and q_1^- domains and 1.34 μ_B for the q_2

domain. We stress that these values are significantly different from those obtained from NMR as well. In magnetic structures with wave vectors of $(1/2, 1/2, c)$ in the body-centered lattice, the magnetic interaction is independent of c between the nearest neighbor c-planes and hence has a similar energy between each domain. This may be a main reason why the antiferromagnetic domain-superlattice structure is stabilized as the peculiar ground magnetic structure. Furthermore, due to the small energy difference between each domain, thermal and/or quantum fluctuations of each domain are likely sources for the estimate in M_{AF} being probe-dependent in $CeRh_2Si_2$. This novel magnetic state may be responsible for the small critical pressure $P_c \sim 0.9$ GPa regardless of the large value of T_{N1}.

4.3.3 Nuclear spin-lattice relaxation rate, $1/T_1$

Measurements of the nuclear spin-lattice relaxation rate, $1/T_1$ were performed at $f =$ 11.1 MHz for $CePd_2Si_2$, $LaPd_2Si_2$ and $LaRh_2Si_2$. The $1/T_1$ in $CeRh_2Si_2$ was measured at $f = 25.1$ MHz at the Al peak in an entire temperature range. $1/T_1$ in all the compounds was uniquely determined with a single T_1 component. Figure 4.12 shows the temperature dependence of $1/T_1$ in $CePd_2Si_2$ (closed circles) and $CeRh_2Si_2$ (closed triangles) together with those in $LaPd_2Si_2$ (open circles) and $LaRh_2Si_2$ (open triangles). A $T_1T =$ constant behavior for $LaPd_2Si_2$ and $LaRh_2Si_2$ is observed with respective value of $(T_1T)^{-1} \sim 0.079$ $(K\cdot sec)^{-1}$ and 0.040 $(K\cdot sec)^{-1}$. The $1/T_1$ in $CeRh_2Si_2$ is in agreement with the previous results [24].

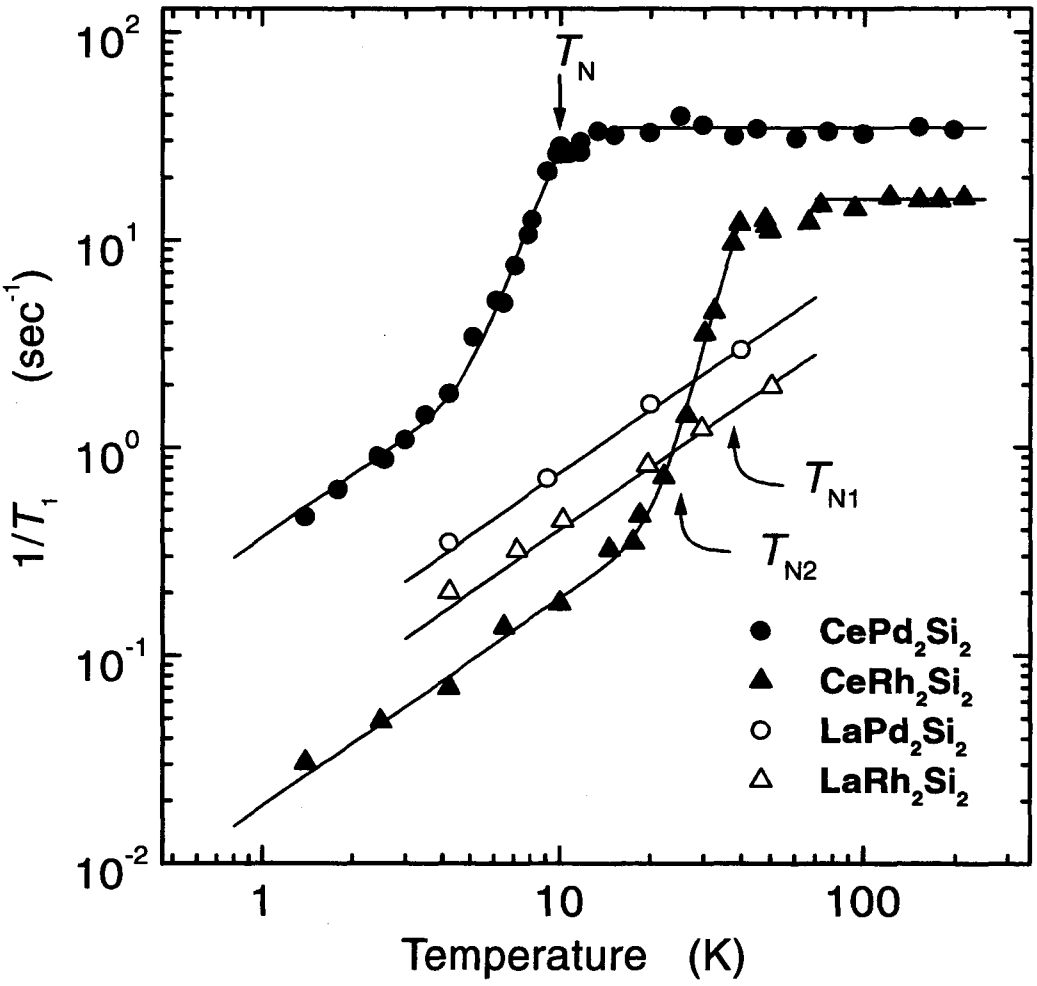

Figure 4.12 Temperature variations of the spin-lattice relaxation rate, $1/T_1$ for $CePd_2Si_2$ (closed circles), $CeRh_2Si_2$ (closed triangles), $LaPd_2Si_2$ (open circles) and $LaRh_2Si_2$ (open triangles).

paramagnetic state

In the high temperature region, the c-f hybridization is not so strong that the experimental relaxation rate, $(1/T_1)_{\rm exp}$ can be decomposed to two parts; the relaxation rate from the $4f$ electrons and the conduction electrons,

$$\left(\frac{1}{T_1}\right)_{\rm exp} = \left(\frac{1}{T_1}\right)_{4f} + \left(\frac{1}{T_1}\right)_{\rm cond}. \tag{4.1}$$

The latter could be known from $1/T_1$ in $LaPd_2Si_2$ and $LaRh_2Si_2$ without Ce ions. The correlation rate in fluctuations of $4f$ electrons, $1/\tau_{\rm NMR}$ can be estimated with the following relation obtained from eq. (1.6),

$$\frac{1}{\tau_{\rm NMR}} = 2Nk_{\rm B}T\gamma_{\rm n}^2 z\left(\frac{K_{4f}}{z}\right)^2 \frac{(T_1)_{4f}}{\chi}. \tag{4.2}$$

Here $\gamma_{\rm n}$ and K_{4f} are the nuclear gyromagnetic ratio of ^{29}Si nucleus and the Knight shift originating from the $4f$ electrons, respectively. K_{4f} is evaluated from subtracting contribution of the conduction electrons, which is estimated from the Knight shift of $LaPd_2Si_2$ with T-independent, $K_{\rm s} = 0.10\%$. We assume $z = 5$, the number of nearest neighboring Ce ions from Si site. Fig. 4.13 (b) shows the temperature variations of $\hbar/\tau_{\rm NMR}$ and the quasi-elastic neutron scattering linewidth $\Gamma/2$ in $CePd_2Si_2$ [26], where $\Gamma/2$ is the direct measurement of $\hbar/\tau$. Both the temperature variations of $\hbar/\tau_{\rm NMR}$ and $\Gamma/2$ reveal significant deviations from a linear Korringa-type behavior.

The ratio $(\hbar/\tau_{\rm NMR})/(\Gamma/2)$ shown in Fig. 4.13 (a) is constant above 50 K. The constant behavior and the greater value of $(\hbar/\tau_{\rm NMR})/(\Gamma/2)$ than 1 indicates that the local field at Si site is affected by the uncorrelated spin fluctuations of Ce ions in spatial region more than first-nearest neighboring Ce ions. Below 50 K, $(\hbar/\tau_{\rm NMR})/(\Gamma/2)$ decreases gradually, suggesting that the spin fluctuations become correlated and coherent due to the strong c-f hybridization on cooling. The above discussion based on local moment regime is not valid in the low temperature close to $T_{\rm K}$, and instead the discussion based on coherent Kondo regime must be done.

In the high-temperature region, local spin fluctuations of $4f$ moments dominate the relaxation process, $1/T_1$ being nearly temperature independent above 12 K and 100 K for $CePd_2Si_2$ and $CeRh_2Si_2$, respectively. Empirically, the temperature at which $1/T_1$ starts to decrease from the T-independent behavior is regarded as a Kondo temperature $T_{\rm K}$ below which the systems enter a crossover regime towards the HF state. The $T_{\rm K}$ in $CePd_2Si_2$ is 12 K which is in good agreement with $T_{\rm K} \sim 10$ K determined from the quasi-elastic ND [25, 26]. The fact that $T_{\rm K}$ is comparable with the $T_{\rm N}$ in $CePd_2Si_2$ implies that the antiferromagnetic ordered state occurs before the HF state is fully established and its nature is anticipated to hold a localized character rather than an itinerant character. On the other hand, the $T_{\rm K}$ in $CeRh_2Si_2$ is estimated to be as high as $\sim$ 100 K, being much

higher than $T_K \sim 33$ K deduced from ND [26]. The fact that T_K is much higher than the T_N in $CeRh_2Si_2$ means that the antiferromagnetic order must be in the itinerant regime which makes magnetic interactions different from the conventional RKKY interaction.

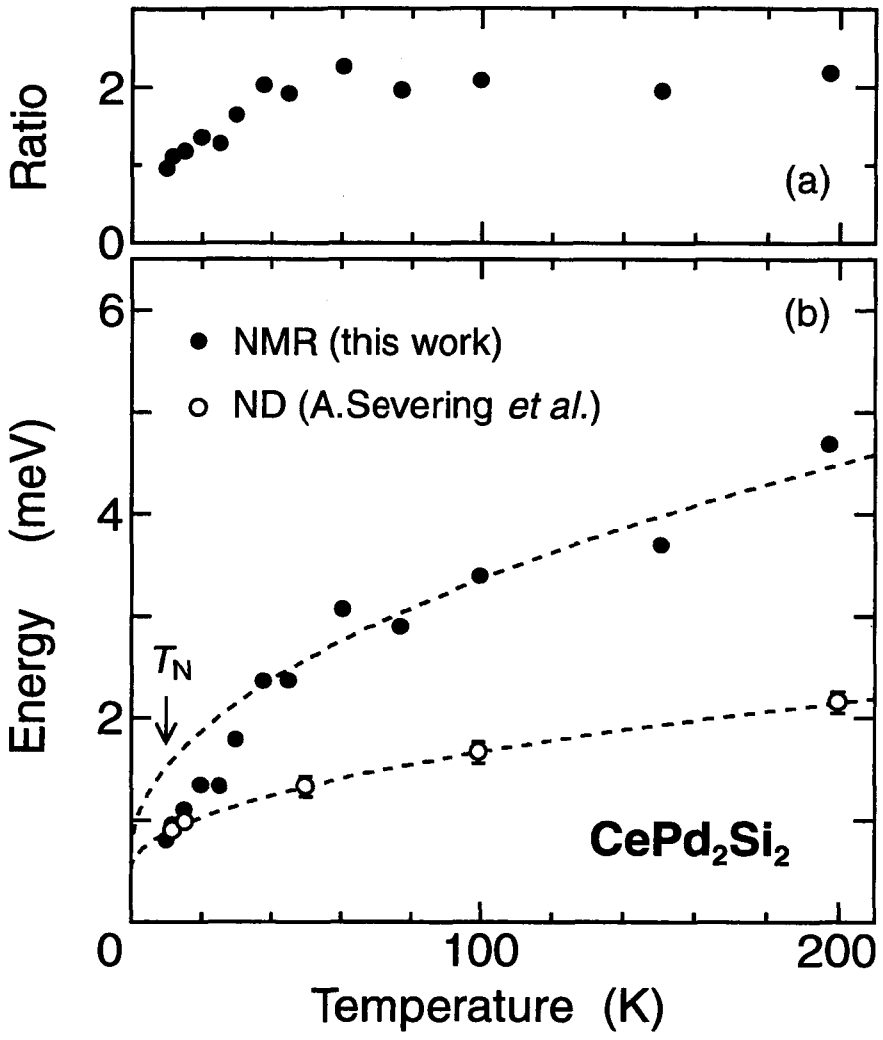

Figure 4.13 (a) The temperature dependence of the ratio, $(\hbar/\tau_{NMR})/(\Gamma/2)$. (b) The temperature variations of $\hbar/\tau_{NMR}$ obtained from this work (closed circles) and the quasi-elastic neutron scattering linewidth $\Gamma/2$ (open circles) [26] in $CePd_2Si_2$. These energies can be described with square-root dependences of $\hbar/\tau_{NMR}$ above 50 K and $\Gamma/2$ above $T_K \sim 10$ K as indicated by dash lines [27].

antiferromagnetic state

The $1/T_1$'s in both the compounds drop rapidly below T_N without any critical divergence near T_N. Any anomaly in $1/T_1$ is not appreciable around $T_{N2} = 25$ K in $CeRh_2Si_2$. Experimentally, $1/T_1$ below T_N is well reproduced by the following expression as

$$\frac{1}{T_1T} = A + B\exp\left(-\frac{E_g}{k_BT}\right),$$

as indicated by solid line of Fig. 4.12. An exponential drop in $1/T_1$ may be due to a partial loss of low-lying excitations below T_N. The energy gap E_g in $CePd_2Si_2$ is estimated to be 2.37 meV which is in good agreement with $E_g \sim 2.3$ meV in the spin-wave excitation spectrum probed by ND [25, 28]. The first term A is the quasi-particle contribution. The value of $1/T_1T \sim 0.33$ $(\text{sec}\cdot\text{K})^{-1}$ in $CePd_2Si_2$ below 4 K is larger than $1/T_1T \sim 0.079$ $(\text{sec}\cdot\text{K})^{-1}$ in $LaPd_2Si_2$. This suggests that a part of f-electrons which do not participate the antiferromagnetic ordered moments may have an itinerant character to form the HF state even far below T_N. On the other hand, the value of $1/T_1T \sim 0.0188$ $(\text{sec}\cdot\text{K})^{-1}$ in $CeRh_2Si_2$ below 10 K is smaller than $1/T_1T \sim 0.0402$ $(\text{sec}\cdot\text{K})^{-1}$ in $LaRh_2Si_2$. This result indicates that the Fermi-liquid excitation below 10 K is considered to originate from the HF band, which is the consequence of the strong c-f hybridization, since $1/T_1$ cannot be explained by the sum of two relaxation contributions from itinerant $4f$ electrons and conduction electrons. The result of $1/T_1$ also suggests that the magnetic order in $CeRh_2Si_2$ occurs in the HF regime, consistent with above-mentioned experimental results of higher T_K and the small ordered moments.

4.4 Conclusion

The Si-NMR studies in $CePd_2Si_2$ and $CeRh_2Si_2$ have revealed the novel differences in magnetic characteristics. The NMR results in $CePd_2Si_2$ are consistent with those obtained from the neutron-diffraction experiments as regarding the sizes in M_{AF}, T_K and the gap in the spin-wave excitation spectrum.

In contrast, the NMR results in $CeRh_2Si_2$ are unconventional. The further another splitting in NMR spectrum at $T_{N2} = 25$ K was found, indicating the novel magnetic structure consisting of independent antiferromagnetic domains. A notable result is that M_{AF}(NMR) = 0.36 and 0.22 μ_B are significantly smaller than M_{AF}(ND) = 1.86 and 1.69 μ_B. We have suggested that the correlation time in fluctuations of f-electron moments is longer than the characteristic time of observation for thermal neutrons, but shorter than that for NMR. This probe dependence of M_{AF} was observed in the the uranium HF compounds UPt_3 and URu_2Si_2. Relevant to this, we propose that quantum spin fluctuations are responsible for this probe-dependence of M_{AF}. A probable source for quantum spin fluctuations may originate from fluctuations of each domain due to the small difference between the energies of each domain suggested from the recent neutron-diffraction experiments [14].

References

[1] B. H. Grier, J. M. Lawrence, V. Muragai, and R. D. Parks, Phys. Rev. B **29**, 2664 (1984).

[2] J. D. Thompson, R. D. Parks, and H. Borges, J. Magn. Magn. Mater. **54-57**, 377 (1986).

[3] P. Link, D. Jaccard, and P. Lejay, Physica B **223-224**, 50 (1996).

[4] T. Graf, J. D. Thompson, M. F. Hundley, R. Movshovich, Z. Fisk, D. Mandrus, R. A. Fisher, and N. E. Phillips, Phys. Rev. Lett. **78**, 3769 (1997).

[5] S. kawarazaki, M. Sato, Y. Miyako, N. Metoki, and M. Nishi, Proceedings of the 22nd International Conference on Low Temperature Physics, LT'99.

[6] F. M. Grosche, S. R. Julian, N. D. Mathur, and G. G. Lonzarich, Physica B **223-224**, 50 (1996); F. M. Grosche, S. R. Julian, N. D. Mathur, F. V. Carter, and G. G. Lonzarich, Physica B **237-238**, 197 (1997).

[7] S. R. Julian, C. Pfleiderer, F. M. Grosche, N. D. Mathur, G. J. McMullan, A. J. Diver, I. R. Walker, and G. G. Lonzarich, J. Phys.: Condens. Matter **8**, 9675 (1996).

[8] R. Movshovich, T. Graf, D. Mandrus, M. F. Hundley, J. D. Thompson, R. A. Fisher, N. E. Phillips, and J. L. Smith, Physica B **223-224**, 126 (1996); R. Movshovich, T. Graf, D. Mandrus, J. D. Thompson, J. L. Smith, and Z. Fisk, Phys. Rev. B **53**, 8241 (1996).

[9] T. Muramatsu, M. Takimoto, T. C. Kobayashi, K. Shimizu, K. Amaya, S. Araki, and Y. Ōnuki, Proceedings of the International Conference on Strongly Correlated Electron Systems, SCES'99.

[10] R. A. Steeman, E. Frikkee, R. B. Helmholdt A. A. Menovsky, J. van den Berg, G. J. Nieuwenhuys, and J. A. Mydosh, Solid State Comm. **66**, 103 (1988).

[11] S. Kawarazaki, Y. Kobashi, T. Taniguchi, Y. Miyako, and H. Amitsuka, J. Phys. Soc. Jpn. **63**, 716 (1994).

[12] S. Kawarazaki, Y. Kobashi, J. A. Fernandez-Baca, S. Murayama, Y. Ōnuki, and Y. Miyako, Physica B **206-207**, 298 (1995).

[13] T. Graf, M. F. Hundley, R. Modler, R. Movshovich, J. D. Thompson, D. Mandrus, R. A. Fisher, and N. E. Phillips, Phys. Rev. B **57**, 7442 (1998).

[14] S. Kawarazaki, M. Sato, N. Chigusa, Y. Miyako, N. Metoki, Y. Koike, M. Nishi, unpublished.

[15] S. Quezel, J. Rossat-Mignod, B. Chevalier, P. Lejay, and J. Etourneau, Solid State Comm. **49**, 685 (1984).

[16] R. Settai, A. Misawa, S. Araki, M. Kosaki, K. Sugiyama, T. Takeuchi, K. Kindo, Y. Haga, E, Yamamoto, and Y. Ōnuki, J. Phys. Soc. Jpn. **66**, 2260 (1997).

[17] G. Aeppli, E. Bucher, C. Broholm, J. K. Kjems, J. Baumann, and J. Hufnagl, Phys. Rev. Lett. **60**, 615 (1988); G. Aeppli, D. Bishop, C. Broholm, E. Bucher, K. Simensmeyer, M. Steiner, and N. Stüsser, Phys. Rev. Lett. **63**, 676 (1989).

[18] R. H. Heffner, D. W. Cooke, A. L. Giorgi, R. L. Hutson, M. E. Schillaci, H. D. Rempp, J. L. Smith, J. O. Willis, D. E. MacLaughlin, C. Boekema, R. L. Lichiti, J. Oostens, and A. B. Denison, Phys. Rev. B **39**, 11345 (1989).

[19] Y. Kohori, M. Kyogaku, T. Kohara, K. Asayama, H. Amitsuka, and Y. Miyako, J. Mag. Mag. Mater. **90-91**, 510 (1990).

[20] H. Tou, Y. Kitaoka, K. Asayama, N. Kimura, Y. Ōnuki, E. Yamamoto, and K. Maezawa, Phys. Rev. Lett. **77**, 1374 (1996).

[21] C. Broholm, J. K. Kjems, W. J. L. Buyers, P. Matthews, T. T. M. Palstra, A. A. Menovsky, and J. A. Mydosh, Phys. Rev. Lett. **58**, 1467 (1987); C. Broholm, H. Lin, P. Matthews, T. E. Mason, W. J. L. Buyers, M. F. Collins, A. A. Menovsky, J. A. Mydosh, and J. K. Kjems, Phys. Rev. B **43**, 12809 (1991).

[22] M. B. MacLaughlin, C. Boekema, R. L. Lichti, and J. Oostens, Phys. Rev. **B37**, 3153 (1988).

[23] Y. Kohori, K. Matsuda, and T. Kohara, J. Phys. Soc. Jpn. **65**, 1083 (1996).

[24] K. Fujiwara, K. Kumagai, C. Sekine, and S. Murayama, Physica B **186-188**, 517 (1993).

[25] B. H. Grier, J. M. Lawrence, S. Horn, and J. D. Thompson, J. Phys. C **21**, 1099 (1988).

[26] A. Severing, E. Holland-Moritz, and B. Frick, Phys. Rev. B **39**, 4164 (1989).

[27] N. E. Bickers, D. L. Cox, and J. W. Wilkins, Phys. Rev. Lett. **54**, 230 (1985).

[28] F. Hippert, B. Hennion, J.-M. Mignot, and P. Lejay, J. Magn. Magn. Mater. **108**, 177 (1992).

Chapter 5

Ru-NMR/NQR study of metamagnetic transition in $CeRu_2Si_2$

5.1 Introduction

The heavy-fermion (HF) compound $CeRu_2Si_2$ crystallizes in the $ThCr_2Si_2$-type structure and shows a rather large value of the temperature-linear coefficient in the specific heat, $\gamma \sim 350$ mJ/mol·K^2 [1]. Although any long-range magnetic order has not been observed down to 20 mK [2, 3] except for the μSR report [4], some antiferromagnetic (AF) order takes place by the substitution of $\sim 8\%$ La for Ce [5], or of $\sim 6\%$ Ge for Si [6]. It suggests that $CeRu_2Si_2$ is close to the quantum critical transition from a Pauli paramagnetic to a long-range magnetically ordered state. Among rich variety of ground states realizing in the HF compounds, the polarized magnetic phase of $CeRu_2Si_2$ is particularly interesting, since a large continuous jump of the magnetization occurs at $H_M = 7.7$ T as indicated in Fig. 5.1 [7, 8].

From systematic measurements such as susceptibility, thermal expansion [9] and specific heat[10] under the magnetic field, it was shown that the effective mass is enhanced at H_M, whereas it is reduced for $H > H_M$. From these results, it was suggested that an application of magnetic field higher than H_M disturbed the HF state appreciably.

Inelastic neutron scattering experiments [11] provided valuable information about a possible evolution in spin fluctuation spectra around H_M. Fig. 5.2 shows q-scan spectra performed at $H = 0$ at an energy $\hbar\omega \sim 1.6$ meV, showing the presence of two competing magnetic correlations. These AF intersite contributions are superimposed to a large localized (q-independent) part well above the background level. The effect of the magnetic field on these neutron intensities is shown in Fig. 5.3. The q-independent magnetic response is nearly independent of the magnetic field, whereas the magnetic signal peaked at the q-vector (0.7, 0.7,0) collapse at H_M. The result suggests that the metamagnetic transition is associated with a drastic change of the magnetic correlations corresponding to the depression of AF intersite spin fluctuations and the emergence of ferromagnetic correlations above H_M. A high value reached by the magnetic polarization leads to a situation similar to ferromagnetism in this regular array of Ce ions.

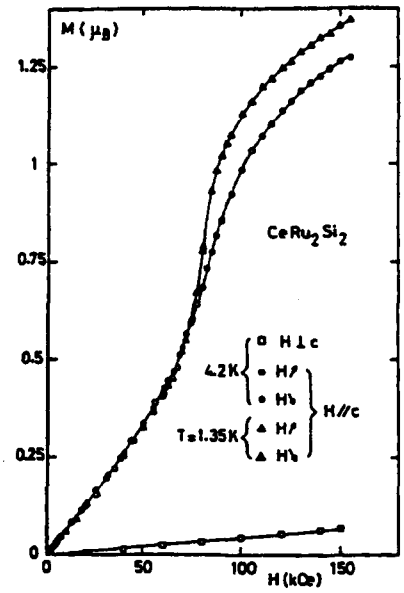

Figure 5.1 Magnetization of $CeRu_2Si_2$ measured parallel and perpendicular to c-axis in increasing and decreasing field at 4.2 and 1.35 K [8].

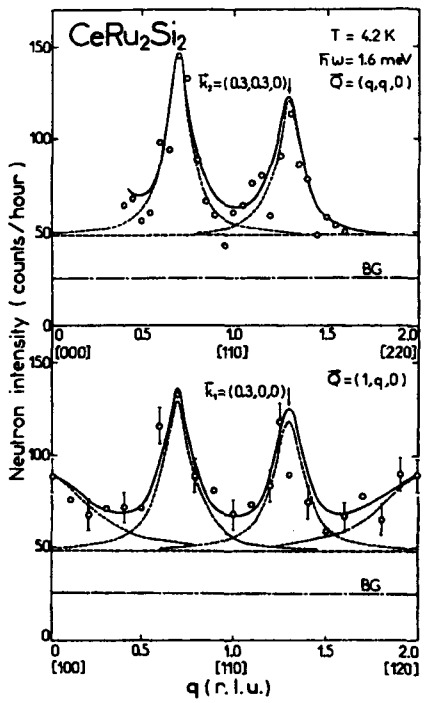

Figure 5.2 q-scans performed at constant energy transfer, $\hbar\omega \sim 1.6$ meV in $CeRu_2Si_2$ at $H = 0$ T [11].

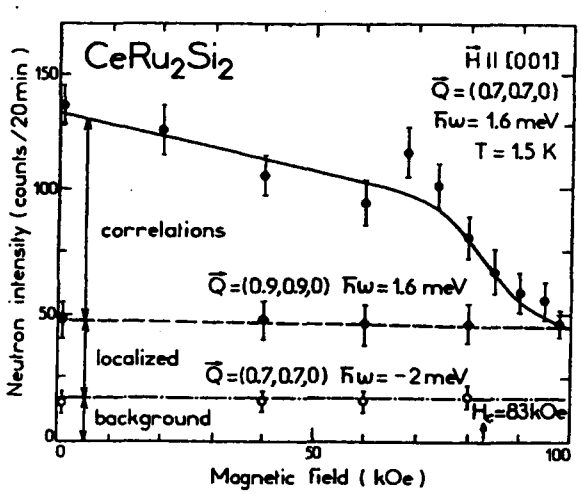

Figure 5.3 Field variations of the neutron intensities at 1.5 K: closed circles for (0.7, 0.7, 0), closed boxes for (0.9, 0.9, 0) and open circles at negative energy transfer for the background determination [11].

In order to investigate a low-lying excitation in the HF state, ^{29}Si-NMR studies in $CeRu_2Si_2$ were reported for $H < H_M$ [12, 13]. Fig. 1.5 shows the temperature dependence of nuclear spin-lattice relaxation rate, $1/T_1$ in $CeRu_2Si_2$ at $H \sim 1.1$ T [14]. From the constant behavior in $1/T_1T$ and the Knight shift against the temperature, it was claimed that the HF state was realized below 8 K and that Kondo temperature, T_K was around 20 K in good agreement with the estimation from the quasi-elastic of neutron scattering linewidth [12]. A systematic NMR investigation is, however, not yet performed either above H_M nor in zero magnetic field. In this chapter, we describe the first Ru-NQR and -NMR studies in $CeRu_2Si_2$ and $LaRu_2Si_2$. A successful observation of Ru-NQR signal has allowed us to obtain the magnetic property in zero magnetic field.

5.2 Sample and characterization

Polycrystalline sample of $CeRu_2Si_2$ was prepared from high purity starting materials. The sample was crushed into powder with diameter less than 35 μm. Powder sample is preferentially aligned with the c axis parallel to the external field as reported in the Si-NMR measurement [12].

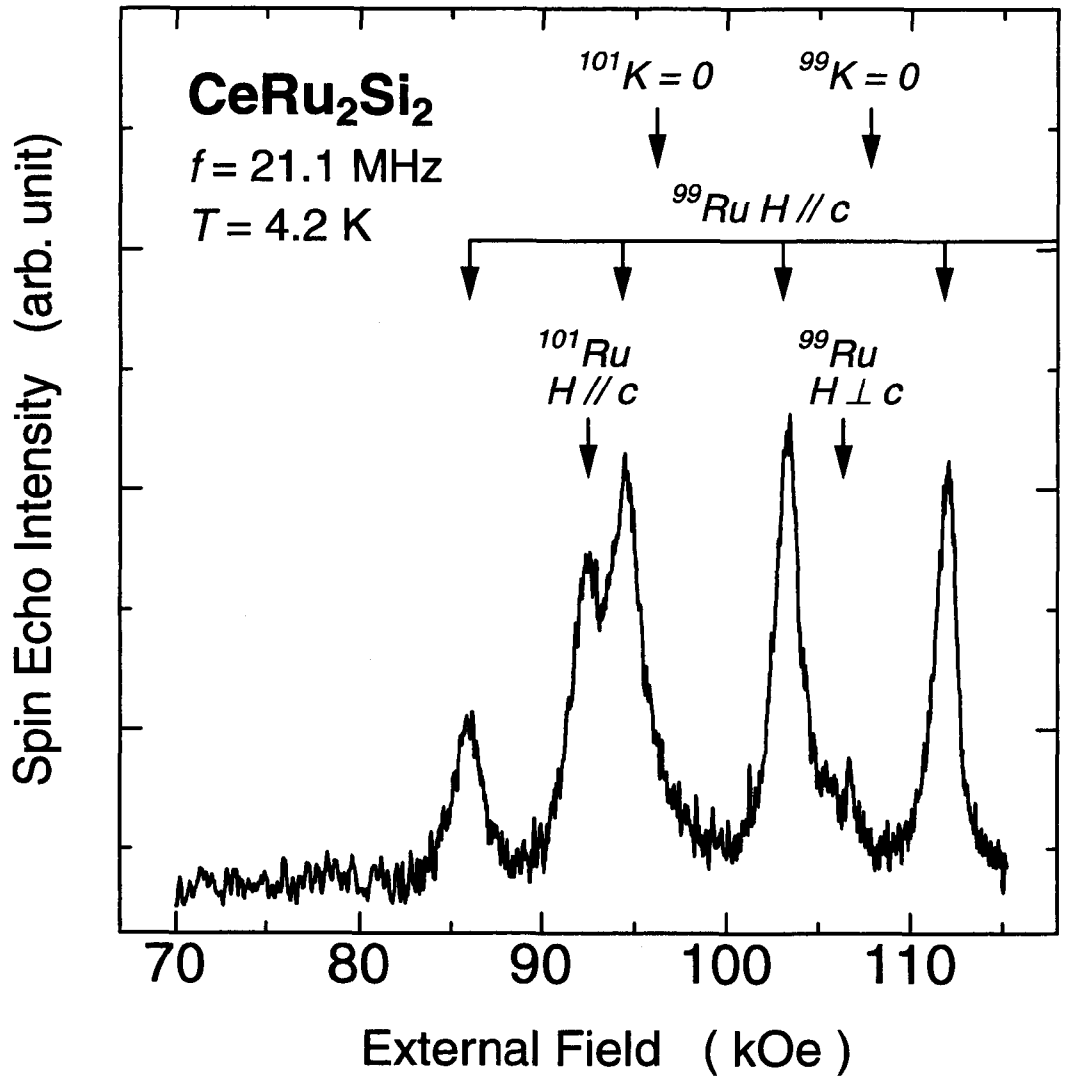

Figure 5.4 Field-swept Ru-NMR spectrum in the oriented powder of $CeRu_2Si_2$. Well-articulated spectrum originates from the electric quadruple interaction for $I = 5/2$ for two Ru isotopes. Upper down arrows denote each peak corresponding to the quadruple split-transition of ^{99}Ru for $H\|c$ axis. The central transition of ^{101}Ru for $H\|c$ axis is only observable due to its larger nuclear quadruple moment.

Figure. 5.4 shows a field-swept Ru-NMR spectrum for the oriented powder at 21.1 MHz and 4.2 K. The well-articulated shape is composed of four transitions from the electric

quadruple interaction for ^{99}Ru ($I = 5/2$) and of a central transition for ^{101}Ru. The ^{99}Ru NQR signal originating from $\pm 3/2 \leftrightarrow \pm 5/2$ transition was observed at 3.61 MHz with a full-width at half-maximum of 0.1 MHz. The ^{101}Ru-NQR spectrum at 4.2 K are shown in Fig. 5.5. The lower and higher frequency resonance lines arise from $\pm 1/2 \leftrightarrow \pm 3/2$ and $\pm 3/2 \leftrightarrow \pm 5/2$ transitions, respectively. From these spectra, the quadruple frequency and the asymmetry parameter of ^{99}Ru were obtained to be $\nu_Q \sim 1.75$ MHz and $\eta \sim 0$ with the principal axis along the c axis, respectively.

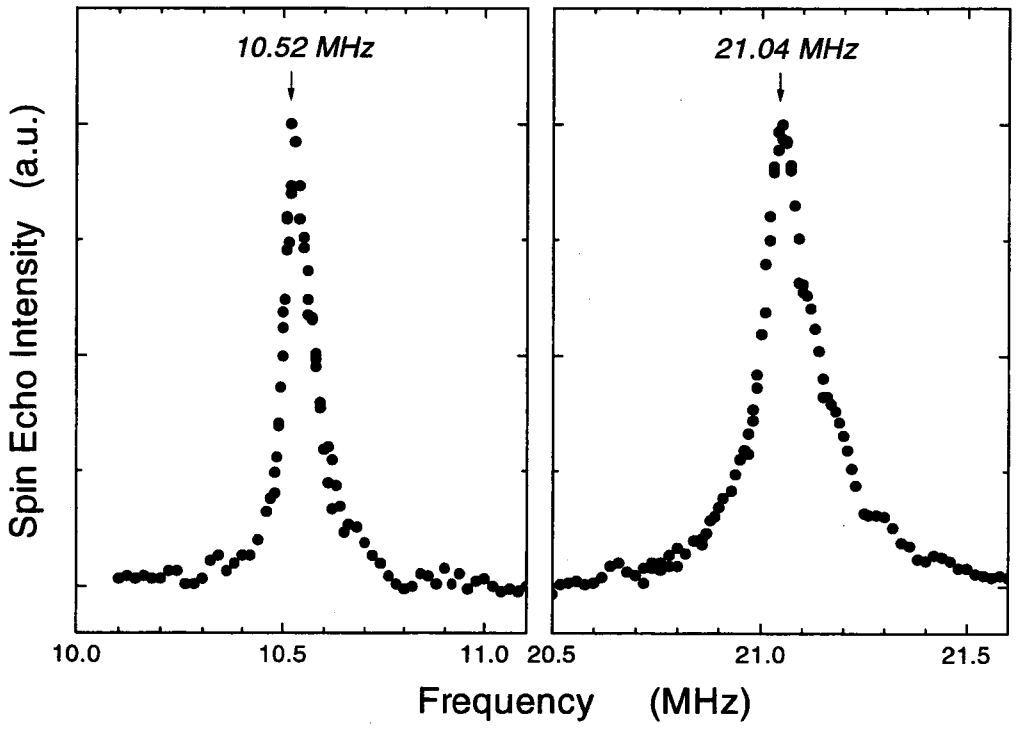

Figure 5.5 ^{101}Ru-NQR spectra obtained at 4.2 K. The lower and higher frequency resonance lines arise from $\pm 1/2 \leftrightarrow \pm 3/2$ and $\pm 3/2 \leftrightarrow \pm 5/2$ transitions, respectively. The quadruple frequency of ^{101}Ru was determined precisely 10.52 MHz.

5.3 Results and discussion

5.3.1 Hyperfine field

The magnetization (M) along the c axis in $CeRu_2Si_2$ is not linear for $H > H_M$ due to the polarized state through the metamagnetic transition. A detailed temperature variation of M for $H > H_M$ was obtained from the temperature dependence of the hyperfine field $\Delta H_{hf} = H_0 - H_{res}$ at the Ru sites where $H_0 = 21.1$ MHz/$^{99}\gamma_n$ is the field which corresponds to $K = 0$, and H_{res} is the resonance field. Fig. 5.6 indicates the respective temperature dependence of $\Delta H_{hf\parallel}$ parallel to the c axis for various fields from 2.93 to 15.5 T together with $\Delta H_{hf\perp}$ perpendicular to the c axis at 10.7 T. The $\Delta H_{hf\parallel}$ at 2.93 T was obtained only in a temperature range of 1.4 – 4.2 K due to the weak signal the NMR signal. As seen in Fig. 5.6, the $\Delta H_{hf\parallel}$'s at 9.0 and 10.3 T in the high-field spin-polarized state continue to increase upon cooling down to 1.4 K, whereas the $\Delta H_{hf\parallel}$ at 2.93 T, where the magnetization is proportional to the field, stays constant. The latter result is consistent with the previous Si Knight shift data $K_\parallel = \Delta H_{hf\parallel}/H_{res}$ at ~ 1.1 T [12].

The $\Delta H_{hf\parallel}$ at the Ru sites induced by H_0 involves the $4f$- electron contribution through conduction-electron spin polarizations and the orbital contribution at the Ru sites and is hence expressed by

$$\Delta H_{hf}(H,T) = H_{res} - H_0 = A_{hf(orb)}\chi_{orb}H_{res} + A_{hf(4f)}M(H_0,T) \tag{5.1}$$

where χ_{orb} and $M(H_0,T)$ are the $4d$ orbital susceptibility and the magnetization per atom in units of μ_B, and $A_{hf(orb)}$ and $A_{hf(4f)}$ are the corresponding hyperfine coupling constants, respectively. Since $K_{orb} = A_{hf(orb)}\chi_{orb}/\mu_B$, we obtain

$$\Delta H_{hf} = K_{orb}\, H_{res} + A_{hf(4f)}\, M \tag{5.2}$$

$$\frac{\Delta H_{hf}}{H_{res}} = K_{orb} + A_{hf(4f)}\,\frac{M}{H_{res}}. \tag{5.3}$$

$\Delta H_{hf}/H_{res}$ is plotted against M/H_{res} in Fig. 5.7 where the magnetization data reported by Haen *et al.* were used [8]. From a linear variation of $\Delta H_{hf\parallel}/H_{res}$ vs M/H_{res} as shown in Fig. 5.7, $K_{orb\parallel}$ and $A_{hf(4f)}$ are extracted to be 0.76% and 3.67 kOe/μ_B, respectively. The estimated $K_{orb\parallel}$ is almost the same as the Ru Knight shift in $LaRu_2Si_2$, 0.72%, indicating that $K_{orb\parallel}$ originates only from the Ru-$4d$ contribution, but not from the Ce contribution. Since $\Delta H_{hf\perp}/H_{res}$ is comparable to $K_{orb\parallel}$, $\Delta H_{hf\perp}$ is not affected by the spin contribution from the $4f$ electrons. The positive and small value of $A_{hf(4f)} = 3.67$ kOe/μ_B is considered to originate from the Fermi contact interaction by $5s$-electron spin polarization induced through the hybridization with the $4f$ electrons.

It should be noted that $\Delta H_{hf\parallel}/H_{res}$ vs M/H_{res} plots for the constant H of 10.3 T at various temperatures and for the constant temperature of 4.2 K under various magnetic fields is on a single line across the metamagnetic transition. The $A_{hf(4f)}$ does not change

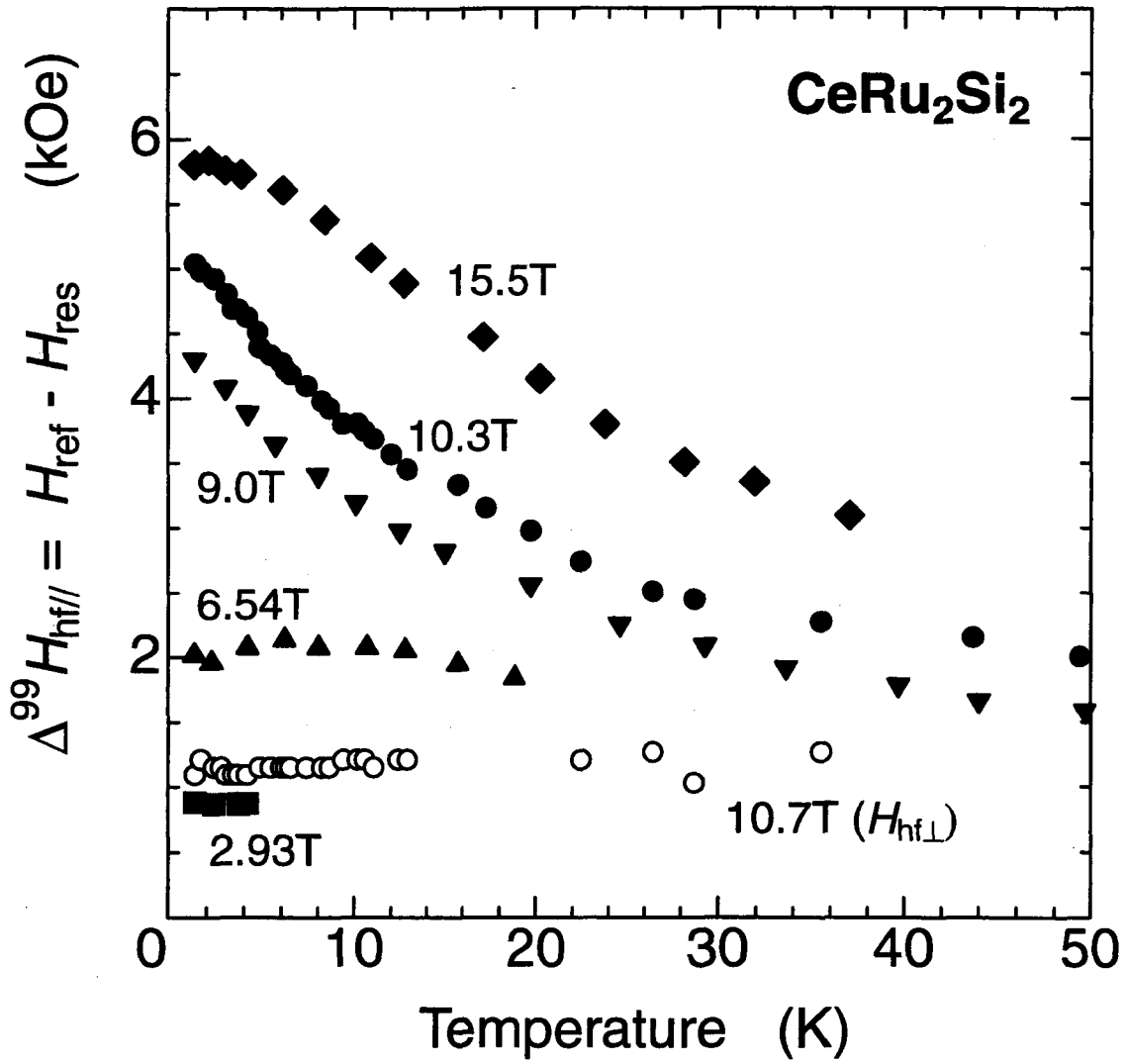

Figure 5.6 Temperature dependence of the hyperfine field, $\Delta H_{\mathrm{hf}\parallel} = H_0 - H_{\mathrm{res}}$ parallel to the c axis for various fields. Temperature dependence of $\Delta H_{\mathrm{hf}\perp}$ perpendicular to the c axis at 10.7 T is also shown.

at all through the metamagnetic transition, indicating no drastic change in the electronic state as observed by magnetization [15], specific heat [10] and transport measurements [16] in contrast to the large change observed in quantum oscillation experiments [17, 18]. This apparent discrepancy may be directly linked to the microscopic formation of the quasi-particle bands.

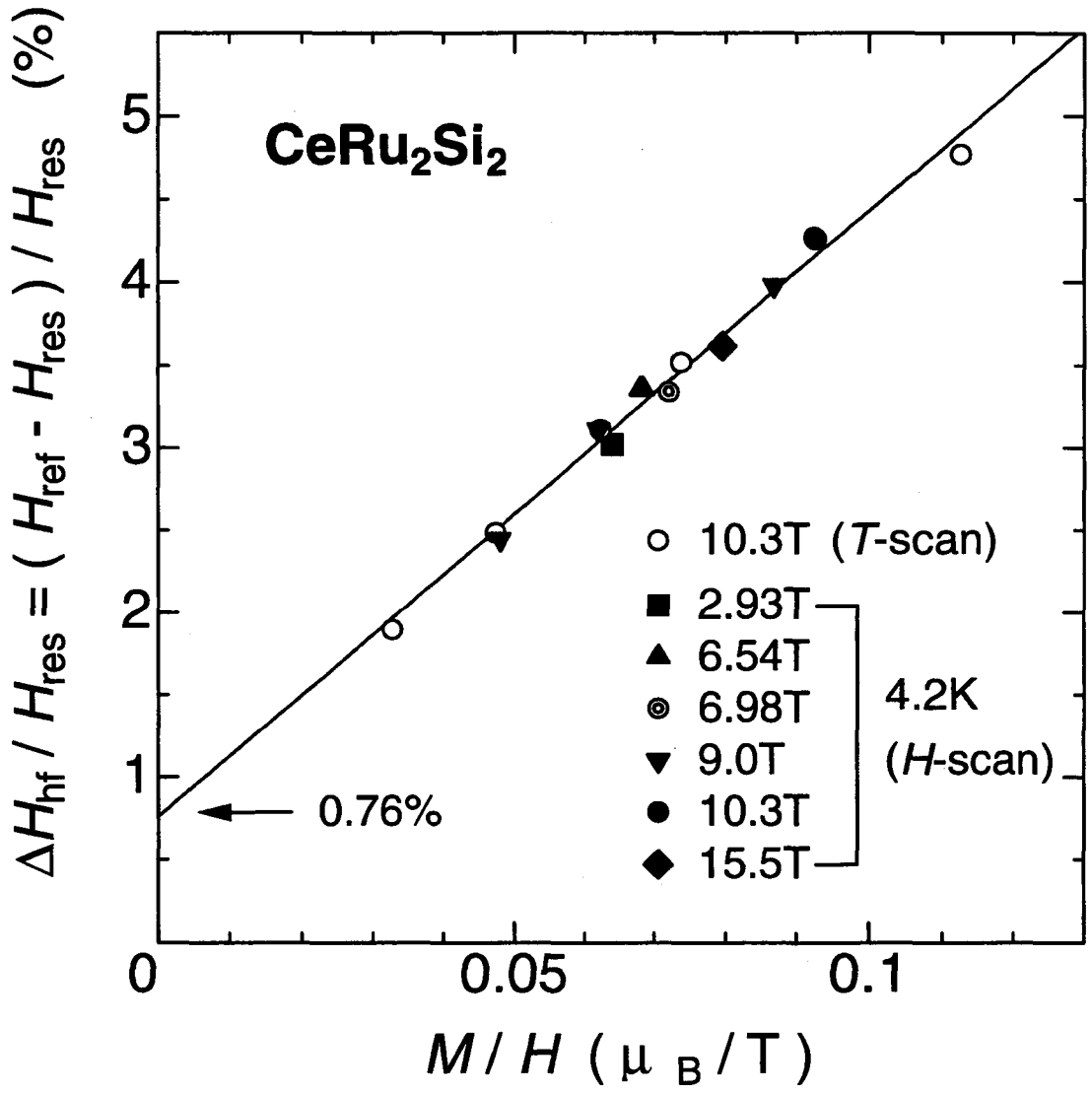

Figure 5.7 $\Delta H_{\mathrm{hf}\parallel}/H_{\mathrm{res}}$ vs M/H_{res} plot. The magnetization data was referred from Ref. [8]. Open circles and other marks correspond to the data obtained in the temperature variation under the constant H of 10.3 T and in the H variation at the constant temperature of 4.2 K, respectively.

Figure 5.8 shows the temperature dependence of the magnetization along the c-axis divided by the external field, H, M/H obtained from the Ru NMR shift and the previous Si NMR data at ~1.14 T from the Si NMR Knight shift with $A_{\mathrm{hf}} \sim 2.21$ (kOe/μ_{B}) [8].

As indicated in the figure, the temperature dependence of M/H is remarkably different between the low and high field below 15 K, where a non-linear response appears in the field-swept magnetization process. This temperature is denoted as the onset temperature, $T_{\rm M}$ for the emergence of the metamagnetic transition. The nearly T-independent behavior below 15 K in the low magnetic field regime is understood as a consequence of the formation of the HF state. Therefore, the monotonous increase below 15 K in the high magnetic field regime shows that the temperature population effect is huge in this polarized state above $H_{\rm M}$. It should be noted that M/H stays constant below 4 K at $H \sim 15.5$ T as seen in the inset of Fig. 5.8, where $1/T_1T$ is also constant as discussed later, suggesting the formation of the different kind of the Fermi-liquid state at $H \ll H_{\rm M}$.

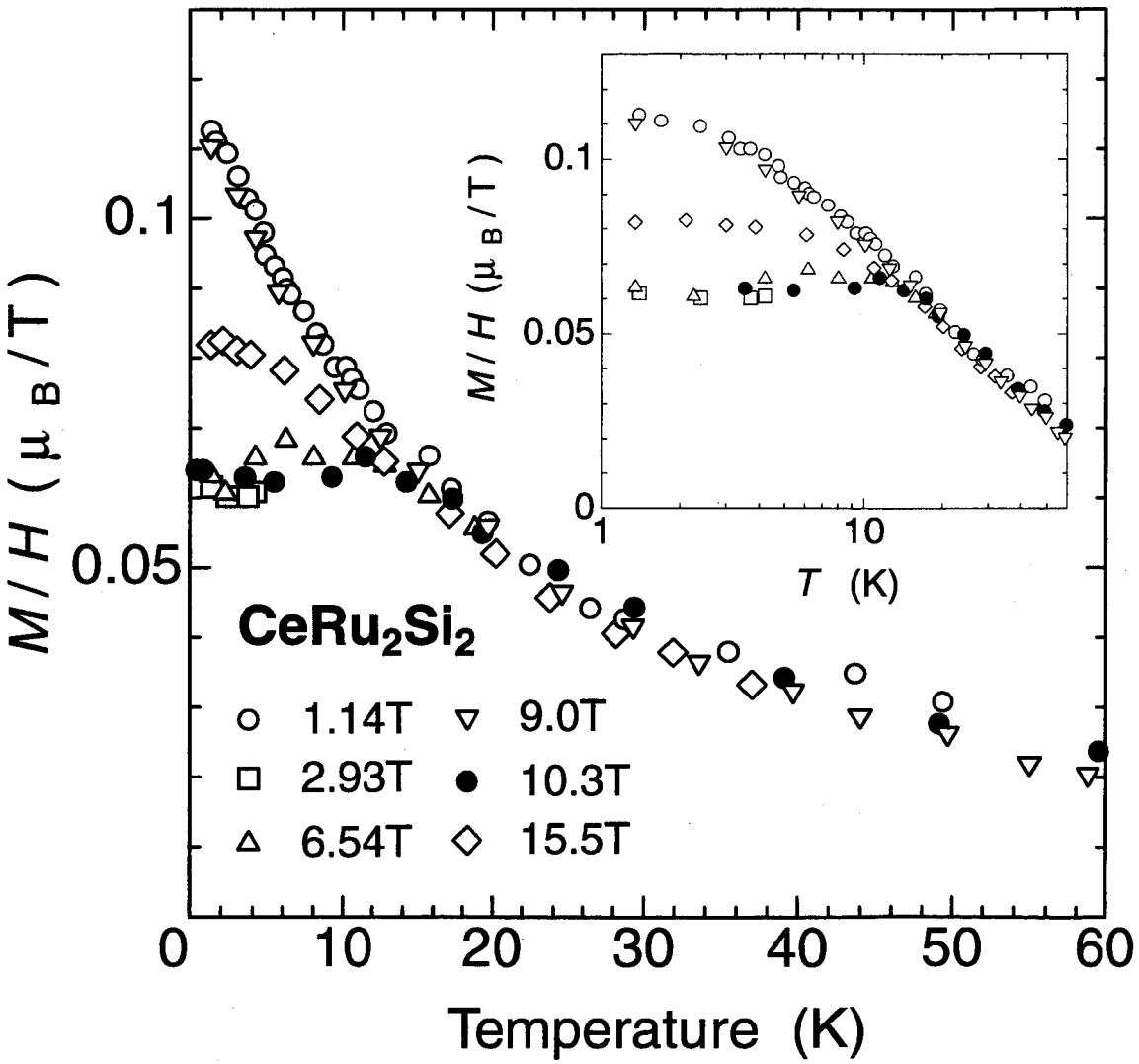

Figure 5.8 Temperature dependence of the M/H deduced from the hyperfine fields at the Ru and Si sites with the relation of eq. (5.3). Inset shows the same data on a logarithmic scale.

5.3.2 Nuclear spin-lattice relaxation rate, $1/T_1$

In Figs. 5.9 (a) and (b), we show the NMR and NQR relaxation behaviors of Ru nuclei ($I = 5/2$), respectively. $1/T_1$'s under magnetic fields were measured by the NMR at the transition of $-1/2 \leftrightarrow +1/2$, while $1/T_1$'s under zero magnetic field were measured by the NQR method for the $\pm 3/2 \leftrightarrow \pm 5/2$ transition. The magnetization recovery for the NMR transition is given by

$$\frac{M(\infty) - M(t)}{M(\infty)} = 0.02857 \exp(-t/T_1) + 0.18 \exp(-6t/T_1) + 0.7936 \exp(-15t/T_1), \quad (5.4)$$

while the recovery for NQR transition is as follows,

$$\frac{M(\infty) - M(t)}{M(\infty)} = \frac{3}{7} \exp(-3t/T_1) + \frac{4}{7} \exp(-10t/T_1), \quad (5.5)$$

where $M(t)$ is the nuclear magnetization at a time t after saturation pulses.

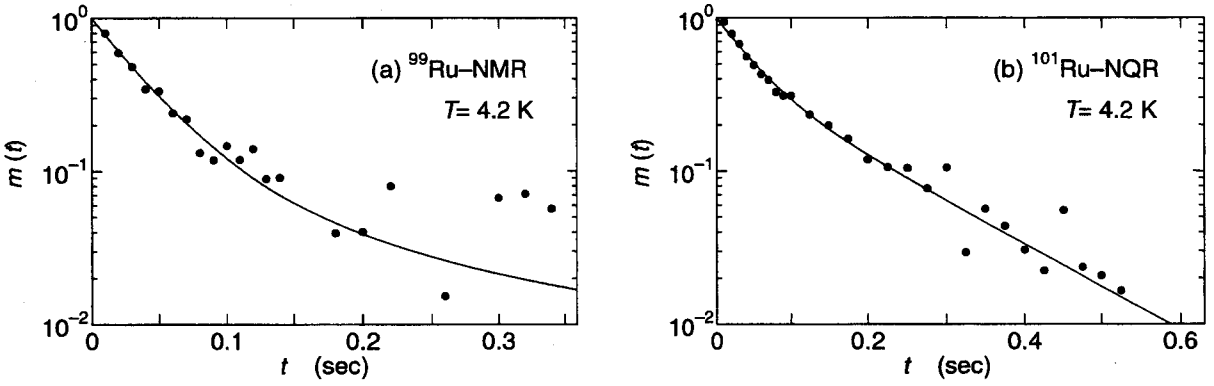

Figure 5.9 Typical behaviors of nuclear magnetization recovery for (a) ^{99}Ru NMR at $-1/2 \leftrightarrow +1/2$ transition around $H \sim 9.0$ T and (b) ^{101}Ru NQR at $\pm 3/2 \leftrightarrow \pm 5/2$ transition at $H = 0$ T in $CeRu_2Si_2$. $m(t)$ stands for $(M(\infty) - M(t))/M(\infty)$. The solid lines are the least square fitting to eq. (5.4) for ^{99}Ru NMR and eq. (5.5) for ^{101}Ru NQR.

The temperature variations of nuclear-spin lattice relaxation rate divided by temperature, $1/T_1T$ below and above H_M are shown in Figs. 5.10 (a) and (b), respectively. As seen in Fig. 5.10 (a), $1/T_1T$'s in zero field and 2.93 T below 8 K stay constant. In the low field regime, the experimental value of $^{99}(1/T_1TK_{iso}^2) = 8.16 \times 10^3$ (sec·K)$^{-1}$ is comparable to the calculated one of $1/T_1TK^2 = \pi\hbar\ ^{99}\gamma_n^2 k_B/\mu_B^2 = 8.04 \times 10^3$ (sec·K)$^{-1}$ based upon the quasi-particle Korringa relation. Here K_{iso} is estimated from $K_{iso} \sim K_{\parallel}/3$ since $K_{\perp}$ is negligible as mentioned above. The HF state below 8 K seems to be dominated by q-independent excitations since the phenomenological magnetic coherence length involves only few lattice distance [11]. This fact is in good agreement with the analysis made in the formalism developed by Moriya [19], where the parameter y_0, inversely proportional to the staggered susceptibility, is relatively large [20].

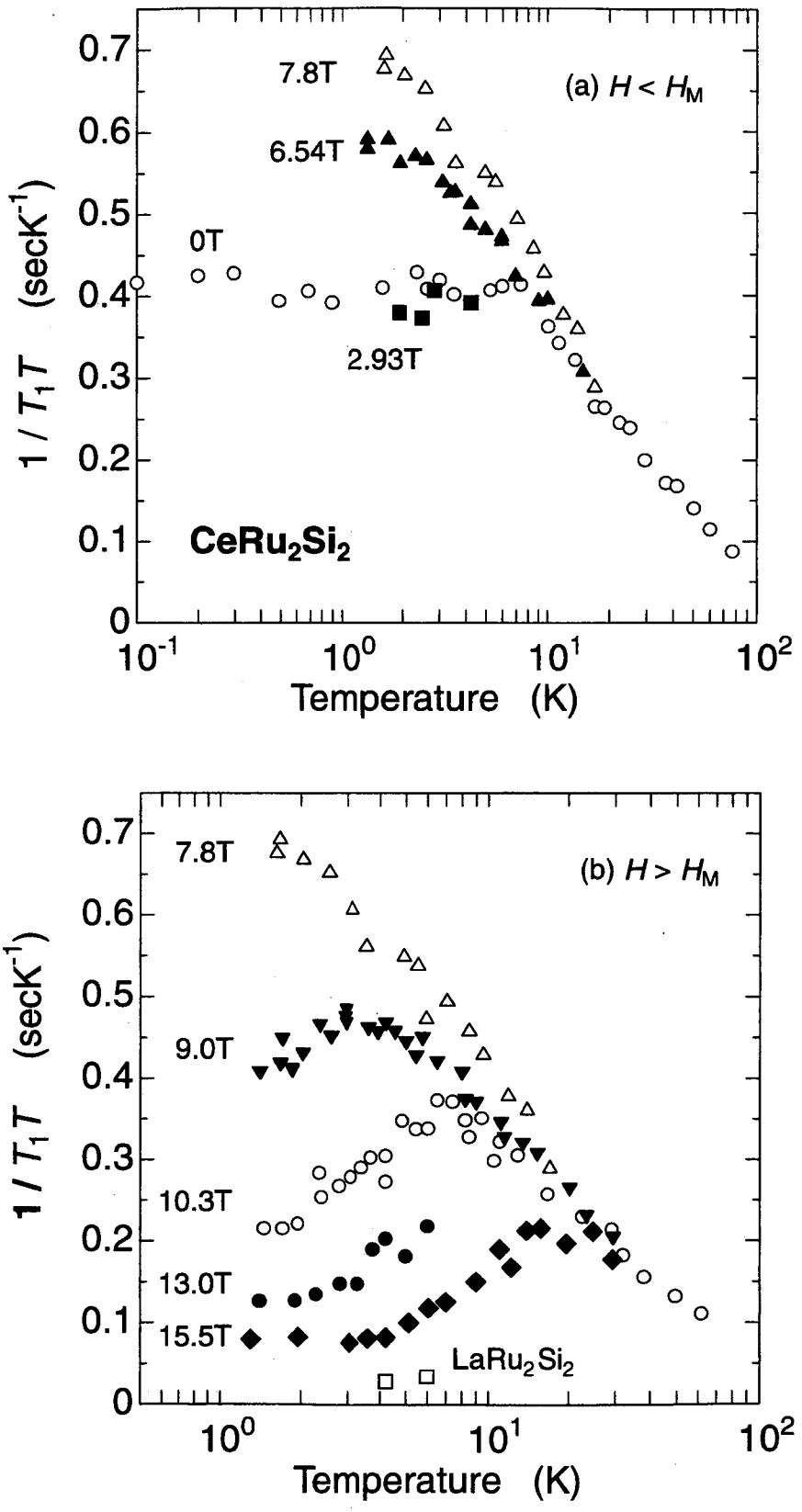

Figure 5.10 Temperature variations of $1/T_1T$ (a) below and (b) above H_M. The $1/T_1T$ of $LaRu_2Si_2$ at 10.3 T is also shown for comparison (open box symbols).

By contrast, $1/T_1T$ below 8 K increases with the increasing field and that at H_M = 7.7 T continues to increase upon cooling as if there exists a critical anomaly almost at $T = 0$ K. As the field increases further, $1/T_1T$ is dramatically suppressed and a peak of $1/T_1T$ emerges around 4 K, 7 K and 20 K for H = 9, 10.3 and 15.5 T, respectively as shown in Fig. 5.10 (b). It should be noted that the $1/T_1T$ = constant in the high field regime holds below temperatures much lower than 8 K in the low field regime.

By using an effective density of states (DOS) , $N_{\rm eff}(E_F)$ at the Fermi level in the HF state, we may assume that $1/T_1T \propto N_{\rm eff}(E_F)^2 \propto \gamma^2$ where $\gamma = C/T$ is the temperature-linear coefficient in the specific heat (C) at $T \rightarrow 0$. In this context, the field-induced suppression in $1/T_1T$ under 7.7, 10.3 and 15.5 T at 1.4 K may be related with the reduction in $N_{\rm eff}(E_F)$. The field dependences of $\sqrt{1/T_1T}$ (open circles) and C/T (closed circles) [10] are shown in Fig. 5.11. The apparent good scaling of $1/T_1T \propto N_{\rm eff}(E_F)^2 \propto \gamma^2$ reflects the fact that $CeRu_2Si_2$ never reaches a magnetic instability even at H_M since each quantity should have a different temperature-dependence near the critical point [19].

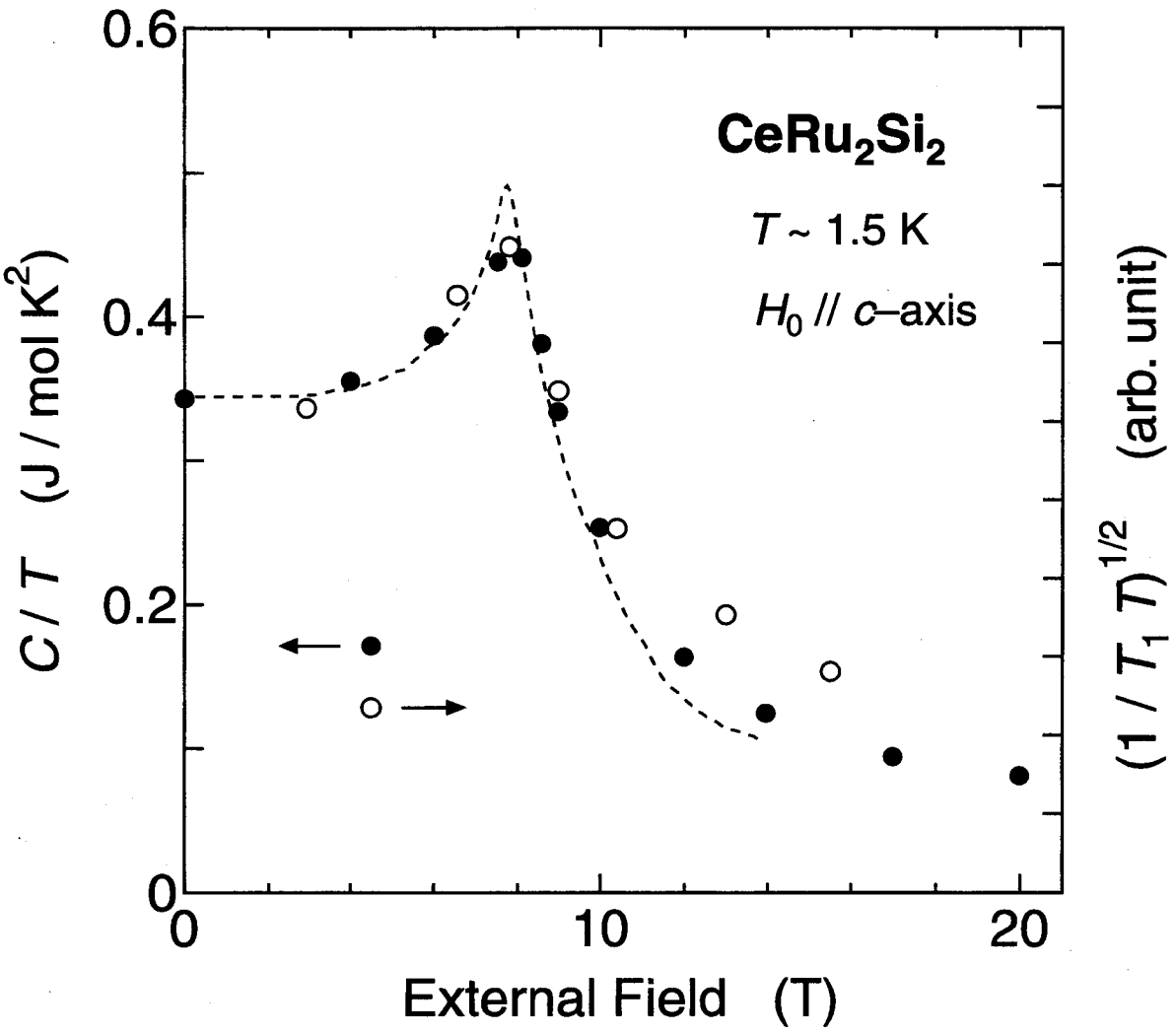

Figure 5.11 Field dependence of $\sqrt{1/T_1T}$ and C/T [10] at 1.5 K, showing the apparent good scaling of $1/T_1T \propto D(E_F)^2 \propto \gamma^2$.

5.3.3 Discussion

The H-T pseudo phase diagram derived from the present results is shown in Fig. 5.12, where the temperature T_p at which $1/T_1T$ shows the peak and T_f below which it holds constant are plotted by square and circle in Fig. 5.12, respectively. T_p and T_f may correspond to the maximum and minimum reported from the previous specific heat and thermal expansion experiments as indicated by up and down triangles in Fig. 5.12, respectively [9, 10]. The similar phase diagrams were derived from recent specific heat [21] and thermal conductivity [22] experiments. In $H < H_M$, the constant behavior in $1/T_1T$ and Knight shift ($K_\parallel$) below 8 K are characteristic for the HF state as mentioned above.

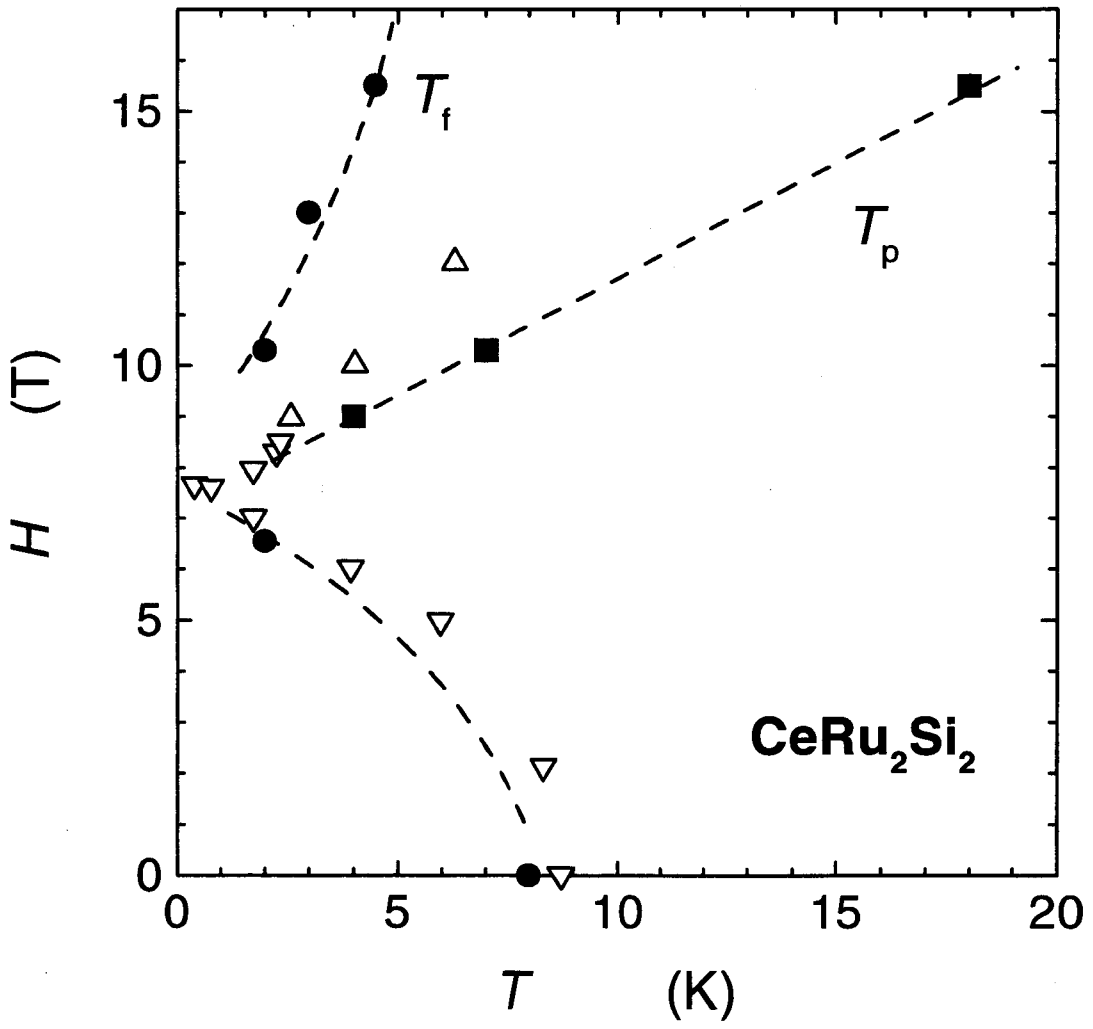

Figure 5.12 H-T pseudo phase diagram derived from the present NMR results. Up and down triangles correspond to the maximum in temperature dependence of C/T and the minimum in the thermal expansion coefficient, respectively [9, 10].

In $H > H_M$, the $1/T_1T$ = constant law appears below T_f where M/H becomes almost temperature independent. However, the emergence of peak in $1/T_1T$ above H_M reflects the fact that the $4f$ state renormalized at the low temperature above H_M is quite different from the case in the unpolarized state. Unusual behavior is that although T_f in $H > 9$ T is lower than $T_f = 8$ K in $H < 3$ T, the value of $1/T_1T$ = constant, which is successively suppressed with the increasing H, is smaller than the value below H_M. This latter result has some relevance to the fact that $1/T_1T$ exhibits a peak at T_p higher than T_f. It means that although the DOS at the Fermi level is much reduced in $H > H_M$, the Fermi liquid state becomes only valid well below $T_f = 8$ K for the HF state in $H < H_M$. This anomalous renormalization process of $4f$ electrons is inherent to the spin-polarized state where $M/H = \chi(H,T)$ increases down to T_f and is saturated with a larger value than that in $H < H_M$ as shown in Fig. 5.8. It is suggested that the HF bandwidth and DOS in the polarized state are much reduced as compared with those in the unpolarized state and at the metamagnetic transition, since most weight of $4f$ state in HF state is considered to be transferred into the ferromagnetically polarized state well below the Fermi level.

The fact that the value of $1/T_1T$ = constant at 15.5 T is significantly larger than that in $LaRu_2Si_2$ suggests that the renormalized $4f$ contribution produces the larger DOS at 15.5 T than that in $LaRu_2Si_2$. In this context, the present result seems to be not compatible with the dHvA result which indicated that the Fermi surface of $CeRu_2Si_2$ is analogous to that of $LaRu_2Si_2$ above H_M [17].

Next we compare the NMR result with the recent results of inelastic neutron scattering experiments [23]. The nuclear relaxation study provides a first insight on the low-energy excitation which can not be reached easily by inelastic neutron experiments. Recent development of the latter technique shows that the AF correlation with characteristic energy ($\sim k_B T_M$) is replaced above H_M by a quasi-static long-range ferromagnetic correlation with a low energy window (< 4 K). This is in good agreement with the rapid decrease in $1/T_1T$ implying a creation of a highly polarized state and with still the occurrence of a temperature dependent Knight shift. Let us stress that polarized neutron experiments, mainly sensitive to a change in the $4f$ magnetic form factor, shows also no indication of its modification through H_M in good agreement with the unchange of the hyperfine coupling constant [23].

5.4 Conclusion

We have investigated the microscopic magnetic properties of the field-induced crossover behavior of the HF state in $CeRu_2Si_2$ by Ru-NMR and NQR measurements.

In the low-field regime, the ordinary HF state below 8 K is evidenced from the quasi-particle Korringa relation. At $H_M \sim 7.7$ T, $1/T_1T$ continues to increase upon cooling to 1.4 K, suggesting a very low characteristic energy. The scaling of $1/T_1T \propto \gamma^2$ at low temperature across H_M reflects the fact that $CeRu_2Si_2$ never reaches a magnetic instability. In the high-field spin-polarized state, the size in $1/T_1T$ and the temperature where $1/T_1T =$ constant law holds are very smaller than those in the unpolarized regime. It is considered that the weight of $4f$ state which depends on the external field at $H > H_M$ is transferred below T_p into the ferromagnetically polarized state below the Fermi level and that the remaining weight forms the HF state below T_f. Therefore k_BT_M is the characteristic energy of the deformation of the HF band below H_M.

The novel crossover in the HF state takes place not only in the H variation but also in the T variation across the metamagnetic transition in $CeRu_2Si_2$. The H-T pseudo phase diagram was developed from the $1/T_1$ and other experimental results.

References

[1] R.A. Fisher, C. Marcenat, N. E. Phillips, P. Haen, F. Lapierre, P. Lejay, J. Flouquet, and J. Voiron, J. Low Temp. Phys. **84**, 49 (1991).

[2] L. C. Gupta, D. E. MacLaughlin, C. Tien, C. Godart, M. A. Edwards, and R. D. Parks, Phys. Rev. B **28**, 3673, (1983).

[3] J. L. Tholence, P. Haen, D. Jaccard, P. Lejay, J. Flouquet, and H. F. Braun, J. Appl. Phys. **57**, 3172 (1985).

[4] A. Amato, C. Baines, R. Feyerherm, J. Flouquet, F. N. Gygax, P. Lejay, A. Schenck, and U. Zimmermann, Physica B **186-188**, 276 (1993).

[5] S. Quezel, P. Burlet, J. L. Jacoud, L. P. Regnault, J. Rossat-Mignod, C. Vettier, P. Lejay, and J. Flouquet, J. Magn. Magn. Matter. **76-77**, 403 (1988).

[6] P. Haen, F. Mallmann, M.-J. Besnus, J.-P. Kappler, F. Bourdarot, P. Burlet, and T. Fukuhara, J. Phys. Soc. Jpn. (Suppl B) **65**, 16 (1996).

[7] M.J. Besnus, J. P. Kappler, P. Lehmann, and A. Meyer, Solid State Commun. **55**, 779 (1985).

[8] P. Haen, J. Flouquet, P. Lapierre, P. Lejay, and G. Remenyi, J. Low. Temp. Phys. **67**, 391 (1987).

[9] A. Lacerda, A. de Visser, L. Puech, P. Lejay, P. Haen, J. Flouquet, J. Voiron, and F. J. Ohkawa, Phys. Rev. B **40**, 11429 (1989).

[10] H. P. van der Meulen, A. de Visser, J. J. M. Franse, T. T. J. M. Berendschot, J. A. A. Perenboom, H. van Kempen, A. Lacerda, P. Lejay, and J. Flouquet, Phys. Rev. B **44**, 814 (1991).

[11] J. Rossat-Mignod, L. P. Regnault, J. L. Jacoud, C. Vettier, P. Lejay, J. Flouquet, E. Walker, D. Jaccard, and A. Amato, J. Magn. Magn. Mater. **76 - 77**, 376 (1988).

[12] Y. Kitaoka, H. Arimoto, Y. Kohori, and K. Asayama, J. Phys. Soc. Jpn. **54**, 3236 (1985).

[13] K. Fujiwara, K. Kumagai, C. Sekine, and S. Murayama, Physica B **186-188**, 517 (1993).

[14] Nuclear Magnetic Resonance in Heavy Fermion systems: Theoretical and Experimental Aspects of Valence Fluctuations and Heavy Fermions, eds. L. C. Gupta and S. K. Malik (Plenum, 1987) 297, Y. Kitaoka, K. Ueda, T. Kohara, Y. Kohori, and K. Asayama.

[15] T. Sakakibara, T. Tenya, K. Matsuhira, H. Mitamura, H. Amitsuka, K. Maezawa, and Y. Ōnuki, Phys. Rev. B **51**, 12030 (1995).

[16] S. Kambe, S. Raymond, H. Suderow, J. Mc Donough, B. Fak, L. P. Regnault, R. Calemczuk, and J. Flouquet, Physica B **223 - 224**, 135 (1996).

[17] H. Aoki, S. Ujii, A. K. Albessard, and Y. Ōnuki, J. Phys. Soc. Jpn. **62**, 3157 (1993).

[18] S. R. Julian, F. S. Tautz, G. J. McMillan, and G. G. Lonzarich, Physica B **199 - 200**, 63 (1994).

[19] T. Moriya and T. Takimoto, J. Phys. Soc. Jpn. **64**, 960 (1997).

[20] S. Kambe, S. Raymond, L. P. Regnault, J. Flouquet, P. Lejay, and P. Haen, J. Phys. Soc. Jpn. **65**, 3294 (1996).

[21] Y. Aoki, T. D. Matsuda, H. Sugawara, H. Sato, H. Ohkuni, R. Settai, Y. Ōnuki, E. Yamamoto, Y. Haga, A. V. Andreev, V. Sechovsky, L. Havela, H. Ikeda, and K. Miyake, J. Magn. Magn. Mater. **177-181**, 271 (1998).

[22] M. Sera, S. Kobayashi, M. Hiroi, N. Kobayashi, H. Ohkuni, and Y. Ōnuki, Phys. Rev. B **56**, 13689 (1997).

[23] S. Raymond, L. P. Regnault, S. Kambe, J. Flouquet, and P. Lejay, J. Phys.: Condens. Matter **10**, 2363 (1998).

Published works

1. Y. Kawasaki, K Ishida, Y. Kitaoka, and K. Asayama: "Si-NMR study of antiferromagnetic heavy-fermion compounds $CePd_2Si_2$ and $CeRh_2Si_2$", Physical Review B **58**, 8634 (1998).

2. M. Imada, M. Tsunekawa, T. Iwasaki, S. Suga, Y. Ōnuki, F. Iga, M. Kasatani, Y. Kawasaki, K. Ishida, Y. Kitaoka, and K. Asayama: "Photoemission of CeX_2Y_2 and $Ce(Pd_{1-x}Cu_x)_3$", Journal of Magnetism and Magnetic Materials **177-181**, 387 (1998).

3. K. Ishida, Y. Kawasaki, Y. Kitaoka, K. Asayama, H. Nakamura, and J. Flouquet: "Ru NMR and NQR probes of the metamagnetic transition in $CeRu_2Si_2$", Physical Review B **57**, R11054 (1998).

4. K. Ishida, Y. Kawasaki, Y. Kitaoka, K. Asayama, H. Nakamura, and J. Flouquet: "Ru-NQR and NMR Study of Metamagnetic Transition in $CeRu_2Si_2$", Physics of Strongly Correlated Electron Systems; JJAP Series 11, 12 (1998).

5. K. Ishida, Y. Kawasaki, K. Tabuchi, K. Kashima, Y. Kitaoka, K. Asayama, C. Geibel, and F. Steglich: "Evolution from Magnetically Ordered to Unconventional Superconducting Phase in a series of $Ce_xCu_2Si_2$ Compounds: Cu-NQR Study", Physics of Strongly Correlated Electron Systems; JJAP Series 11, 35 (1998).

6. Y. Kawasaki, K. Ishida, Y. Kitaoka, K. Asayama, H. Nakamura, and J. Flouquet: "Ru-NMR study of pseudo-metamagnetic transition in $CeRu_2Si_2$", Physica B **259-261**, 77 (1999).

7. K. Ishida, Y. Kawasaki, K. Tabuchi, K. Kashima, Y. Kitaoka, K. Asayama, C. Geibel, and F. Steglich: "Evolution from Magnetism to Unconventional Superconductivity in a series of $Ce_xCu_2Si_2$ Compounds Probed by Cu NQR", Physical Review Letters **82**, 5353 (1999).

8. K. Ishida, Y. Kawasaki, K. Tabuchi, K. Kashima, Y. Kitaoka, K. Asayama, C. Geibel, and F. Steglich: "Crossover behavior from magnetism to superconductivity in $Ce_xCu_2Si_2$", Physica B **259-261**, 678 (1999).

9. Y. Kawasaki, K. Ishida, Y. Kitaoka, K. Asayama, C. Geibel, and F. Steglich: "Magnetism and superconductivity of $Ce_{1+x}Cu_{2+y}Si_2$ under pressure", to be published in *the Proceedings of the International Conference on Strongly Correlated Electron Systems 1999.*

10. H. Okura, K. Ishida, Y. Kawasaki, Y. Kitaoka, Y. Yamamoto, Y. Miyako, T. Fukuhara, and Maezawa: "Ru NQR studies in La and Ge-doped $CeRu_2Si_2$", to be published in *the Proceedings of the International Conference on Strongly Correlated Electron Systems 1999.*

11. C. Thessieu, K. Ishida, S. Kawasaki, T. Mito, Y. Kawasaki, G. -q. Zheng, Y. Kitaoka, and Y. Ōnuki: "In-NQR study of $CeIn_3$ under pressure", to be published in *the Proceedings of the International Conference on Strongly Correlated Electron Systems 1999.*

12. W. Higemoto, A. Koda, R. Kadono, K. Ishida, Y. Kawasaki, Y. Kitaoka, C. Geibel, and F. Steglich: "Magnetism of heavy fermion superconductor $CeCu_2(Si_{1-x}Ge_x)_2$ Compounds: probed by muon", to be published in *the Proceedings of the International Conference on Muon Spin Rotation, Relaxation and Resonance 1999.*

13. K. Ishida, Y. Kawasaki, T. Mito, C. Thessieu, G. -q. Zheng, Y. Kitaoka, C. Geibel, and F. Steglich: "Cu-NQR sturdy of magnetism and superconductivity in $Ce_{1+x}Cu_{2+y}Si_2$ under pressure", to be published in *the Proceedings of the International Symposium on Physics of Solids Under High Pressure Using Nuclear Probes 1999.*

Parts of this thesis were already published:

Chapter 3:	*5, 7, 8, 9, 13.*
Chapter 4:	*1.*
Chapter 5:	*3, 4, 6.*

Acknowledgments

Above all, it is a pleasure to express my gratitude to Prof. Yoshio Kitaoka, who enlightens and leads me with a foresight throughout this work. I would like to express thanks to emeritus Prof. Kunisuke Asayama for giving me the opportunity to study the heavy-fermion physics and for gentle and patient encouragement.

I would particularly like to thank Dr. Kenji Ishida and Dr. Guo-qing Zheng, who always give me helpful suggestions and support through this work.

The experimental studies were performed thanks to the patient support for the high pressure technique by Dr. Takeshi Mito, Dr. Christophe Thessieu, and Mr. Andrei Kornilof. My thanks are also due to Dr. Hideki Tou, Dr. Koichi Nakamura, and Dr. Akihiro Koda for their stimulating discussion and practical advice for the low temperature experiments, to Dr. Koichi Magishi, Dr. Shinji Matsumoto, Dr. Yo Tokunaga, and Dr. Hidekazu Mukuda for their helpful discussion and cordial encouragement. The cooperation of colleagues in our group is gratefully acknowledged.

I am deeply indebted to Prof. Yoshichika Ōnuki, Dr. Hiroyuki Nakamura, Prof. Christoph Geibel, and Prof. Frank Steglich, who provided the high quality samples in this study. I am grateful, also, to Prof. Syuzo Kawarazaki, Prof. Jacques Flouquet, Prof. Tatsuo C. Kobayashi, Prof. Kazumasa Miyake, and Prof. Hiroshi Kohno for their comments and valuable suggestions.

Finally, I wish to thank my parents for their support over the years.